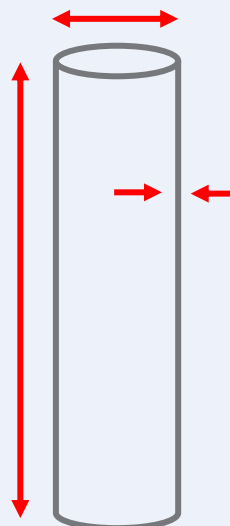

The plugging effect on the design of open-ended steel pipe piles

K.H.M. Harms

2021

Delft University of Technology
Civil Engineering and Geosciences
MSc. Civil Engineering – Geo-Engineering



The plugging effect on the design of open-ended steel pipe piles

by

K.H.M. Harms

to obtain the degree of Master of Science in Civil Engineering
at the Delft University of Technology,
to be defended publicly on 22-11-2021

Student number: 4451589
Project duration: February 1, 2021 – November 22, 2021
Thesis committee: Prof. dr. ir. K.G. Gavin, TU Delft, chair
Ir. R. van de Kamp, Rijkswaterstaat
Dr. G. Giardina, TU Delft
Dr. ir. F. Pisanò, TU Delft

An electronic version of this thesis is available at <http://repository.tudelft.nl/>.

Preface

This thesis is written to obtain the MSc. degree of Civil Engineering with track Geo-Engineering at the faculty of Civil Engineering and Geosciences from the TU Delft and is done in cooperation with Rijkswaterstaat.

I would like to thank Renger and Ken for being great supervisors. Graduating during a pandemic has not always been the most exciting, but thank you both for your support and making it work. And thank you to the rest of my committee for the constructive feedback and critical questions that were much needed. Also thank you Dirk de Lange from Deltares for helping me a lot, too. In many ways a thesis is actually more a team effort than it is individual work and everybody's help is massively appreciated.

This thesis was done in cooperation with Rijkswaterstaat, which is the executive agency of the Ministry of Infrastructure and Water Management of the Netherlands and responsible for e.g. the Dutch highway system, public structures and water safety. Rijkswaterstaat is often involved in the development of new design guidelines and CUR committees, and as such this paper primarily focuses on the evaluation and analysis of design codes in relation to plugging. The experience to graduate at Rijkswaterstaat was really valuable and showed me interesting aspects of geotechnical engineering.

One thing I learned about foundation design is that you know nothing for certain but that everything matters. It is not a field where one approach fits all, nor will it be. However, the amount of research done on open-ended piles is astonishing and I learned a lot from this project, but as with anything, you learn that there is a lot we know and a lot we do not. I hope to contribute in some way a bit to the things we do know in this ongoing field of research.

*K.H.M. Harms
Delft, November 2021*

Abstract

The design of open-ended piles means choosing the right dimensions (length, diameter and wall thickness) so that a design method predicts an axial capacity for a pile in combination with a soil profile with a CPT. Plugging of soil inside the pile can cause soil displacement around the pile, which influences the capacity of the pile. The many uncertainties of the plugging effect and the limited amount of load tests on which design codes are often based can cause significant over- or under-prediction which has negative financial and/or structural effects.

This research looks at the workings of three design methods for piles loaded in compression and tension by modelling capacity for different soil profiles, varying parameters and load tests. Compared methods are from the NEN 9997-1 (NEN), CUR 2001-8 report (CUR) and a newly developed international standard (ISO). It is generally accepted that the NEN is overly simplistic and research shows the CUR to be generally over-predicting capacity, but the implications of these flaws are not in detail investigated. Per method, the behaviour of shaft and base resistances/capacities and total axial capacity were modelled for constant q_c 's, real CPT's and applied to case studies. Case studies, where possible, are focused on Dutch soil condition to see how the ISO would apply. The capacities were modelled over the whole domain of the CPT to get insight in general behaviour of the methods and to see where potential weaknesses lie. Also an evaluation on installation effects as residual stresses and pile ageing was done.

It appears the CUR and NEN both have demonstrable flaws that negatively impact their capacity predictions, and most notable are their approach on shaft friction that translates to non-optimal shaft capacity profiles. Also, their response on increasing diameters of concern, as design methods are in enormous disagreement on capacities for piles with diameters larger than 1 m. Predictions compared to each other can vary threefold and differ with 8.5 MN.

The CUR generally over-predicts capacities in looser sands but under-predicts for deeper tests. The NEN generally under-predicts for denser sands but is sometimes largest of three for looser sands. General under-prediction does not necessarily mean the method is conservative. The ISO performs in most cases best, and uses a predictive plug length to influence both shaft and base capacity. The NEN is poorly suited for design, the CUR is in particular unsuited for longer piles or diameters larger than 1 m. The ISO is an improvement on current design guidelines for the Netherlands and a good step in incorporating plugging in the design for open-ended piles.

List of Figures

1.1	Possible closed- and open-ended pile states	2
2.1	Stress components in a plugged open-ended pile loaded in compression	6
2.2	Research from F. Chow, 1997 and Lehane et al., 1993 showing friction fatigue	8
2.3	Components Mohr-Coulomb failure criterion (τ_f versus σ'_r) for a (closed-ended) pile in load test, by Lehane et al. (1993)	8
2.4	Arch developments from Li et al., 2019	9
2.5	Influence <i>IFR</i> on q_{plug} and q_{ann} , from Lehane and Gavin, 2001	10
2.6	Base resistance components from Kim et al., 2002	10
2.7	Mechanisms causing reduction in tensile loading compared to compressive loading from ICP, 2005	11
2.8	Components for IFR and PLR, based on Paik and Salgado, 2003	12
2.9	Measuring <i>IFR</i> , from K. Paik et al., 2003	13
2.10	<i>IFR</i> and <i>PLR</i> results for three piles in the same soil, from Jeong et al., 2015	14
2.11	Results from Gudavalli, 2014 for piles with $D = 0.5\text{ m}$	15
2.12	Field evidence for the rigid plugging criterion (equations 2.12 and 2.13), from ICP, 2005	16
2.13	Schematic representation of the creation of residual stress from F. Chow, 1997	17
2.14	Influence of residual stress corrections loads in gravelly sand load test, from Han et al., 2020	18
2.15	<i>PLR</i> versus D_i , from JIP, 2020. Equation 4.7 in legend is equation 2.24 below.	22
3.1	Schematic representation of methodology	23
4.1	Shaft friction along a pile in homogeneous sand ($L = 50\text{ m}$, $q_c = 35\text{ MPa}$, $D = 1.3\text{ m}$, $t = 0.016\text{ m}$)	27
4.2	Shaft friction of Fig. 4.1a from 40 – 50 m with averages	28
4.3	Friction fatigue effect of τ_f for ISO and CUR in constant q_c (35 MPa): a reduction in τ_f is apparent when the pile is driven down (pile tip level goes from 35 to 45 m). $D = 1.3\text{ m}$, $t = 0.016\text{ m}$	29
4.4	Capacities for constant q_c , compression	30
4.5	Capacity for constant q_c from 5 MPa to 50 MPa for a pile with $D = 1.3\text{ m}$, $t = 0.016\text{ m}$ ($t/D = 0.012$)	31
4.6	Capacities for depth trends for a pile with $D = 1.03\text{ m}$ and $t = 0.016\text{ m}$	32
4.7	Effect of diameter on NEN for increasing diameter in synthetic q_c of 15 MPa	33
4.8	Diameter effect on shear stress for $q_c = 15\text{ MPa}$	33
4.9	Diameter effect on base resistance	34
4.10	Diameter effect on $Q_{cur} - Q_{iso}$ for different q_c	35
4.11	Capacities for constant q_c profiles, tension	35
4.12	Maasvlakte CPT profile with base resistances for a pile with $D = 0.5\text{ m}$ and $t = 0.008\text{ m}$	36
4.13	Resulting capacities from Fig. 4.12 for two piles. Below left black dot: pile is assumed to plug during loading. Pile does not plug on the right red line of the NEN	37
4.14	Utrecht CPT profile with base resistances for a pile with $D = 0.5\text{ m}$ and $t = 0.016\text{ m}$	38
4.15	Influence of increasing/decreasing D on $q_{b,nen}$	39
4.16	Resulting capacities from CPT in Fig. 4.14 for two piles. From black dot, the NEN predicts plugging. Pile is predicted non-plugging in Q_{nen} with $D = 1.3\text{ m}$	39
4.17	Breakdown of capacity components from Utrecht for CUR and ISO for two piles	40
4.18	Enschede CPT profile with base resistances for a pile with $D = 0.5\text{ m}$ and $t = 0.008\text{ m}$	41
4.19	Resulting capacities from CPT in Fig. 4.18 for two piles. After black dot and in between blue/red dots, $Q_{b,nen} < Q_{fr,nen,i}$ and pile is assumed to plug	41

4.20 Database CUR for open-ended piles loaded in compression - colours indicate test sites	42
5.1 <i>PLR</i> and <i>IFR</i> of EURIPIDES I	46
5.2 Results for EURIPIDES test 1 a-c, black dots are Q_m -values from Yang et al., 2016	47
5.3 Predicted and measured shaft frictions, with measured shaft friction from JIP, 2020	48
5.4 CPT profile and capacities for EURIPIDES II	49
5.5 q_c profile and gravel content from Han et al., 2020	50
5.6 Predicted and measured shaft frictions	51
5.7 Hoogzand 1-c	52
5.8 Hoogzand 3-c	53
5.9 Hoogzand 1-c shaft friction profiles, measured values from JIP, 2020	54
5.10 Tokyo load test cone resistance and resulting base capacity	55
5.11 EURIPIDES capacity prediction for tension, black dots are $Q_{t,m}$	56
5.12 Hoogzand capacity prediction for tension, black dots are $Q_{t,m}$	56
5.13 q_c profile and capacity predictions for Blessington tests S2-S5 (tension)	57
5.14 Variations of <i>PLR</i> on Q_{iso} for Hoogzand III	59
B.1 Database CUR for open-ended piles loaded in compression - colours indicate sites	68
B.2 Database CUR for open-ended piles loaded in tension - colours indicate sites	68
C.1 CPT from Maasvlakte (q_c measured with $q_{c,avg}$)	71
C.3 Effect of increasing diameter on CUR and ISO for $q_c = 15 \text{ MPa}$	72
C.2 Effect of varying synthetic q_c on capacities CUR and ISO	72
C.5 Database CUR for open-ended piles loaded in compression - colours indicate sites	72
C.4 $Q_{fr,i}$ and Q_b for NEN in CPT Utrecht for a pile with $D = 0.5 \text{ m}$. When $Q_{fr,i} < Q_b$, the pile plugs (according to the NEN)	73
C.6 Database CUR for open-ended piles loaded in tension - colours indicate sites	73
C.7 Database CUR for open-ended piles loaded in tension - colours indicate sites	73
D.1 Equilibrium of soil element, from Randolph, 2003	75
D.2 Equation from Jeong et al., 2015	76

Notation

List of symbols

α_p	pile class factor from the NEN for compression
α_s	pile class factor from the NEN for shaft friction in compression, $\alpha_s = 0.006$ for open-ended piles
α_t	pile class factor from the NEN for shaft friction in tension, $\alpha_t = 0.004$ for open-ended piles
β	friction ratio, $\beta = \tau_f / \sigma'_v$, or pile foot class factor for the NEN
δ_f	interface friction angle
γ'	effective volumetric weight of the soil, generally for sands $\gamma' \approx 10 \text{ kN/m}^3$
σ'_{rc}	effective radial stress at equilibrium
σ'_{rd}	effective radial stress due to dilation or lateral expansion
σ'_v	effective vertical stress
τ_f	shear stress (or shaft friction) at failure
φ'	angle of internal friction
A_b	base area of pile, $A_b = \pi D_0^2 / 4$
A_{re}	effective area ratio, "the ratio of the displacement induced to that of a fully plugged pile" (JIP, 2020), $A_{re} = 1 - FFR(D_i/D)^2 \approx 1 - PLR(D_i/D)^2$
d_{CPT}	diameter of CPT, $d_{CPT} = 0.0356 \text{ m}$
D	diameter
D_0	outer diameter
D_{50}	mean particle diameter
D_i	inner diameter
D_r	relative density
DR	displacement ratio, parameter accounting for the closedness of a pile, $DR = 1 - (D_i/D_0)^2$
FFR	Final Filling Ratio, average IFR for a distance of multiple diameters near pile tip
f_t/f_c	factor for loading direction, $f_t/f_c = 1.0$ in compression and 0.75 in tension
h	distance from pile tip, $h = L - z$
h/R^*	normalised distance from pile tip
IFR	Incremental Filling ratio, $IFR = dL_{plug}/dPTL$
K	coefficient of lateral earth pressure
L	length of pile
L/D	pile slenderness
L_{plug}	length of plug
p_a	reference atmospheric pressure, $p_a = 100 \text{ kPa}$
PLR	plug length ratio, L_{plug}/L , often the average IFR over a certain distance from pile tip
PTL	pile tip level
q_{ann}	annulus resistance from pile tip
q_b	base resistance
q_b/q_c	normalised base resistance
q_c	cone resistance from CPT
$q_{c,avg}$	average cone resistance $1.5D$ above and below pile tip
q_p	average cone resistance $1.5D$ above and below pile tip
q_{plug}	plug resistance

Q	axial capacity, the load an open-ended pile can bear to for a displacement of 10% its diameter (compression) or total measured load (tension)
Q_{ann}	annulus capacity
Q_{eb}	end bearing capacity
Q_{fr}	frictional capacity
Q_{plug}	plug capacity
$Q_{t,c}/Q_{t,m}$	performance, or total calculated capacity divided by total measured capacity
R	pile radius
R^*	effective pile radius, radius a closed-ended pile would have with same A_{ann} , $R^* = R \cdot DR^{0.5}$
t	wall thickness of pile
z	depth

General subscripts

0.1D	10% of diameter, a common pile displacement for which $Q_{t,m}$ is defined
avg	average
ann	annulus
b	base
c	calculated (subscript for Q) or at equilibrium (subscript for e.g. σ'_{rc})
eb	end-bearing
f	failure
fr	friction
i	inner
m	measured
o	outer
rc	radial at equilibrium
rd	radial due to dilation
rf	radial at failure
s	shaft
t	tension or total
v	vertical

Acronyms

API	American Petroleum Institute
CUR	Civieltechnisch Centrum Uitvoering Research en Regelgeving
CPT	Cone Penetration Test
DEM	Discrete Element Method
EURIPIDES	European Initiative on Piles in Dense Sands
FEM	Finite Element Method
ICL	Imperial College London
ICP	Imperial College Pile, former MTD
JIP	Joint Industry Project
NEN	Nederlandse Normen
RWS	Rijkswaterstaat
UWA	University of Western Australia

Summary

The design of open-ended steel pipe piles means choosing the dimensions of the pile - length, diameter and wall thickness - so that the axial capacity is predicted in combination with a CPT. Axial capacity is defined as the maximum load a pile can bear to induce a displacement of 10% its diameter. Plugging greatly influences axial capacity but is often poorly accounted for in design methods. The many uncertainties of the plugging effect and the limited amount of load tests on which design codes are often based can cause significant over- or under-prediction which has negative financial and/or structural effects. This research evaluated three design methods: two of which are common in the Netherlands, being the NEN 9991-7 (NEN) and the CUR 2001-8 report (CUR), and a newly established international method (ISO).

The NEN relates cone resistance q_c directly to shaft friction with constant α -factors and limiting values. For base resistance, the NEN use the Koppejan averaging method and a plugging condition where the minimum of internal shaft capacity or base capacity contributes to capacity. The CUR is primarily based on the EURIPIDES tests and assumes only the fully plugged condition in its base resistance. The ISO is a merge of existing methods and uses the Mohr-Coulomb failure criterion for shaft friction with empirical formulations. It uses the plug length ratio in its shaft and base capacity and this allows to predict capacity for partially plugged conditions.

Design code characteristics

The shaft resistances, base resistances and capacities for each methods were plotted for different situations: a constant q_c , real CPT's, variations for dimensions and these conclusions were then linked to case studies. The three methods vary significantly in predicted capacities. The ISO proved to be the most best method.

The NEN is poorly suited for design methods because the constant α -factors are inadequate for accurate capacity predictions and result in no implied friction fatigue. The limiting values for shaft friction in combination with the plugging condition severely under-predict capacity in denser sands. Case studies, often done in dense sands, confirm this. The NEN often predicts the lowest capacity, but it is not always a conservative method.

The CUR assumes the vast majority of its shaft friction to be concentrated near the pile tip, causing a large friction fatigue component near the pile tip. This stress concentration near the pile tip implies that weak/strong zones farther from the pile tip have little influence on shaft capacity. The shaft capacity profile has an asymptotic trend due to this concentration near the pile tip. Consequently, the CUR under-predicts those in shaft and total capacity. Normalised base resistance q_b/q_c increases with decreasing q_c which causes a significant over-prediction for base resistance in looser sands.

The ISO has a concentration of shear stress near the pile tip which decreases at increasing distance from the tip. This causes friction fatigue and the shaft capacity profile to increase over depth. Consequently, the total capacity has a stronger depth trend than the CUR. The normalised base resistance q_b/q_c is constant for the ISO, so independent of q_c . This directly relates base resistance to cone resistance, independent of the q_c value near the pile tip. The ISO method uses a predicted Plug Length Ratio (before installation) but this has large uncertainties. Correcting with a measured Plug Length Ratio (after installation), the change of capacity is within acceptable bounds.

The CUR is sensitive for changes in diameter, if the diameter is increased the capacity also significantly increases. There are two reasons in the CUR's formulation for this: a larger diameter increases the shaft friction profile for the CUR, and the CUR generally predicts higher base resistance which, for a larger diameter, gives a higher base capacity. It is not recommended to the use the CUR for piles with for piles with a diameter larger than 1 meter. A case study confirmed this over-prediction for base capacity. The ISO is more stable for changes in diameter, as q_b/q_c is constant for q_c changes and shaft friction

decreases over the length and especially near the pile tip which is reasonable due to a lesser degree of soil displacement as t/D generally decreases for larger diameters.

The large base resistance of the CUR and the depth trend of the ISO cause the CUR to predict highest capacities for shallow depths and looser sands (low q_c), while the ISO often predicts the highest capacity for deeper depths and denser sands (high q_c).

Case studies

Discussed case studies are EURIPIDES and Hoogzand (compression and tension), Tokyo, tension tests in Blessington and a test in gravelly sand. The ISO performed better than the CUR in the case studies for compression as well as tension. The NEN is generally The depth trend of the ISO and constant q_b/q_c are important reasons why the ISO performs better than the CUR.

EURIPIDES showed that the ISO is correct in the depth trend of capacity, which is an important reason why the ISO performs better for longer piles where shaft capacity often is larger than base capacity.

Both the CUR and the ISO work well in over-consolidated sand (Hoogzand). The large stress concentration near the pile was not seen in measured shaft frictions, not even in the over-consolidated sand of Hoogzand. Neither was the approximately constant shaft friction profile implied by the NEN seen anywhere.

The over-prediction of the CUR for large diameters is confirmed by the Tokyo test. Also the ISO over-predicted base capacity and this may be because there is weak zone below the pile tip.

Shaft capacity in gravel is heavily over-predicted by all methods as larger grain size cause less surface for friction to act upon. Design codes are suited to predict base capacity in gravelly sand. A correction for residual stresses reduced the measured shaft capacity which increased the over-prediction.

The ISO performed best for pile ageing tests, but this is also includes many uncertainties and is difficult to incorporate in a design code.

From the available data, the ISO is the most effective way of predicting capacity in the Netherlands. There is still a lack in representative load test in Dutch soil conditions. Improving design of open-ended piles requires more load tests and the biggest gain can be made in more accurate formulations for shaft friction.

Contents

List of Figures	vii
Notation	ix
1 Introduction	1
1.1 Plugging and design of open-ended steel pipe piles	1
1.2 Research topic	2
1.3 Document structure	3
2 Axial capacity of open-ended piles and the mechanisms of plugging	5
2.1 Axial capacity of open-ended piles	5
2.1.1 Shaft resistance expressions	7
2.1.2 Base resistance and plugging	8
2.1.3 Tension	11
2.2 Plugging during installation and loading.	11
2.2.1 Installation	11
2.2.2 Loading	13
2.3 Diameter and relative density in relation to plugging	14
2.3.1 Pile diameter	14
2.3.2 Relative density.	16
2.4 Installation effects	17
2.4.1 Residual stresses.	17
2.4.2 Pile ageing	18
2.5 Problems in modelling plugging	18
2.6 Empirical design methods	19
2.6.1 NEN 9997-1.	19
2.6.2 CUR 2001-8	20
2.6.3 Unified API/ISO.	21
3 Methodology	23
3.1 Synthetic q_c versus real CPT's.	24
3.2 Case studies	25
3.3 Numerical approach	25
4 Results: Design code analysis	27
4.1 Shaft friction with synthetic CPT	27
4.2 Axial capacity with synthetic CPT's, compression	29
4.2.1 Influence q_c	30
4.2.2 Influence diameter and wall thickness.	32
4.3 Axial capacities with synthetic CPT's, tension	35
4.4 Axial capacities with CPT's	36
4.4.1 Maasvlakte, deep and dense sand layer	36
4.4.2 Utrecht, shallow and loose sand layer.	38
4.4.3 Enschede, two shallow and locally dense sand layers	41
4.5 Database background of CUR and ISO	42
4.6 Summarised conclusions.	43
5 Results: Case studies	45
5.1 Euripides I a-c, compression.	45
5.1.1 Dimensions and condition	45
5.1.2 Results	46

5.2	Euripides II, compression	49
5.3	Han, F. et al. (2020) - Gravelly sand, compression	50
5.4	Hoogzand I and III, compression	52
5.4.1	Dimensions and conditions	52
5.4.2	Results	52
5.5	Tokyo, compression	54
5.6	Tension	55
5.6.1	EURIPIDES and Hoogzand	55
5.6.2	Blessington	57
5.7	Accuracy on performance and plugging prediction	58
5.7.1	Performance calculations	58
5.7.2	PLR_{ISO}	58
5.8	Future load tests	59
5.9	Summarised conclusions case studies	60
6	Recommendations and conclusion	61
A	Summarised equations per design method	65
B	Database overview of pile load tests	67
B.1	CUR.	67
B.2	ISO	69
B.3	Collected pile load tests from Yang et al., 2016.	69
C	Additional plots	71
D	The 1D plugging equation	75

Introduction

1.1. Plugging and design of open-ended steel pipe piles

Open-ended steel pipe piles are a type of foundation piles, often tubular in shape and commonly used in on- and offshore practices. Offshore examples are typically found under windmills and oil platforms. Onshore examples can be found under flats, bridgeheads, pillars, and as part of a combiwall. Open-ended piles are easier to install to greater depths and require less blow counts (K. Paik et al., 2003). Other reasons for the wide use of open-ended steel pipe piles are their high axial capacities, light weight and pleasant workability (Ko and Jeong, 2015). This makes it possible to easier install them to greater depths where closed-ended piles would not be able to be driven to.

An open-ended pile develops shaft resistances on the exterior as well as the interior of the pile, whereas a closed-ended pile has no internal friction. Soil entering the inside of a pile during installation mobilises a resistance between the soil and the pile that can induce arching of soil, causing a plug to form. Plugging of the pile occurs when the soil enters the inside of pile at a rate smaller than the pile driving, or when no soil enters at all. Multiple factors influence the capacity of open-ended steel pipe piles, such as pile diameter, installation depth, the soil's relative density, the soil's friction angle and installation method (Labenski et al., 2016). Piles can also plug during loading. A fully plugged pile can be approximated as a closed-ended pile. Depending on full or no plugging and in what stage (installation or loading), open-ended pipe piles behave similar to either displacement piles when it is fully plugged or as replacement or partial displacement piles when the pile is unplugged.

Open-ended piles obtain their base capacity from the resistance beneath the annulus and internal shaft friction, in contrast with closed-ended piles that obtain their base resistance from the pile tip. Figure 1.1 shows the mentioned pile types.

The design of open-ended piles means calculating a pile's dimensions - length, diameter and wall thickness - that predict a certain axial capacity for a given soil profile measured with a Cone Penetration Test (CPT).

In the Netherlands, the design of open-ended pile is often done based on the NEN 9997-1 (called the NEN) or with the CUR 2001-8 (called the CUR), both of which are empirical design methods based on a CPT's cone resistance q_c . However, these have fundamentally different underlying assumptions and approximations to shaft friction and end bearing. The NEN considers the plugging effect during loading, while the CUR 2001-8 assumes full plugging to take place after a certain installation depth. Other design methods also developed internationally, such as the IC-05 (England), UWA-05 (Australia) and NGI-05 (Norway). These (including the CUR 2001-8) were unified into a new CPT-based design method in JIP, 2020 (called the ISO) which is considered state of the art in design practice. This relatively new design method incorporates partial plugging in shaft and base resistance.

A key factor in predicting the axial capacity of an open-ended pile is the formation of a potential plug

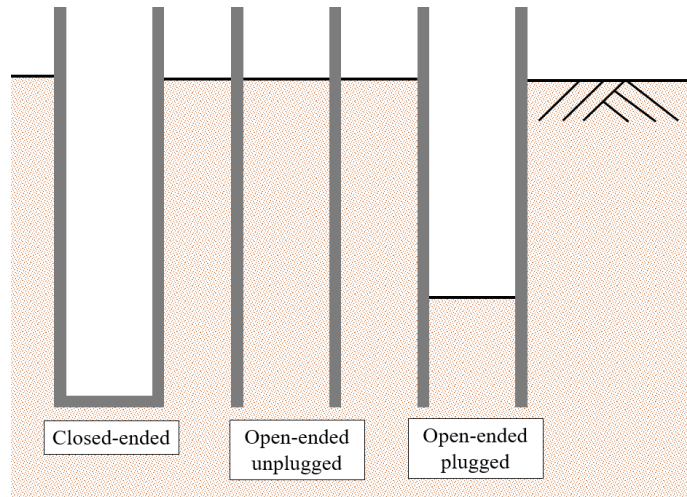


Figure 1.1: Possible closed- and open-ended pile states

(Yu and Yang, 2012). However, (accessible) plugging measurements are typically rare and test loads are not common in the Netherlands, which makes it difficult to approach the plugging problem with observational data. Observational data of field load tests on large-diameter piles ($D > 0.5 \text{ m}$) is generally rare, site-specific and difficult to couple to design codes. Therefore, the degree of soil displacement inside a pile often is not specifically accounted for in a design method.

A way to measure the effectiveness of a design method is dividing the measured capacity of a load test by a predicted capacity and see how close this value is to 1. This is called the performance of a method. Over-predicting axial capacity may lead to unwanted structural risks as more capacity is predicted than a pile can bear, while under-predicting leads potentially to either more piles to be installed or unnecessary resources used as dimensions are unnecessarily large. Both over- and under-predicting an open-ended pile's capacity can be costly and these risks may withhold contractors or engineering firms from using open-ended piles in their project.

1.2. Research topic

There is significant room for improvement considering Dutch standards on the design of open-ended piles. The current standards (NEN 9997-1 and CUR 2001-8) have both certain limitations.

The NEN is not an internationally recognized as a design method but a norm used by Rijkswaterstaat. The NEN is never included in literature or used in performance databases, but it is known that is generally a reductive method of calculating axial capacity. This is mainly because it uses constant α factors to relate q_c to shaft and base resistance, in combination with limiting values for both (*afsnuiten*).

The CUR 2001-8 dates back from 2001 and is based on a small database of piles (12 for compression). Research from, for example, J. A. Schneider et al., 2008 shows the CUR 2001-8 generally tends to over-predict axial capacities in compression and under-predicts piles in tension. It is often not researched in detail why methods under- or over-predict. It could be due to coincidence, large variability in predicting capacities, inherent limitations of the method's approach, etc. Apart from that, it is not researched how they behave with varying parameters or soil conditions and what their inherent weaknesses are.

The new international standard from JIP, 2020 (ISO) may be applicable to Dutch soil conditions and more accurately predict axial capacity of open-ended piles in relation to plugging. Performance calculations from JIP, 2020 shows the ISO to be better performing than the CUR, and likely better than the NEN, too .

It is unknown how these three design methods behave compared to each other on larger scales than individual performance calculations. There is no performance database on the NEN while it is important for Dutch standards. Evaluations on realistic shaft and base resistances for these methods are necessary to more accurately predict the axial capacity of open-ended steel pipe piles which is strongly

influenced by plugging. Varying important parameters can expose weaknesses they may not have been calibrated for. Also other installation effects are often not accounted for in a design methods. A critical evaluation on the three design methods - NEN, CUR and ISO - from a theoretical, programming and practical perspective can improve the design of open-ended piles in the Netherlands significantly.

Therefore, this thesis aims to answer the following research question: *How can the design of open-ended pipe piles in the Netherlands be optimised?* This concerns driven, circular steel open-ended pipe piles in siliceous sands loaded in compression and tension. In order to answer this, this question is supported by the following 5 sub-questions.

1. How is the capacity of pipe piles obtained and how do design methods approach axial capacity?
2. What are the characteristics for capacity, shaft resistance and base resistance of the discussed design methods?
3. What are the implications of these methods for varying parameters and soil conditions?
4. How effective are these methods and their characteristics based on real load tests?

1.3. Document structure

This thesis is divided into chapters that are aimed at covering the sub-questions.

- Chapter 2 contains a literature review on the axial capacity of open-ended piles and discusses the mechanisms of plugging and its effect on axial capacity, as well as certain installation effects and means to quantify plugging.
- Chapter 3 is the methodology in which the approach to the main research question and sub-questions 2-4 is discussed.
- Chapter 4 covers the results on the (numerical) analysis of the discussed design methods and evaluated their effectiveness and weaknesses via a constant q_c and real CPT's. Varying parameters and soil conditions are evaluated to look at general trends for each.
- Chapter 5 links the conclusions obtained in chapter 4 to a number of case studies and looks at how the future tests can improve current design of open-ended piles.
- Chapter 6 contains conclusions and recommendations.

2

Axial capacity of open-ended piles and the mechanisms of plugging

2.1. Axial capacity of open-ended piles

Open-ended pipe piles obtain their axial capacity Q (measured in force) from friction components along the shaft of the pile and base resistance from the pile tip. The capacity of an open-ended pile is defined as the load it can bear for a displacement of 10% the diameter. Common design methods (those discussed in this chapter) consider the capacity from outer shaft friction Q_{fr} and base capacity Q_b separately and sum them for the axial capacity with

$$Q = Q_b + Q_{fr} \quad (2.1)$$

where Q is the total axial capacity, Q_b is base capacity and Q_{fr} is shaft capacity.

In reality this summation is not fully correct, as there is also an interaction between the two around the pile tip, so they are not fully independent (CUR, 2001). The base capacity of an open-ended pile consists of two components, being the capacity of the annulus Q_{ann} and the minimum of the plug and capacity Q_{plug} of the internal shaft friction $Q_{fr,i}$, leading to

$$Q_b = Q_{ann} + \min(Q_{plug}, Q_{fr,i}) \quad (2.2)$$

where Q_b is the base capacity, Q_{ann} is annulus capacity, Q_{plug} is plug capacity and $Q_{fr,i}$ is inner shaft capacity.

When $Q_{plug} < Q_{fr,i}$, the pile is plugged, while when $Q_{fr,i} < Q_{plug}$, the pile is unplugged and cored. Q_{plug} is defined as the plug resistance q_{plug} it can bear over its inner area $A_{b,i}$, or

$$Q_{plug} = A_{b,i}q_{plug} = \frac{\pi D_i^2}{4}q_{plug} \quad (2.3)$$

where Q_{plug} is the plug capacity, D_i is the inner diameter of the pile and q_{plug} is plug resistance. $Q_{fr,i}$ is the force obtained from inner shaft friction over the shaft area of the plug, or

$$Q_{fr,i} = \pi D L_{plug} \tau_{f,i} \quad (2.4)$$

where $Q_{fr,i}$ is the inner shaft capacity, D_o is the outer diameter, L_{plug} the length of the plug and $\tau_{f,i}$ the internal shaft friction.

The difficulty in determining axial capacity with equation 2.2 lies in determining q_{plug} and/or $\tau_{f,i}$. Both which depend on many different factors and mechanisms that are complex to integrate into reliable design equations. Q_{ann} and Q_{plug} are often merged into Q_b with an empirical formula in a single term q_b that can be used for the axial capacity. As such, the A pile's inner shaft friction $\tau_{f,i}$ should be larger than the base resistance of the plug for plugging to occur, consequently causing no relative movement between the soil inside the pile and the pile itself. That explains the minimum term in equation 2.2, in essence discerning between a plugged and unplugged pile.

The API method, the first design method for piles, considers only two states of an open-ended pile: a fully plugged pile and a fully unplugged pile. The lowest of the two was judged as normative, but this is a reductive way of predicting capacity and it does not consider partially plugged cases.

When the shaft friction τ_f is known, it can be integrated over the length on its circumference, resulting in the shaft capacity of the pile with

$$Q_{fr} = \pi D_o \int_0^L \tau_f(z) dz \quad (2.5)$$

where Q_{fr} is the shaft capacity, D_o is the outer diameter and τ_f the external shaft friction.

Figure 2.1 shows the stress components that contribute to the capacity of an open-ended pile. Contrary to closed-ended piles, open-ended piles develop internal friction components and a potential plug resistance, whereas closed-ended piles only have external friction components and base resistance from the pile tip.

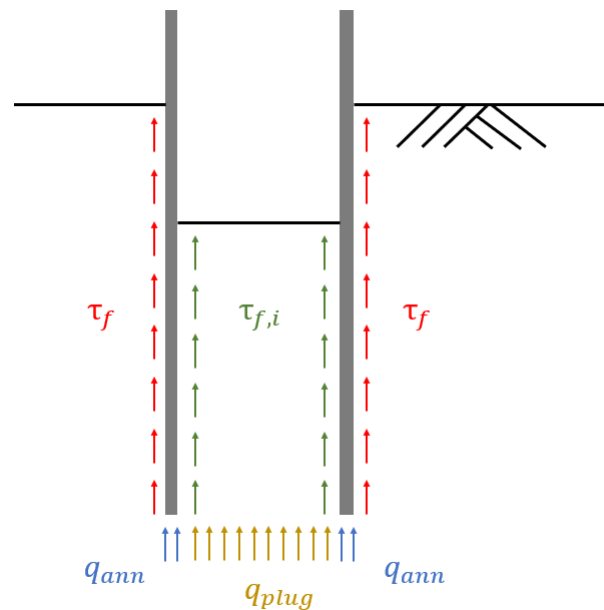


Figure 2.1: Stress components in a plugged open-ended pile loaded in compression

Theoretically, the axial capacity of a pile is obtained from the shaft frictions τ_f (outer) and $\tau_{f,i}$ (inner), and base resistances of the pile from the annulus q_{ann} and a potential plug q_{plug} (Labenski et al., 2016). Also here, design methods often merge terms, such as q_{plug} and q_{ann} into an empirical expression to q_b . Shaft friction is often empirically approached, because it depends on factors that a CPT is not always capable of determining such as the soil's shear resistance, pile roughness and the radial stress on the shaft (Labenski et al., 2016).

Also the plug in a pipe pile is dependent on multiple factors. Often noted throughout literature are pile dimensions, the interface friction angle, the relative density D_r and the installation method (e.g. Labenski et al., 2016). However, there are others such as inner pipe surface roughness, sand compressibility and also driving energy.

This research covers design methods that are meant for piles installed by driving. Open-ended piles can also be installed due to vibration. Vibration causes a reduction in cone resistance and leads to less axial capacity for a pile. This was shown in an article by van Dalen, 2013 in the magazine *Geotechniek*.

2.1.1. Shaft resistance expressions

The first design code on piles came from the American Petroleum Institute (API) in 1969 and assumed a shear resistance τ_f by means of an earth pressure approach with

$$\tau_f = K \sigma'_v \tan(\delta_f) = \beta \sigma'_v \leq \tau_{max} \quad (2.6)$$

where the shaft friction τ_f is related to the vertical effective stress σ'_v with the earth pressure coefficient K and the interface friction angle δ_f .

The difficulty in the API method lies in obtaining representative values for K and σ'_v that account for soil heterogeneity. This led to capacity predictions that varied a lot from measured capacities. A test from Imperial College London on a closed-ended steel pile showed a correlation between τ_f and q_c , initiating the development of empirically based design methods (D. Gavin, 2011).

The ICP design code (Imperial College Pile, formerly known as MTD) used pile tests to propose shaft friction τ_f for displacement piles to follow Mohr Coulomb's failure criterion with

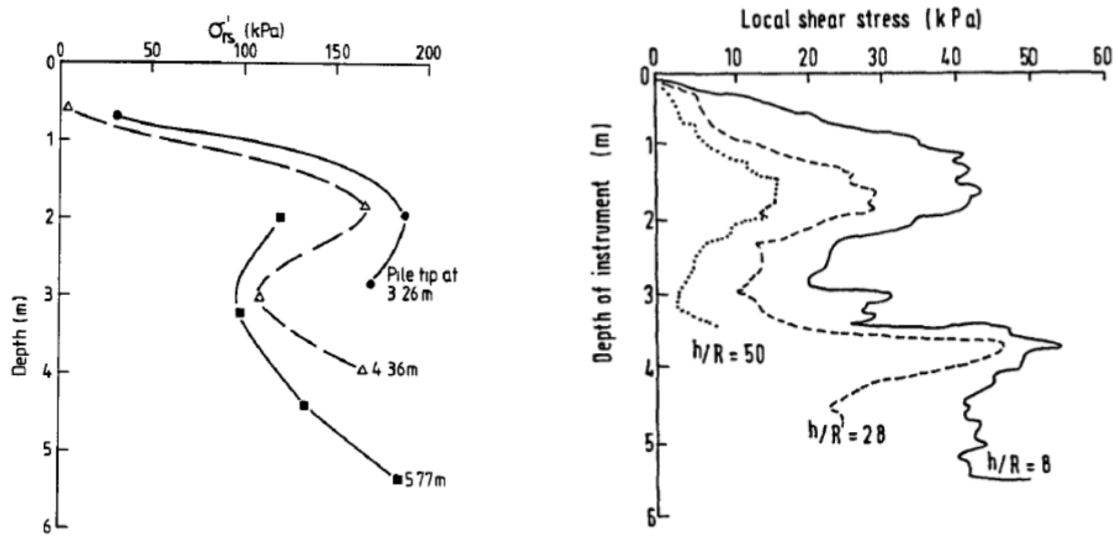
$$\tau_f = \sigma'_{rf} \tan \delta_f = (\sigma'_{rc} + \Delta\sigma'_{rd}) \tan \delta_f \quad (2.7)$$

where σ'_{rf} is the radial effective stress at failure, σ'_{rc} stationary radial effective stress (at equilibrium), $\Delta\sigma'_{rd}$ is a change in radial effective stress due to dilation or lateral expansion and δ_{cv} the constant volume friction angle.

The interface friction angle δ_f is the operational value, but this equals the constant volume friction angle for sands in case dilation/contraction has ceased (ICP, 2005). Equation 2.7 was first initiated for closed-ended piles, but pile tests at Dunkirk showed that it is also applicable to open-ended piles with different empirical formulations for σ'_{rc} and $\Delta\sigma'_{rd}$.

Approaching shear stress with equation 2.7 was an improvement as shaft friction measurements showed that it was not accurate to correlate it with the API method because it only takes into account the vertical effective stress. Multiple researches (e.g. F. Chow, 1997, Lehane et al., 1993) noted the dependency of relative pile tip depth h on the radial effective stress σ'_{rc} , and in particular the decrease of σ'_{rc} on a fixed depth point as the pile is driven further down. This reduction of stress for a fixed point as the pile is driven further down is often referred to as friction fatigue. It plays an important role in approximating the shaft resistance, an effect that is not accounted for in the API method. The mechanisms of friction fatigue are relatively unknown due to measurements being easily disturbed by residual loads, damaging of instruments during installation and discerning between internal and external shaft friction (White and Lehane, 2004). Figure 2.2a shows that the stress on $z = 2 \text{ m}$ reduces as the pile is driven down from 2.6 to 5.77 m.

Figure 2.2 shows the effect of friction fatigue from literature.



(a) Influence on local stationary stress σ'_{rc} on pile tip penetration from F. Chow, 1997 (b) h/R influence on τ_f for cone-ended pile by Lehane et al. (1993)

Figure 2.2: Research from F. Chow, 1997 and Lehane et al., 1993 showing friction fatigue

Figure 2.3 shows a possible stress path for shear stress following the Mohr Coulomb criterion as in equation 2.7. Currently used design methods for open-ended piles (such as the ISO method) still rely on this Mohr Coulomb criterion and empirically derive expressions for σ'_{rc} and $\Delta\sigma'_{rd}$ that fit open-ended pile behaviour. An initial reduction in radial effective stress σ'_r can be seen in Figure 2.3, which is due to rotation of stresses when a pile is driven (F. C. Chow and Jardine, 1996). This rotation is more notable with piles loaded in tension.

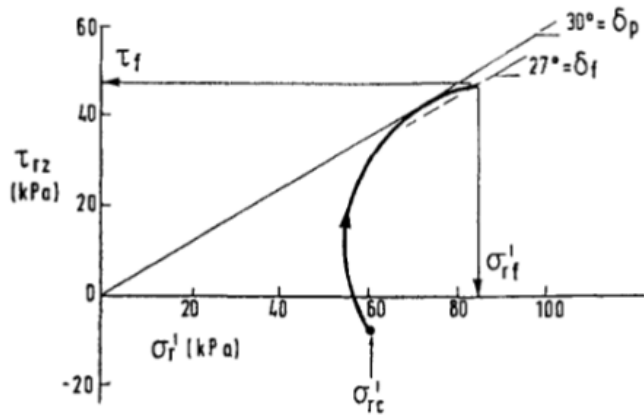


Figure 2.3: Components Mohr-Coulomb failure criterion (τ_f versus σ'_r) for a (closed-ended) pile in load test, by Lehane et al. (1993)

The UWA-05 method was another improvement in design methods and related the Final Filling Ratio FFR which is the mean Incremental Filling Ratio IFR over a couple of times the diameter. The UWA-05 showed to be a significant improvement compared to the CUR in terms of performance (J. A. Schneider et al., 2008). Its shaft friction formulation also follows the form of equation 2.7.

2.1.2. Base resistance and plugging

The base resistance of open-ended piles is obtained via internal shaft friction or plug resistance and resistance of the annulus. Internal skin friction develops during strong arching of the soil due to high effective angles of internal friction ϕ' and strong dilation, both of which are influenced by a high relative

density D_r (ICP, 2005). Generally as pile diameter increases, arching effects decrease. Arching of the soil is numerically evaluated by Li et al., 2019 and shows arching by means of the Discrete Element Method which made it able to observe principle stress rotation, seen in Fig. 2.4.

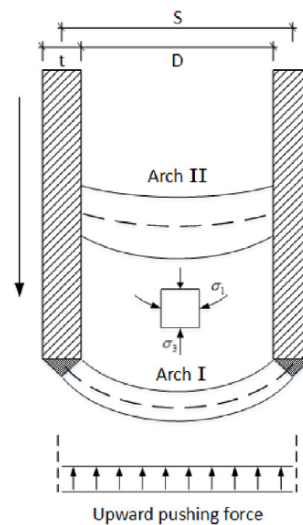


Figure 2.4: Arch developments from Li et al., 2019

In Fig. 2.4 there are two arches. Arch I develops first when soil enters the pile and dominates when D/t is small. Arch II also notably develops due to the shape of the pile tip. Arching cannot develop for large D as there are too many grains between the walls to transfer the load to the other side via the arch and the load is 'lost', withholding the build up of inner shaft friction.

When a pile is fully plugged, it has a base capacity lower than that of a closed-ended pile because of the local settlement needed to develop the arch and the soil beneath the soil column which has not been given the same stressing and stiffening during driving (F. C. Chow and Jardine, 1996). The underlying reason of these are that the pile behaves as a closed-ended pile at a certain point during its driving, and not from the start of driving.

Gavin and Lehane (2001) did a study on the base capacity of jacked pipe piles and found the basal response of the plugged piles were stiffer than that of unplugged ones. This was shown by measuring the Incremental Filling Ratio IFR for piles during jacking and during loading.

The IFR is a good way of measuring plugging during installation (chapter 2.2) and is defined by the change in length of the plug dL_{plug} divided by change of embedded length of the pile (pile tip level) during driving $dPTL$, or $IFR = dL_{plug}/dPTL$. If the Incremental Filling Ratio IFR equals 1, the soil column inside the pile does not move downwards with the pile, and no plug appears (Labenski et al., 2016). As the IFR decreases and the becomes plugged, more soil is pushed around the pile, thereby increasing radial stress, and q_{plug} increases.

Gavin and Lehane argued that q_{plug} to be directly related to q_c and IFR . Fig. 2.5a shows a relationship of $q_{plug} \approx q_c$ for fully plugged piles with $IFR = 0$, which decreases linearly by approximation to unplugged state with $IFR = 1$. From load-settlement curves, the plug stress at failure appeared to be directly proportional to overall plug stiffness. These two conclusions combined lead to base stiffness related to q_c and IFR in a similar way as q_{plug} . As such, the base stiffness of a pile with $IFR < 0.8$ (i.e. the left hand grouping of load test measurements in Fig. 2.5a) is almost completely defined by the stiffness of the sand below the pile as $q_{plug} \approx q_c$.

Almost all piles plugged during the static load test. When a pile is fully plugged ($IFR = 0$), it behaves as a closed-ended pile since plug resistance is roughly equal to cone resistance and q_{ann} approximately equal to q_c and independent of the IFR , see also Figures 2.5a and 2.5b.

Also it can be seen that an IFR of 1 means low stresses and consequently lower stiffness. Fully coring piles during jacking ($IFR = 1$) have a plug capacity of roughly 10 – 20 %

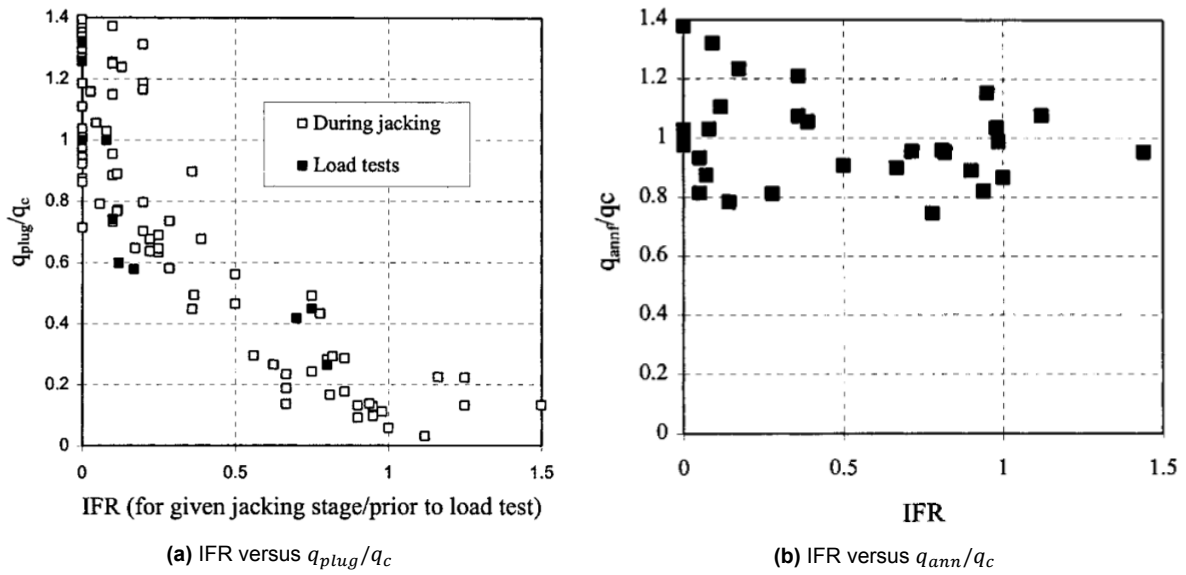


Figure 2.5: Influence IFR on q_{plug} and q_{ann} , from Lehane and Gavin, 2001

In full-scale load tests, strain gauges are often used to separate base and shaft resistance. A double pile wall system can be used to measure and separate resistance components of open-ended piles. Figure 2.6 shows how Q_b from can be separated into Q_{ann} and Q_{plug} under the assumption that the resistance (load/distance) between lowest gauge and pile base is the same as that of the second lowest gauge and lowest gauge (i.e. the dotted line).

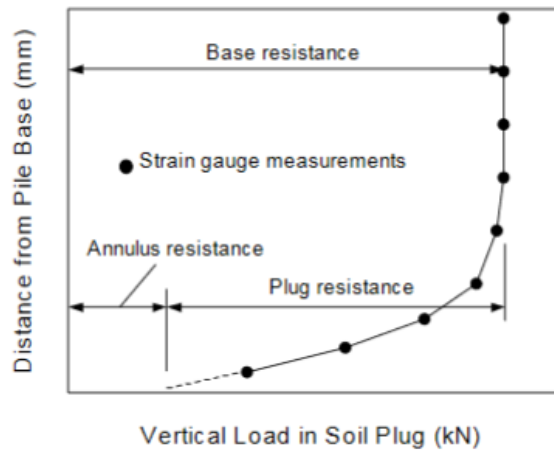


Figure 2.6: Base resistance components from Kim et al., 2002

2.1.3. Tension

Piles loaded in tension do not have a base resistance as the loading is in the opposite direction. The shaft resistance for piles loaded in tension is typically reduced by a factor on shaft resistance in compression due to rotation in principle stress and contraction of the pile causing a reduction in radial effective stress. Figure 2.7 from the IC-05 method illustrates these.

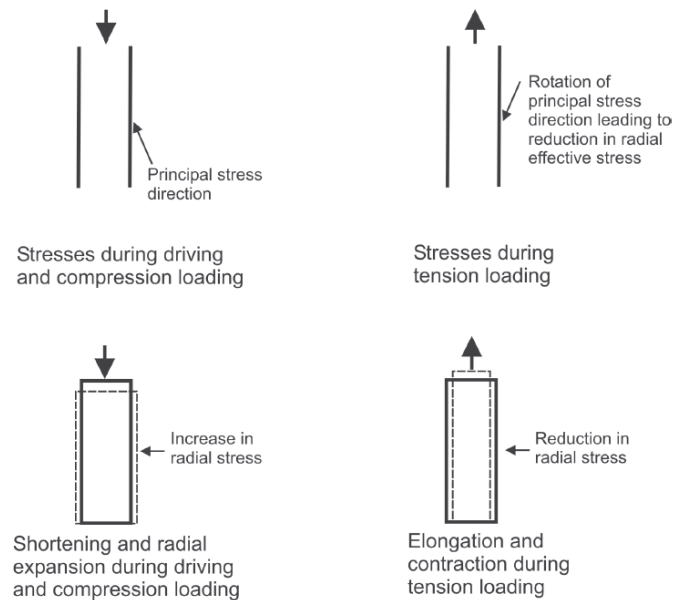


Figure 2.7: Mechanisms causing reduction in tensile loading compared to compressive loading from ICP, 2005

The principal stress direction induced during driving of the pile is reversed when the loading direction is changed to tension, but this loses some of the mobilized radial effective stress when the pile is installed during driving (compression). Also the pile contracts and elongates during tension as loading is in opposite direction as driving. Typically a reduction factor is put on the shaft friction prediction in compression to translate it to tension because of these two mechanisms.

2.2. Plugging during installation and loading

There are two ways a pile can plug: during driving (installation) and during static loading. Plugging may also influence dynamic behaviour, but that is not covered in this research. Both plugging mechanisms are shortly discussed.

2.2.1. Installation

During pile installation, the core in the pile might mobilize enough inner friction between soil and pile to block further soil from entering the pile and will be plugged. The inner friction primarily mobilises the plug, most notably at the bottom of the plug due to the strongest arching influence and a large coefficient of lateral earth pressure K_0 (Yu and Yang, 2012). Soil plugging during installation can be measured by means of the plug length ratio (PLR) and the incremental filling ratio (IFR). The PLR is defined as the length of the plug L_{plug} divided by penetration depth noted here as pile tip level (PTL), whereas the IFR describes the incremental process between L_{plug} and the PTL (Jeong et al., 2015).

$$IFR = \frac{dL_{plug}}{dPTL} \cdot 100(\%) \quad (2.8)$$

$$PLR = \frac{L_{plug}}{PTL} \quad (2.9)$$

where IFR is the Incremental Filling Ratio, L_{plug} is the length of the plug, PLR the Plug Length Ratio and PTL (pile tip level) the embedded length of pile.

If $PLR = 0$, $L_{plug} = 0$ and there is not soil inside the pile, and it can be compared to a closed-ended pile. If $PLR = 1$, the pile is fully filled with soil at the end of installation (i.e. fully coring) and no plug appeared.

Figure 2.8 show the terms for equations 2.8 and 2.9 for two moments during installation. Here, $dL_{plug} = L_{plug1} - L_{plug2}$ and $dPTL = PTL_1 - PTL_2$.

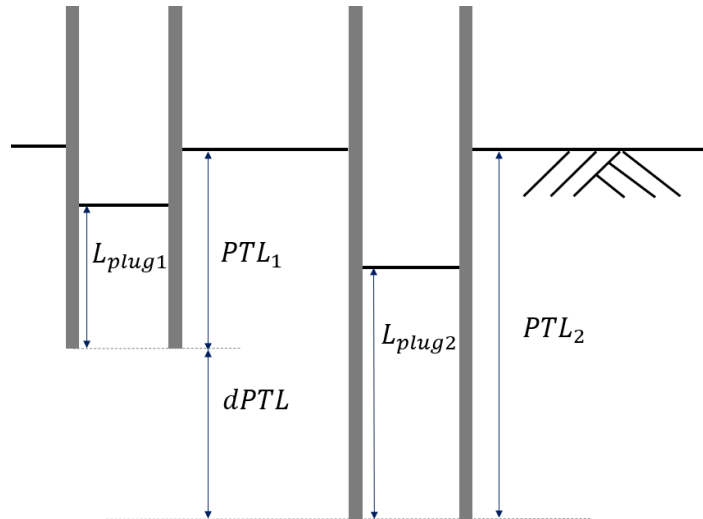


Figure 2.8: Components for IFR and PLR, based on Paik and Salgado, 2003

A fully plugged pile has $IFR = 0$ and can be approximated as a closed-ended pile as no soil has entered the pile while, oppositely, a fully cored (i.e. unplugged) pile has $IFR = 1$. The IFR can be greater than 1 if the rate in which the soil enters the pile is greater than the rate in which the pile is driven down. From its incremental definition, full plugging during installation via IFR implies no relative movement between inner soil column and pile. However, some relative movement between pile and plug may still physically occur if $IFR = 0$ near the pile toe, as a plug is often (slightly) compressible. A common way to measure IFR is given in Fig. 2.9.

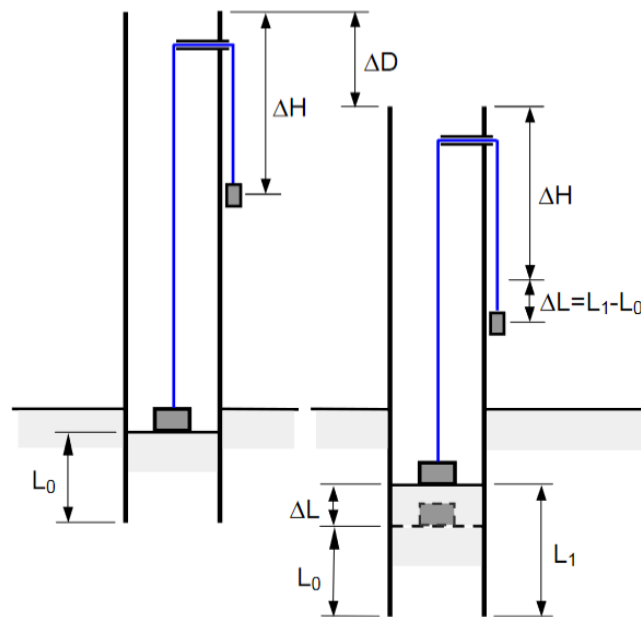


Figure 2.9: Measuring *IFR*, from K. Paik et al., 2003

Figure 2.9 shows that measuring the *IFR* requires a rather complex system that has to be installed and monitored during driving. Plugging measurements are often rare and, in practice, often only the *PLR* is known partly for this reason. Lehane and Gavin, 2001 note that though there is a relationship between q_{plug} and *PLR*, the relationship between q_{plug} and *IFR* is more coherent. The *IFR* might a better way to incorporate plugging in design of an open-ended pile but incorporating the *PLR* or *FFR* might be better achievable for practical concerns.

Paik and Salgado, 2003 have obtained a correlation between the *IFR* and *PLR* with the use of small scale piles in a calibration chamber. Their founded relationship was

$$IFR = 109 \cdot PLR - 22 \quad (2.10)$$

where *IFR* is the Incremental Filling Ratio and *PLR* the Plug Length Ratio.

If the *IFR* is not measured in the field, the authors of Paik and Salgado, 2003 suggest to use equation 2.10 to obtain the *IFR* from the *PLR*. However, the authors of Gudavalli, 2014 note caution on using equation 2.10 as the diameter to particle scale is not the same for small scale piles as for field piles.

Ko and Jeong, 2015 note that, in general, the *IFR* decreases as penetration depth increases and decreasing relative density.

The plugging effect is not always beneficial for a pile during installation as it may impede the pile to be driven further down (Iskander, 2010). A soil plug removal technique will have to be applied, such as jetting out the plug.

2.2.2. Loading

If a pile is plugged during static loading, it means that the plug does not move with respect to the pile. This is for the whole plug by approximation, as the bottom of the plug can slightly move due to compression of the plug. In general, piles that are plugged during static loading have not plugged during driving (Iskander, 2010). If piles plug during static loading, their base resistance is often not equal to that of closed-ended piles due to compressibility of the plug and/or soil below the plug (Iskander, 2010).

Han et al., 2020 note that a pile will always plug under static loading if the plug length is a couple of times the diameter. In other words, regardless of the diameter, static loading will not be able to overcome

the plug capacity (provided the plug length is a couple of time the diameter). Large diameter piles are often driven in unplugged mode because the inertial forces of the plug and plug base resistance are larger than the internal frictional forces (Han et al., 2020).

In Fig. 2.5a it was already discussed that the plug capacity of plugged piles during loading is roughly similar to q_c value of the base. Unplugged piles during jacking have roughly 10 – 20 % plug capacity of the q_c at the base. See also chapter 2.1.2.

2.3. Diameter and relative density in relation to plugging

Plugging is dependent on many factors. The focus on this research is on q_c -dependent design methods in relation to pile dimensions, that is why pile diameter and relative density (often correlated with q_c) are discussed. Plugging can also be evaluated in relation to hammer characteristics, interface friction angle, sand compressibility, etc.

2.3.1. Pile diameter

Figures 2.10a and 2.10b show results from Jeong et al., 2015 in which three different piles were installed in the same soil with increasing diameter ($D_{TP-1} = 0.508m$, $D_{TP-2} = 0.711m$, $D_{TP-3} = 0.914m$). This figure clearly shows an increasing IFR when the diameter increases, thereby showing that plugging increases when the pile diameter increases, and that larger piles typically tend to plug in a partially plugged manner.

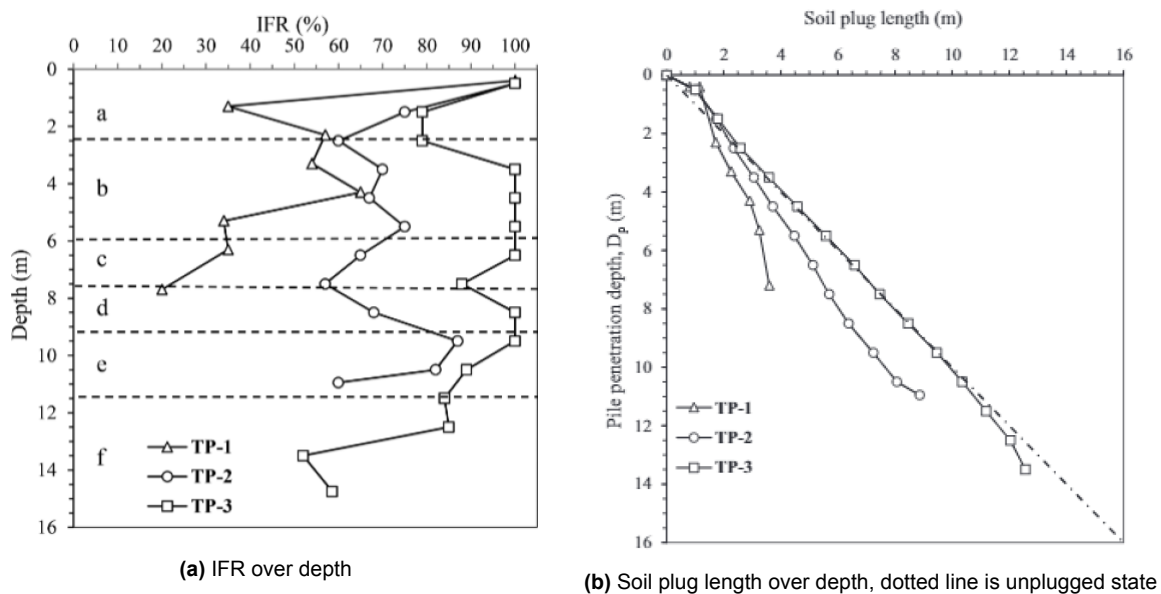


Figure 2.10: IFR and PLR results for three piles in the same soil, from Jeong et al., 2015

This is also supported by Han et al., 2020 who note that inertial forces of the plug and base resistance are larger than the internal shaft friction. When the diameter is increased, the area increases that factor squared and more mass of the plug is in the pile which causes a larger inertia to overcome during driving.

When the diameter is increased, arching of the soil is at a certain point not possible anymore a the pile is driven in unplugged mode.

A study done on soil plugging by Gudavalli, 2014 evaluated a total of 1355 piles with varying diameters (0.406 – 0.914 m) with pile tip levels from 10 – 30 m. The site consisted of dense silty sands (60% sand, 33% fines, 7% gravel) and q_c values were on average 25 MPa until 6 m depth and 42 MPa after that

(Gudavalli, 2014). This is a valuable study as it collects plugging data from a large number of piles installed in the field instead of a laboratory.

Their research showed that the soil plug length can be correlated well to the diameter. Fitted lines for soil plug length over depth did not show a lot of scatter. As the diameter increased, *PLR* values decreased and for the larger diameters the piles were driven in a coring mode. The *PLR* increased from 0.76 to 0.91 for piles that increased for diameter from 0.40 m to 0.91 m.

The proposed equation for the *PLR* based on inner diameter is

$$PLR = (D_i/1.4)^{0.19} \quad (2.11)$$

where *PLR* is the Plug Length Ratio and D_i is the inner diameter.

Even though the findings from Gudavalli, 2014 are very useful since they are based on a large database, they may not directly apply to Dutch soil conditions. The installment of EURIPIDES test 1 a-c (discussed in chapter 5.1) included detailed *PLR* measurements. The predicted *PLR* by equation 2.11 would be 0.875 and standard deviation for the mean *PLR* in this diameter range is 0.051. However, the average measured *PLR*'s per test a-c are 0.977, 1.018 and 1.005 respectively. A notable plug in the EURIPIDES tests was not formed during installation. This is probably due to the different site conditions, as the EURIPIDES pile was first driven through a thick and soft Holocene layer for the first 28 meters.

Figure 2.11 shows the relationship of soil plug lengths on embedded lengths for a set of pile with $D = 0.5$ m. The relatively small spread of measurements from the fitted line suggests a strong correlation between *PLR* and diameter.

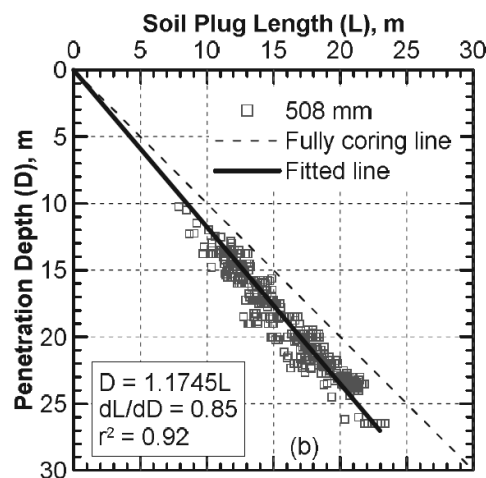


Figure 2.11: Results from Gudavalli, 2014 for piles with $D = 0.5$ m

2.3.2. Relative density

Based on the relative density, the ICP proposed two plugging criteria for the development of a rigid plug during static loading based on the inner diameter with

$$D_i < 0.02(D_r - 30) \quad (2.12)$$

$$D_i/d_{cPT} < 0.083q_c/p_a \quad (2.13)$$

where inner diameter D_i is measured in meters, relative density D_r as a percentage and p_a is the atmospheric reference pressure (100 kPa).

These plugging criterion propose a minimum internal diameter for arching to occur based on D_r .

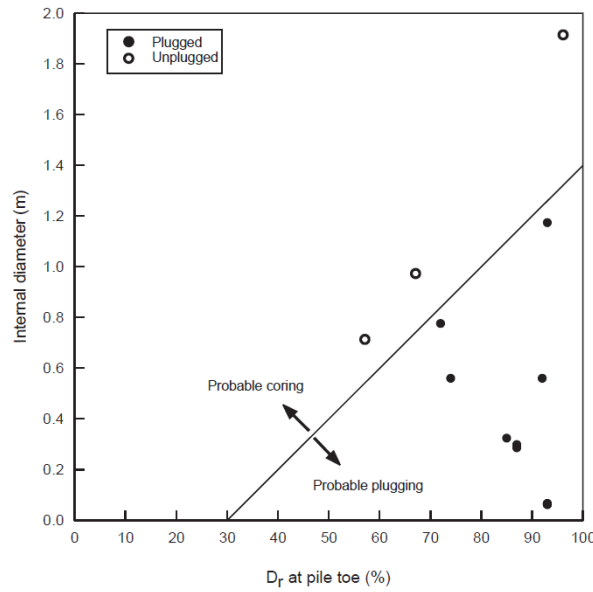


Figure 2.12: Field evidence for the rigid plugging criterion (equations 2.12 and 2.13), from ICP, 2005

Figure 2.12 contains quite limited data and only distinguishes between plugged/unplugged and not the partially plugged condition. Also the origin of data on Fig. 2.12 is untraceable. Still, relating plugging to relative density (from q_c) might perhaps be a better or more reliable way to predict plugging.

There are multiple correlations between q_c and D_r . Assuming normally consolidated sand, one way to estimate relative density is with an empirical formula from Jamiolkowski et al., 2003 with

$$D_r = 0.35 \ln(q_{c1N}/20) \quad (2.14)$$

where D_r is the relative density and q_{c1N} is the normalised cone resistance, given by

$$q_{c1N} = (q_c/p_a)(\sigma'_{v0}/p_a)^{0.5} \quad (2.15)$$

where q_{c1N} is the normalised cone resistance, q_c is the cone resistance, σ'_{v0} is the vertical effective stress and p_a reference atmospheric pressure.

2.4. Installation effects

The axial capacity of open-ended piles is also of influence from certain installation effects. Two of them, residual stresses and pile ageing, are discussed that are also discussed in the case studies of chapter 5.

2.4.1. Residual stresses

Residual loads may reside in the pile, most notably at the base, after installation. A residual base stress $q_{b,res}$ is caused by upward decompression of the soil after hammering and (elastic) unloading of the pile. and equates with negative skin friction $\tau_{f,neg}$ on the shaft. A schematic representation of this mechanism is given by F. Chow, 1997 in Figure 2.13.

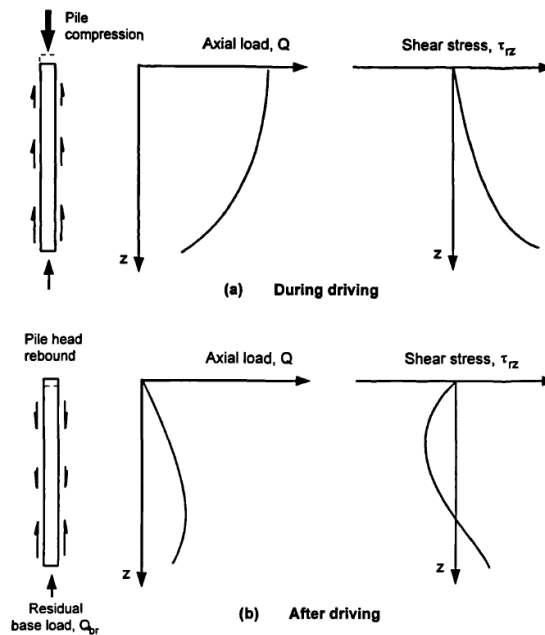


Figure 2.13: Schematic representation of the creation of residual stress from F. Chow, 1997

The load during driving is concentrated at the top of the pile, causing a concentration of shear stress (in opposite direction) near the pile tip. During unloading when the hammer is not in touch with the pile, the pile rebounds and creates negative shear stress at the top of the pile and a concentration of load near the pile tip.

Correcting for these residual loads may lead to a reduction in unit shaft resistance, as $\tau_{f,neg}$ is directed downwards to resist the upward movement from these stresses (Han et al., 2020). Figure 2.14a shows this effect. Figure 2.14b shows the effect of residual load correction on axial capacity components.

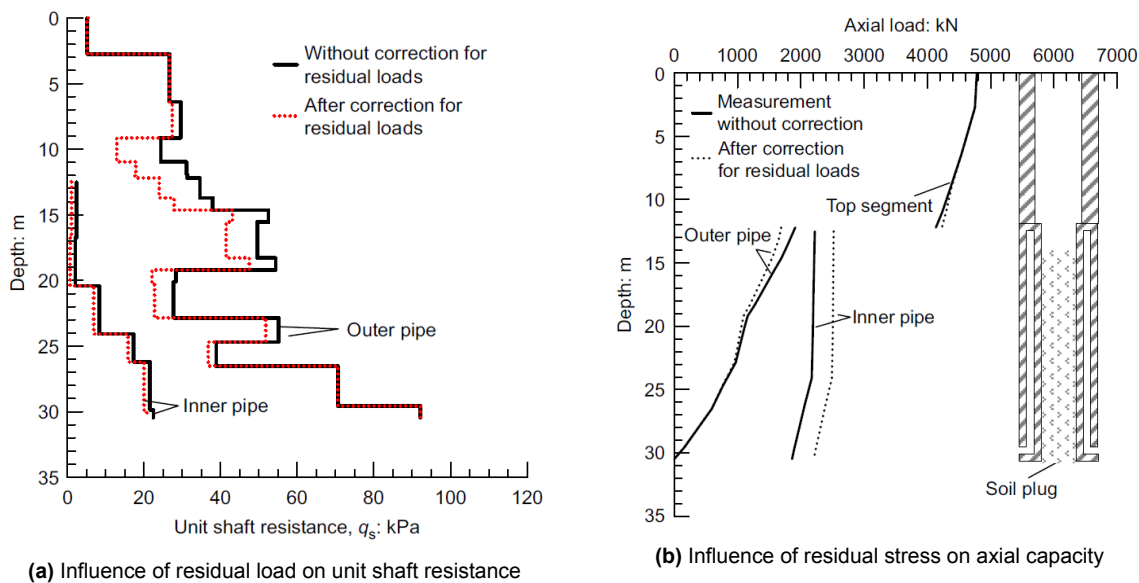


Figure 2.14: Influence of residual stress corrections loads in gravelly sand load test, from Han et al., 2020

The case study chapter in 5.3 covers more the methods' response in relation to residual stresses from the test by Han et al., 2020.

2.4.2. Pile ageing

Pile ageing is a phenomena related to an increase in shaft capacity over time. It does not significantly influence base resistance. Ageing is a noteworthy phenomenon, as case studies indicate the shaft capacity can increase over three times after 100 days of driving (K. Gavin and Igoe, 2021). This is especially important for offshore piles, that have to withstand large tensile forces. The many uncertainties and varying case studies make it difficult to incorporate this in pile design methods. F. Chow, 1997 notes three potential reasons for pile ageing, being corrosion, stress relaxation and increased constrained dilation.

This effect has hardly been studied in the Netherlands, except for the EURIPIDES tests. The EURIPIDES I a-c tests were later re-tested showed an increase between 70 – 90 % in capacity. EURIPIDES test II did not reach failure, and load-displacement curves showed little plastic straining, meaning that the 'new' (time-dependent) capacity significantly increased (ICP, 2005).

The Blessington case study in chapter 5.6.2 shows the effect of pile ageing for pile tests from K. G. Gavin et al., 2013.

2.5. Problems in modelling plugging

There are a number of reasons why plugging has been difficult to model or adopt specifically in design methods and why the plugging effect contains still large amount of uncertainties.

- Not all parameters that affect plugging can be derived from a CPT. Relative density is one of these (though reliable indirect approximations exist), as well as a representative K_0 value to approximate stress distribution inside the pipe. Also, it's not common for every country to have a CPT-based design approach.
- The Dutch shallow subsurface, especially in the West, is built up of a thick layer of soft Holocene sediments under which stiffer Pleistocene sand layers lie which makes it uncertain if and when a potential plug may develop.
- (Accessible) data of recorded plug lengths in practice is rare and often site specific. Offshore installation is often too expensive for including measurement apparatus in piles. Design methods are often based on similar (rather small) databases of relatively old tests.

- The plugging effect can hardly be modeled with Finite Elements because plugging includes large displacements. Open-ended piles can be modelled in Plaxis or Finite Elements, but the plugging effect is limited. Finite Elements are not able to incorporate the large soil deformations that take place during plugging. An option would be to explore plugging with the Material Point Method which is designed for failure with large deformations. However, this method is complex, still in rather experimental stages and computationally expensive.

2.6. Empirical design methods

It is common practice in the Netherlands to calculate axial capacity in conformance with either the CUR 2001-8 report or NEN 9997-1 for open-ended steel pipe piles installed by impact driving. Other international models have also appeared over the years, such as the UWA-05 and NGI-05 methods. In 2020, the Joint-Industry Project (JIP) unified these models (also including the CUR 2001-8) into a new, unaffiliated CPT-based design method, referred to in this report as the ISO. These three methods - shortened to NEN, CUR and ISO - will be discussed and evaluated in this report on their workings and the axial capacity they predict for pipe piles.

The discussed design methods use a CPT's cone resistance q_c as primary input to calculate shaft friction τ_f and base resistance q_b . Each method has its own way of determining shaft friction and base resistance, leading to different capacities and different contributions of shaft capacity and base capacity.

Installation effects, such as plugging, in design codes are often not described separately, but are calibrated on an analytical framework with empirical factors (Iskander, 2010). An example for Dutch design practices are the pile class factors α_p used for $q_{b,nen}$ and α_s used for $\tau_{f,nen}$. In the CUR, this can be seen by the equation for q_b that includes a potential plug capacity in its base resistance.

A CPT's sleeve friction has also been attempted to link to shaft friction, but q_c -based methods are more widely used as sleeve friction generally has a higher variability (J. A. Schneider et al., 2008). More detailed design methods relating q_c to τ_f and q_b with different parameters are based on a database of static load tests, though they are small and consist of on-land tests with small diameters.

The most important parameters, equations and assumptions per method are discussed below. The complete set of equations can be found in Appendix A.

2.6.1. NEN 9997-1

The Dutch method in the NEN is called an α method, directly relating shaft friction τ_f to cone resistance q_c with different but constant α -factors. This is a rather reductive method to obtain the axial capacity based on a linear relationship between q_c and shaft friction and base resistance with a certain limiting value.

To determine base capacity Q_b , the Dutch method suggests

$$Q_b = A_b \cdot q_b, \quad q_{b,max} \leq 15 \text{ MPa} \quad (2.16)$$

where Q_b is the base capacity, A_b is the area of the pile and $q_{b,nen}$ the base resistance determined by the method of Koppejan with a maximum of 15 MPa.

The q_c averaging technique of Koppejan suggests a base resistance q_b based on the zone of influence from the pile during installation and assuming it will fail along the weakest zones. It does so by averaging q_c from 3 trajectories that follow a minimum path rule, meaning that over a certain trajectory x times the diameter above or below the pile tip, the minimum q_c value is normative for averaging to q_b .

The Dutch method prescribes the relation between cone resistance q_c and shaft friction τ_f with

$$\tau_f = \alpha_s \cdot q_s \leq 12 \vee 15 \text{ MPa} \quad (2.17)$$

where τ_f is the shaft friction, α_s is a constant reduction factor based on pile class and type and q_s the q_c profile where limiting values are applied.

The pile class factors in τ_f and q_b incorporate installation effects and soil behaviour caused by the pile driving. For open-ended steel pipe piles, $\alpha_s = 0.006$. Such a constant α_s implies no friction fatigue.

Typically in Dutch design, τ_f is limited to either 12 or 15 *MPa* depending on the layer thickness.

The NEN is a rather reductive method, meaning that a change in α_s covers the change from a driven closed-ended concrete pile of similar dimensions to that of an open-ended steel pipe pile, thereby neglecting differences in both types of piles after installation such as plugging. On top of that, it remains unclear on what data the value of α_s are based and how trustworthy it is. Though there is now some ratification for α_p , there is none for α_s or α_t and it remains unclear how reliable these values are.

For an open-ended pile, base resistance apart from the annulus only plays a role when a plug has developed, but the NEN does not propose a way to obtain inner shaft friction and thus it remains unclear if base capacity has any role at all or if capacity is a summation of outer shaft capacity and inner shaft capacity. Q_{nen} can be determined with

$$Q_{nen} = Q_{fr} + \min(Q_b, Q_{fr,i} + Q_{ann}) \quad (2.18)$$

where the capacity Q_{nen} is the summation of outer shaft capacity Q_{fr} and the minimum of base capacity Q_b and inner frictional capacity $Q_{fr,i}$ plus annulus capacity Q_{ann} .

This relationship, in combination with the α -factors determine plugging behaviour predicted by the NEN. The NEN does not state an explicit approach for $Q_{fr,i}$, and as such it is assumed that the same approach applies for $Q_{fr,i}$ as for Q_{fr} but with a smaller inner diameter D_i .

2.6.2. CUR 2001-8

The CUR Report 2001-8 was established due to lack of a reliable method for base resistance in the former NEN 6743 (i.e. current NEN 9997-1) (CUR, 2001). The method in the CUR 2001-8 report is internationally also known as the Fugro-05 method. It used data from instrumented pile tests to better fit the equations proposed by F. Chow, 1997 and the first IC equations, and used a 'best fit' to propose a new, CPT-based design method, especially for offshore practices. No limiting values are applied.

A significant limitation of the CUR is that it only applies to a set of specific ground and pile conditions, most important of them being a pile's t/D ratio needing to be greater than 1/60. This condition can be met for off-shore piles (for which the CUR was also partially intended), but is almost never met for on-shore piles. In practise, the t/D ratio is often larger than 1/90. Also, the pile length has to be between 5 – 80 in L/D and has to be installed until (full) plugging occurs, which, according to the CUR, happens after pile installation of $8D$ of cumulative sand thickness. This is a very optimistic assumption, as to when plugging occurs is still largely unknown and cannot be compromised to an installation depth. The CUR only considers fully plugged or fully cored conditions.

According to the CUR, the base capacity of an open-ended steel pipe pile can be calculated with

$$Q_b = A_b \cdot 8.5 p_a (q_{c,avg}/p_a)^{0.5} (DR)^{0.25} \quad (2.19)$$

where Q_b is the base capacity, A_b the area of the base, $q_{c,avg}$ is the average q_c on distances $1.5D$ above and below the pile tip level, DR the displacement ratio and p_a the reference atmospheric pressure.

The CUR's equation for q_b originates from three linear elastic, perfectly plastic springs. With a simplified interpretation of the spring analogy and due to the fact that only 10% of the pile tip depth is considered for base resistance, equation for q_b is dependent on σ'_v , D_0 and D_i , with the 'most practical format':

$$q_b/p_a = \alpha (q_{c,avg}/p_a) (\sigma'_v/p_a)^c (D_0)^d (DR)^e \quad (2.20)$$

The CUR does not give an explanation why a power law in this form is deemed fitting, neither are any alternatives considered. In the analysis, it seemed that fitting this formula gave no effect on diameter and vertical effective stress, and it was simplified to equation 2.19.

A pile's inner friction cannot exceed the maximal base capacity minus the wall capacity (CUR, 2001). In other words, the base capacity Q_b according to eq. 2.19 should be smaller than the inner shaft capacity

and base capacity of the wall. Equation 2.21 assumes the pile is plugged, but if a pile is not (fully) plugged, the base capacity can be calculated with

$$Q_{b,unplugged} = Q_{b,wall} + Q_{plug} \quad (2.21)$$

In practice, the lowest result of equations 2.19 and 2.21 is leading.

For the shaft friction, the CUR proposes two separate empirical formulas dependent on a distance from the pile tip of $h/R^* = 4$. The CUR disregards an increase in shaft friction due to dilation, or $\Delta\sigma'_{rd}$ and implies rather strong friction fatigue component $(h/R^*)^{-0.90}$. First suggested by Jardine and Chow, 1996, a $(h/R^*)^{-r}$ term accounts for friction fatigue, and in which $r = 0.38$ gave the best fit for their database which the CUR increased to 0.90 (White and Lehane, 2004).

Two other terms in the CUR's set up are worth explaining, R^* and DR . The effective radius R^* is the radius a closed-ended pile would have with the same cross-sectional area as an open-ended pile, and such an approximation from open-ended to closed-ended relies on a fully plugged pile. The displacement ratio DR is a parameter indicating the closedness of a pile, ranging from 0 (i.e. pile thickness is 0, or infinitely thin) to 1 (i.e. pile is closed-ended, or thickness is equal to radius).

$$DR = 1 - (D_i/D_o)^2 \quad (2.22)$$

where DR is the Displacement Ratio and D_i and D_o the inner and outer diameters.

The CUR provides an indication for base capacity, which is a property regarding the ultimate limit state (USL). However, this cannot be linked to a load-displacement relationship, which is a property regarding the serviceability limit state (SLS). The CUR advises to consult the NEN where empirical load-displacement curves set up for closed-ended piles should give an indication. These in turn does not take the compressibility of the plug into account.

2.6.3. Unified API/ISO

The unified API/ISO method combined four CPT-based design methods (being Fugro-05 described in the CUR 2001-8, ICP-05, NGI-05 and UWA-05) for the axial capacity of piles (open- and closed-ended) for piles open- and closed-ended. Most notable of this method is that it's the only taking the partially plugged condition into account for both shaft and base resistances, whereas the NEN and CUR neglect this. The method does not give any limitations on pile dimensions to which it applies, in contrast to the CUR. The ISO is quite similar in set-up to the UWA-05. In the report's abstract, it states that the method is relatively insensitive for an increase of diameter compared to other methods.

The method determines shaft friction τ_f originating from Coulomb's law with

$$\tau_f = \sigma'_{rf} \tan \delta_f = (f_t/f_c)(\sigma'_{rc} + \Delta\sigma'_{rd}) \tan \delta_f \quad (2.23)$$

where (f_t/f_c) is a coefficient equal to 1 for compression and 0.75 for tension, σ'_{rf} is the radial effective stress at peak friction consisting of the (stationary) radial effective stress σ'_{rc} and the increase in radial effective stress during loading $\Delta\sigma'_{rd}$, and where δ_f is the interface friction angle (JIP, 2020). Empirical relations are set up for σ'_{rc} and $\Delta\sigma'_{rd}$.

The base resistance is determined by relating $q_{b0.1}/q_p$ to effective area ratio A_{re} with a linear best fit formula. The spread on this distribution is reasonably well and based on a reasonable database which includes the CUR's database, except for the micaceous sands at Jamuna.

The method uses the effective area ratio A_{re} affecting shaft friction and accounting for soil displacement by the pile and the soil if the pile is (partially) plugged. An analogous term can be found in the CUR 2001-8 with the displacement ratio DR , accounting for the 'openness' of the pile. The adoption of A_{re} in the design method is important as soil displacement is a significant factor on a pile's axial capacity (J. Schneider et al., 2005). The difference between the CUR and ISO is that the A_{re} incorporates an

empirically derived PLR relationship, shown in Figure 2.15 and equation 2.24. This means that the Plug Length Ratio is already predicted before installation. The scatter between observed values and equation 2.24 can be large, due to the fact that there are many more factors of influence between PLR and D_i .

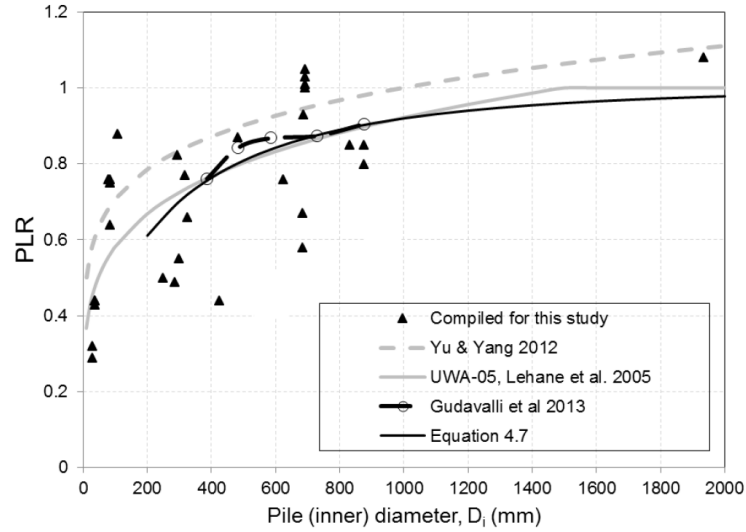


Figure 2.15: PLR versus D_i , from JIP, 2020. Equation 4.7 in legend is equation 2.24 below.

The proposed equation to predict the Plug Length Ratio PLR before installation is

$$PLR = L_{plug}/L \approx \tanh \left[0.3 \left(\frac{D_i}{d_{CPT}} \right)^{0.5} \right] \quad (2.24)$$

where PLR is the Plug Length Ratio, L_{plug} the length of the plug, L the length of the pile, D_i the inner diameter and d_{CPT} the diameter of the CPT cone ($d_{CPT} = 0.0356 \text{ m}$).

3

Methodology

In design methods or database assessments, often there is a performance database where calculated total capacities $Q_{t,c}$ are divided by measured total capacities $Q_{t,m}$. The databases of these performance calculations per method are relatively small, an example is the CUR which is based on 12 tests from 5 different sites. Some methods perform better than others, but underlying reasons why are often not given. Also their behaviour for varying soil conditions in combination with different pile dimensions is not analysed, and this causes large uncertainties to the reliability and applicability of design methods.

Therefore, this research is focused on calculating capacities for each measurement point of a CPT, instead of single capacity calculations. This implies that the length of the pile is variable on the CPT domain, instead of a constant as is the case in a pile load test. This means that for every point on for example a CPT profile the capacity is calculated. There are certain key variables (such as cone resistance, diameter and wall thickness) that can in this way be combined to see their influence on general capacity trends. In this way, certain weaknesses or improvements on a design method can be found. This approach allows to answer sub-question 2 and 3, and is also partly used for sub-question 4.

From there, capacity plots in real CPT's can be made and from these, $Q_{t,c}/Q_{t,m}$ in case studies can be explained.

The design methods discussed in this report are the NEN, the CUR and the ISO. The NEN and the CUR are commonly used in the Netherlands, and the ISO is compared with it to see how current international state of the art is applicable to Dutch soil conditions. These three methods work in different ways and consequently give different capacities for different soil conditions.

Figure 3.1 shows the structure of the research questions in relation to the chapters.

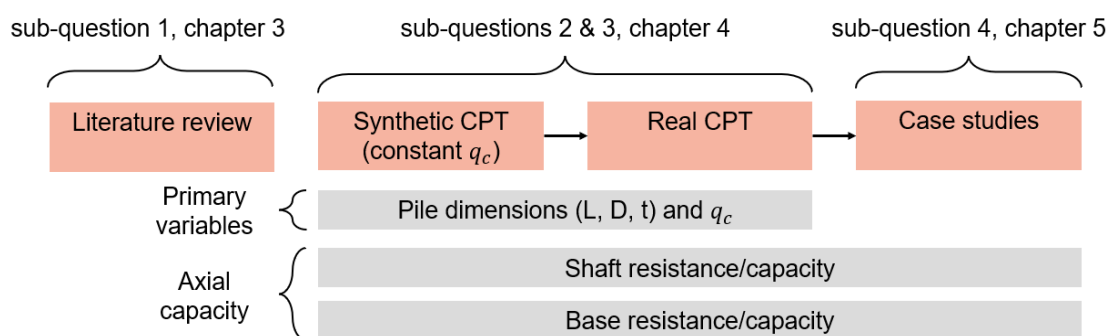


Figure 3.1: Schematic representation of methodology

3.1. Synthetic q_c versus real CPT's

This approach starts by plotting trends for a constant cone resistance q_c , what in this report is called a synthetic analysis. The synthetic analysis allows to see the working of the methods without natural soil variability. This is physically impractical as soil variability is often a present feature as a 20 – 50 m soil profile in the Netherlands is never homogeneous. Also, cone resistance is stress dependent and a high, constant q_c just below ground level never measured because it would require very high stresses. Still, plotting for synthetic q_c shows implied tendencies of the methods that can be used to explain capacity predictions in real CPTs.

First shaft and base resistances are evaluated. Together these two build up the components for capacity and explain a lot on how the capacity of a pile is obtained. Each method deals with effects such as friction fatigue (chapter 2.1.1). Base resistance is only dependent on an averaged q_c similar to a constant q_c and pile dimensions D and t so it is actually not just a synthetic analysis.

After that, capacities are plotted for low and high q_c values. This is a first indication of how different the methods can be potentially. Also capacities per method are plotted for q_c 's from 5 MPa to 50 MPa with steps of 5 MPa. This gives a general indication of the behaviour of the methods for different q_c values and a first indication of which methods predict highest/lowest capacities. A depth trend in q_c (i.e. q_c starting with a low value at the surface and linearly increasing over depth) is also looked at. It is a better representation of real soil conditions instead of constant q_c .

After synthetic q_c , variations in pile dimensions of diameter and thickness is looked at, because they are of big importance too for the capacity. Capacities for different diameters are plotted ranging from small ($D = 0.36$ m) to very large ($D = 2.5$ m). Typical pile diameters and wall thickness are chosen. In general as D increases, t/D decreases and there is less soil displacement of the annulus. With these it can be seen how the methods react in capacity predictions for different pile dimension. Also shaft and base resistances are looked at.

The second part of chapter 4 consists of linking these conclusions too real CPT profiles. The change from synthetic q_c to a real CPT requires additional numerical implementation. An example is varying base resistances over the profile instead of a constant value, and for the NEN the Koppejan averaging method has to be used. For the CUR and ISO, q_c profiles have to be averaged distances $\pm 1.5D$ on every measuring point to compute base resistances.

Three different CPT's from the Netherlands were processed to get insight on the axial capacity of different sand deposits and q_c trends. The capacities for these CPT's were calculated for piles loaded in compression and are named after their location: 'Maasvlakte' has a deep sand and very dense sand layer, 'Utrecht' and shallow and loose sand layer and 'Enschede' two shallow and locally dense sand layers. These three provide general CPT trends that are compared to the synthetic sensitivity and later linked to case studies that is aimed to explain why certain methods do well in one case but are off in another.

For each method per CPT, the capacities are plotted for two diameters of 0.5 m and 1.3 m. These were chosen as there is a general lack of large D tests in the methods, and tendencies of prediction and real behaviour largely unknown. The synthetic analysis also showed that there is large disagreement between the methods for diameters > 0.5 m. In combination with different q_c trends from the CPT, it can be seen where certain flaws or weaknesses for each method lie.

In combination with the synthetic analysis this has not been done before and provides new insight in the working of design methods, their implementations and in what situations they generally might under- or over-predict. With this, sub-questions 2 and 3 are answered.

3.2. Case studies

Case studies are then used to validate the previous findings, answering sub-question 4. Ideally, case studies are chosen that expose the weaknesses of the methods from the synthetic and real CPT analysis. However, there are not many accessible that are relevant to Dutch soil conditions and where data such as Incremental Filling Ratio *IFR* and measured shaft friction are captured. Most relevant will be Dutch tests to see how the ISO method reacts on Dutch conditions. Two available Dutch tests are EURIPIDES and Hoogzand. EURIPIDES is done with a larger diameter and to deeper depths, while Hoogzand is tested in relatively shallow but highly over-consolidated sand. Both tests were also tested in tension.

A large diameter pile test in Tokyo with $D = 2.0 \text{ m}$ is evaluated on base capacity to see how it compares to the response of larger diameters of the CUR and ISO.

Two tests from literature are evaluated in which important installation effects and individual capacity components are accounted for. A test from Han et al., 2020 was done in gravelly sand and separated capacity components and corrected for residual stresses. Tension tests in Blessington from K. Gavin and Igoe, 2021 gave insight in the effect of pile ageing.

The model is adapted to plot capacities over pile tip level and see what trends occur in combination with measured load test values. Predicted capacity components of the shaft and base are separated to see what the most important trends are, their variability and how much they deviate from measured values.

Recommendations on future pile load tests based on chapter 4 and 5 may optimise future design. The predicted Plug Length Ratio *PLR* (so prior to installation) from the ISO method is compared to measured *PLR* (after installation) and how this corrects a predicted capacity with a measured *PLR*.

3.3. Numerical approach

The design equations per method (in App. A) were programmed to obtain the plots with imported CPT's or synthetic q_c . In none of the plots are material factors applied.

The effective vertical stress σ'_v is approximated as $\sigma'_v = \gamma' \cdot z$ with $\gamma' = 10 \text{ kN/m}^3$. This is a reasonable approximation as measurements indicate σ'_v (in e.g. ICP, 2005) to follow this trend and variations do not affect predicted capacities significantly.

The methods use different empirical formulations for shaft friction τ_f . The CUR uses two different expressions, based on the distance from the pile tip level. The NEN and ISO use one expression for the whole pile length. The CUR and the ISO methods both include the parameter h in their equation, being the distance from a soil horizon z to the pile tip L , or $h = L - z$. With L as a variable the same length as z , discretising L and z with indices i and j leads to square matrix $h[i, j]$ with boundary conditions $\tau_f = 0$ when $h < 0$ (i.e. no shear stresses beneath the pile).

In other words, for each pile tip level there is a different h vector. A pile of length 10 m has $h = 3 \text{ m}$ at $z = 7 \text{ m}$, while a pile of length 15 m has $h = 8 \text{ m}$ for that same depth horizon at $z = 7 \text{ m}$. This requires two discretisations along L and z that make build up h from which τ_f can be calculated, taking into account the conditional statements for τ_f from the CUR.

This results in τ_f expressions also being matrices. Calculating shaft capacity from τ_f is done by integrating τ_f over the length of the pile times πD . As such, the shaft capacity of a pile at depth x can be calculated by integrating all shaft friction values 'above' x (i.e. the other dimension of matrix h at x). With the give assumption for σ'_v and with $h = L - z$, the integral of shear stress τ_f over depth z to shaft capacity Q_{fr} for the CUR and ISO cannot be solved to a formulation that does not include its original integral form. Integration by parts returns a remaining expression identical to the expression that was attempted to integrate. A numerical method has to be used for those and the straightforward midpoint

rule is chosen. This means that Q_{fr} is calculated with

$$Q_{fr,PTL} = \pi D \sum \tau_{f,PTL} \Delta z \quad (3.1)$$

This is accurate enough given that a CPT's interval Δz_{cpt} is small compared to its length (usually 0.02 m over 20 – 40 m) and a method's formulations are empirical by nature. Commonly, $\Delta z = 0.02$.

Sensitivity for D and q_c was be done with a third dimension on matrices for τ_f . The model was checked with individual calculations on certain points.

As the NEN relies on α factors relating q_c directly to shear stress, it was not needed to include it within the formulations and conditions for h . The NEN does not give a formulation for internal shaft capacity for its plugging condition, and it was assumed that internal shaft capacity $Q_{fr,i}$ is similar to external shaft capacity Q_{fr} but with inner diameter $D_i = D - 2t$.

For increasing PTL , the q_c requiring also a matrix for $q_c[i,j]$ where. The upper triangle equals 0 as q_c values below a PTL do not contribute to tau_{fr} , but this is not strictly necessary. For every pile penetration $PTL[i]$ there is a q_c profile for $\tau_f[i,j]$ from 0 (ground level) to $z[j]$ (end of pile).

For real CPT's, the NEN relies on the Koppejan averaging method with

$$q_b = \frac{1}{2} \cdot \alpha_p \cdot \beta \cdot s \left(\frac{q_{c,I,avg} + q_{c,II,avg}}{2} + q_{c,III,avg} \right) \leq 15 \text{ MPa} \quad (3.2)$$

where $q_{c,I-III,avg}$ follow minimum path rules for trajectories for certain trajectories scaled by the diameter above or below the pile tip. This was modelled where on each point the trajectory per averaging parameter is normalised by diameter and the trajectory length is chosen that makes q_b as small as possible.

Results: Design code analysis

For a given CPT profile, the design methods may differ significantly in their resulting capacities, but it is not always possible to state whether this difference is caused by the method approach or local soil variability. To isolate the effects of the different methods, the soil's variability is ignored with a synthetic CPT (i.e. constant q_c) to see trends for the method's capacities over depth of pile penetration. A constant q_c does not have practical relevance as soil deposits almost never show a constant q_c , but plotting with constant q_c gives conclusions that can be used to explain capacity predictions for real CPT's.

The most important variables to vary are q_c and diameter. After this tension and real CPT's are evaluated. This was done with on two piles of larger diameters with different dimensions ($D = 0.5\text{ m}$ $t = 0.008\text{ m}$, $D = 1.3\text{ m}$ $t = 0.013\text{ m}$). When the y-axis is named 'Pile tip level (m)', the plot shows capacity over a variable length. The complete sets of formulas per method can be found in Appendix A.

All plots in this chapter were made without applying material factors.

4.1. Shaft friction with synthetic CPT

Figures 4.1a and 4.1b show the shaft friction profiles for constant q_c for compression and tension. Pile dimensions dimensions are $L = 50\text{ m}$, $D = 1.3\text{ m}$ and $t = 0.016\text{ m}$ (so $t/D = 0.012$).

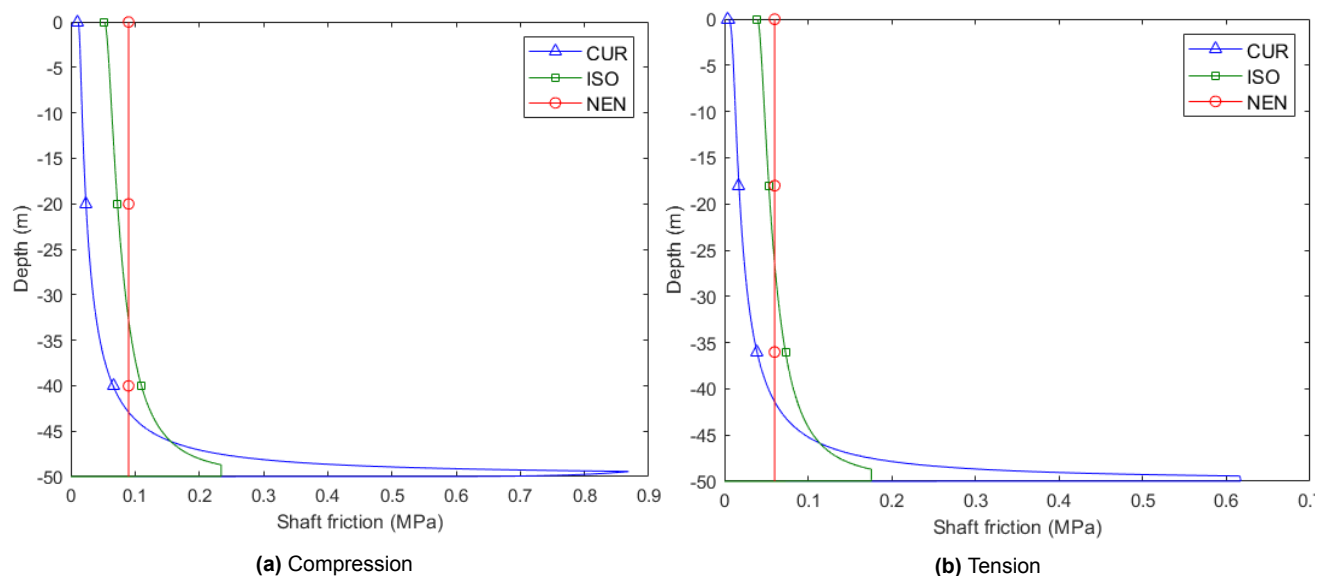


Figure 4.1: Shaft friction along a pile in homogeneous sand ($L = 50\text{ m}$, $q_c = 35\text{ MPa}$, $D = 1.3\text{ m}$, $t = 0.016\text{ m}$)

Per method this leads to the following implications:

- *NEN*. Above 15 MPa, shaft friction τ_f from the NEN becomes linear due to the limiting value applied on τ_f of 12 or 15 MPa depending on layer thickness (eq. 2.17). Consequently the NEN assumes shaft friction to be constantly divided with synthetic q_c . The α factors directly relate q_c to τ_f with a limiting value. There is no friction fatigue implied by the NEN. The NEN implies hardly any interaction between soil particles as the pile is driven down and soil displaced with this constant shaft friction.
- *CUR*. The CUR's shaft friction is very different from the rest with a large peak of shaft friction near the bottom of the pile. This is peak is at a distance $h/R^* = 4$ (eq. A.11) from the pile tip after it quickly reduces to zero towards the tip due to a largely assumed friction fatigue component from the term $(h/(4R))^*$. This requires friction to rise from 0 to 0.87 MPa from 1 – 2 m away from the pile tip. After that shaft friction quickly reduces again with 80 – 90%.

Another way to interpret τ_f of the CUR is that most of the shaft friction contributing to Q_{fr} is near the bottom of the pile and that the influence of zones further up are of little to no importance. Most of the contribution to Q_{fr} is near the pile tip, and this makes Q_{fr} not really dependent on the length of the pile but only of the friction near the pile tip.

- *ISO*. The ISO method also shows some friction fatigue, but less extreme than the CUR. It looks like a combination of the NEN and the CUR, meaning that shaft friction increases near the pile tip (i.e. friction near the pile contributes more to frictional capacity than zones further up), but it is also not extremely different than the constant approach from the NEN.

Roughly 5% of τ_f at the pile tip is caused by the dilation term $\Delta\sigma'_{rd}$ (eq. A.20). The shape of the curve of τ_f for the ISO is mostly caused by the term $[\max(1, (h/D))]^{0.4}$ (eq. A.19), which relates τ_f to the distance from the pile tip h normalised with diameter.

- *Tension*. Figure 4.1b shows the predicted τ_f profiles during tension. The NEN and ISO approach this with a constant reduction on τ_f and the CUR proposes a different formula but effectively also results in more or less a similar profile of smaller magnitude.

Figure 4.2 shows the bottom 10 m of the pile from Fig. 4.1a with average shaft frictions. Considering only this bottom part of the pile is typical for calculating resistance in industry. The large differences of stress concentration at the bottom of the pile is emphasized. On average for this 10 m of pile, the CUR predicts highest average shaft friction, followed by the ISO and last the NEN that inherently predicts constant shaft friction for this case.

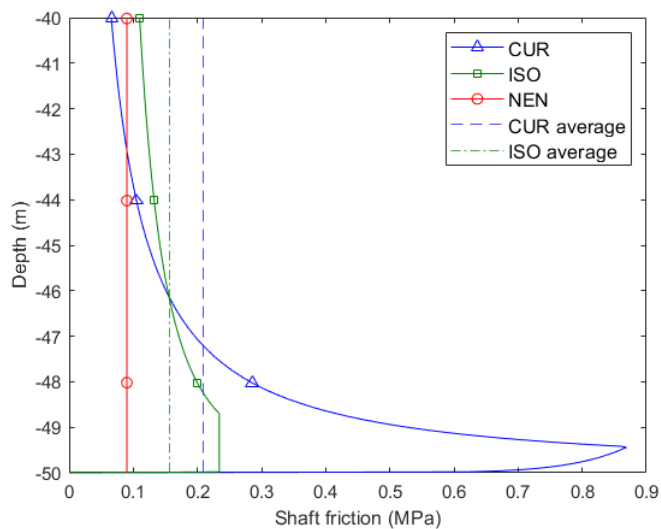


Figure 4.2: Shaft friction of Fig. 4.1a from 40 – 50 m with averages

The concept of friction fatigue is shown in Figure 4.3. Here, the τ_f profiles of the ISO and CUR are plotted for a constant q_c of 35 MPa. It can be seen that the shaft friction for any depth point (chosen was $z = 25m$, red-dashed line) decreases as the pile is driven deeper (i.e. pile tip level moves from 35 to 45 m depth).

The figure is cut off at $\tau_f = 0.25$ MPa but for the CUR it continues to 0.8 – 0.9 MPa. Friction fatigue of the CUR is mostly happening near the pile tip due to the sudden large concentration of shaft friction there.

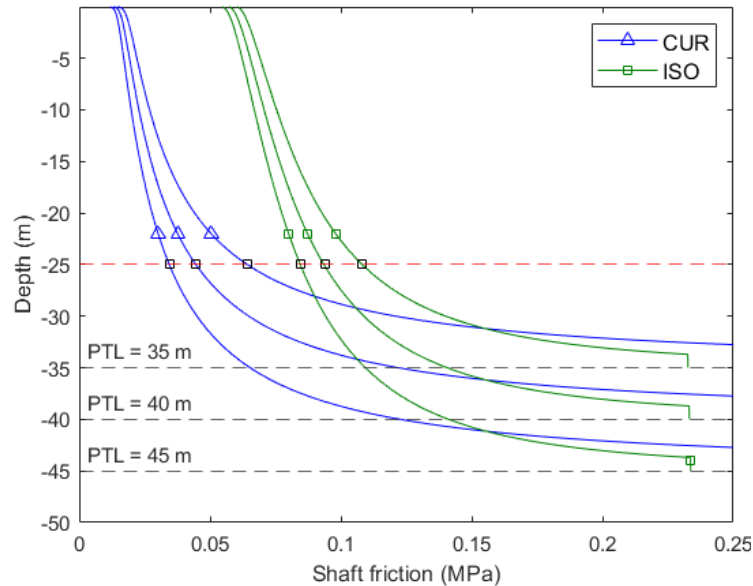


Figure 4.3: Friction fatigue effect of τ_f for ISO and CUR in constant q_c (35 MPa): a reduction in τ_f is apparent when the pile is driven down (pile tip level goes from 35 to 45 m). $D = 1.3$ m, $t = 0.016$ m

4.2. Axial capacity with synthetic CPT's, compression

Axial capacity trends are plotted with all the method's equations (see Appendix A. The most important parameters are q_c (constant and with depth trend) and cross sectional pile dimensions (diameter and thickness).

As the capacities are plotted for every pile length on the y-axis, the plots in this sub-chapter are with a variable pile length on the y-axis, which is not a depth axis. The variable length of the pile is indicated as pile tip penetration or pile tip level.

4.2.1. Influence q_c

Constant q_c

Figure 4.5 shows the capacities per method for a 50 m domain with $q_c = 10 \text{ MPa}$ or 50 MPa for a pile with $D = 1.3 \text{ m}$ and $t = 0.016 \text{ m}$ ($t/D = 0.012$). Differences in capacity over depth are caused by shaft capacity and not base capacity since it is constant for constant q_c .

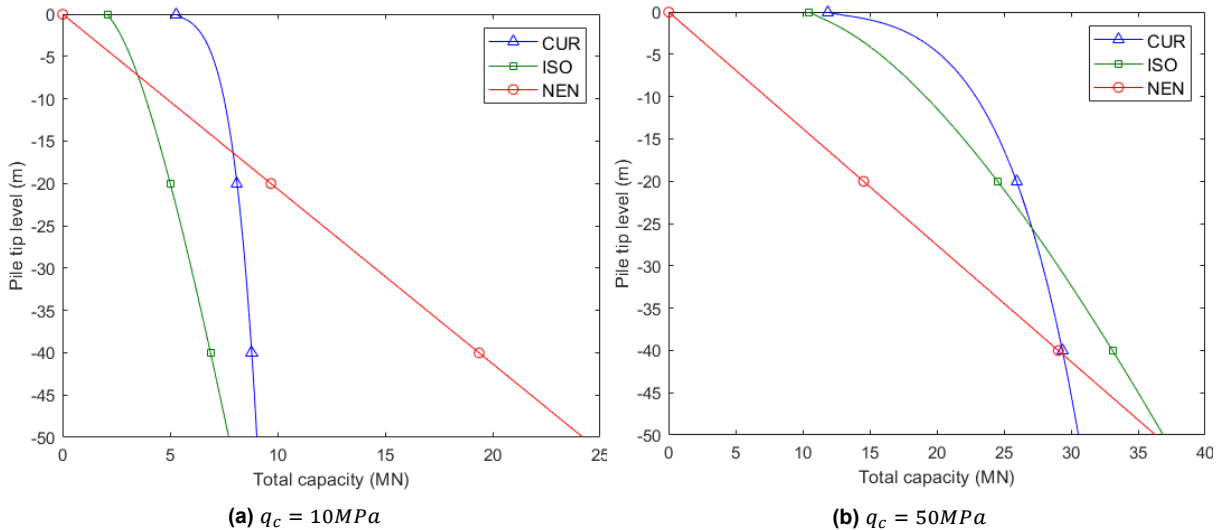


Figure 4.4: Capacities for constant q_c , compression

Fig. 4.5 leads to the following implications:

- Figures 4.4a and 4.4b show how wide the capacities can vary for identical input and constant q_c . The methods vary and disagree a lot on axial capacities.
- *NEN*. The capacity of the NEN is approached with the shaft capacity plus the minimum of the inner shaft capacity and the base capacity (eq. 2.18). The NEN predicts a linear profile due to the α factors and constant q_c , directly relating q_c to axial capacity. There is a slight change between q_c of 10 MPa and 50 MPa due to the limiting values. This is a rather reductive implication for such a significant change in cone resistance.

The limiting values are occasionally argued to calculate in a conservative way. Figure 4.4a shows this may not necessarily be true, as the NEN predicts an enormous difference compared to the CUR and ISO.

- *CUR*. The CUR's capacity behaviour is asymptotic. The asymptotic behaviour follows from Fig. 4.1 where an increase in length would hardly cause an increase in τ_f as the friction is mostly situated at the bottom and the influence of friction far from the pile tip can be neglected. The length of the pile should contribute to shaft capacity for synthetic q_c as an increase in length should give more soil-structure contacts and thus more friction. The CUR generally predicts a higher base capacity than the ISO.
- *ISO*. The ISO has a depth trend in capacity. This follows from Fig. 4.1. As the pile is installed deeper (PTL increases) the shaft friction profile also increases over the whole length of the pile, and not only near the bottom as the CUR implies. This depth trend becomes stronger with higher q_c .

Multiple q_c 's

The influence of q_c is further evaluated by looping over different values ranging from 5, 10, 15, ...50 MPa. Figure 4.5a shows the capacity of the NEN for increasing q_c . To see the differences between CUR and ISO for increasing q_c , the capacity of the ISO was subtracted from the capacity of the CUR in Fig. 4.5b.

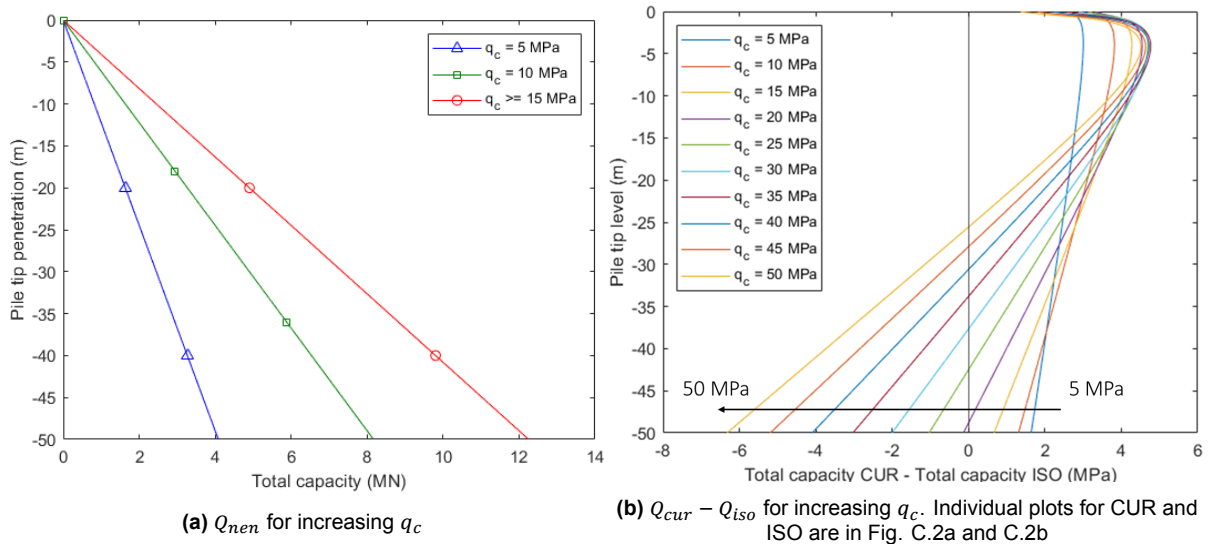


Figure 4.5: Capacity for constant q_c from 5 MPa to 50 MPa for a pile with $D = 1.3$ m, $t = 0.016$ m ($t/D = 0.012$)

Figure 4.5 leads to the following implications:

- *Figure 4.5a.* The effect of limiting values for the NEN on shaft friction has a clear effect: there is not a difference for the capacity profile above $q_c > 15$ MPa. Load tests are often done in sands with $q_c > 15$ MPa, but the NEN will predict a linear capacity profile from that point. There is also no base resistance present for the NEN because the inner friction is smaller than the base resistance. Also for these regions, the NEN predicts a linearly increasing capacity of similar trend.
- *Figure 4.5b.* This Figure plots the difference between the CUR and ISO capacities because it illustrates better the variance between the two methods. For shallow depths (in the Fig. for $z < 25$ m) the capacity of the CUR is higher than the capacity of the ISO. The same is true for low q_c (in the Fig. for $q_c < 25$ MPa). This does not mean that these conditions are always true for these values of q_c and z , but it can be accepted as general trend that for low/shallow z and low q_c (or say loose sand), the CUR predicts higher capacities than the ISO.

The reason for this is that the CUR predicts a higher base capacity but low increase over depth for shaft capacity. The ISO has less base capacity but predicts a depth trend in frictional capacity that at some moment surpasses the CUR's capacity.

q_c depth trend

The capacities were plotted for a q_c depth trend with $q_c(0) = 5 \text{ MPa}$ linearly increasing to $q_c(50) = 35 \text{ MPa}$ in Figure 4.6a and to $q_c(50) = 50 \text{ MPa}$ in Figure 4.6b.

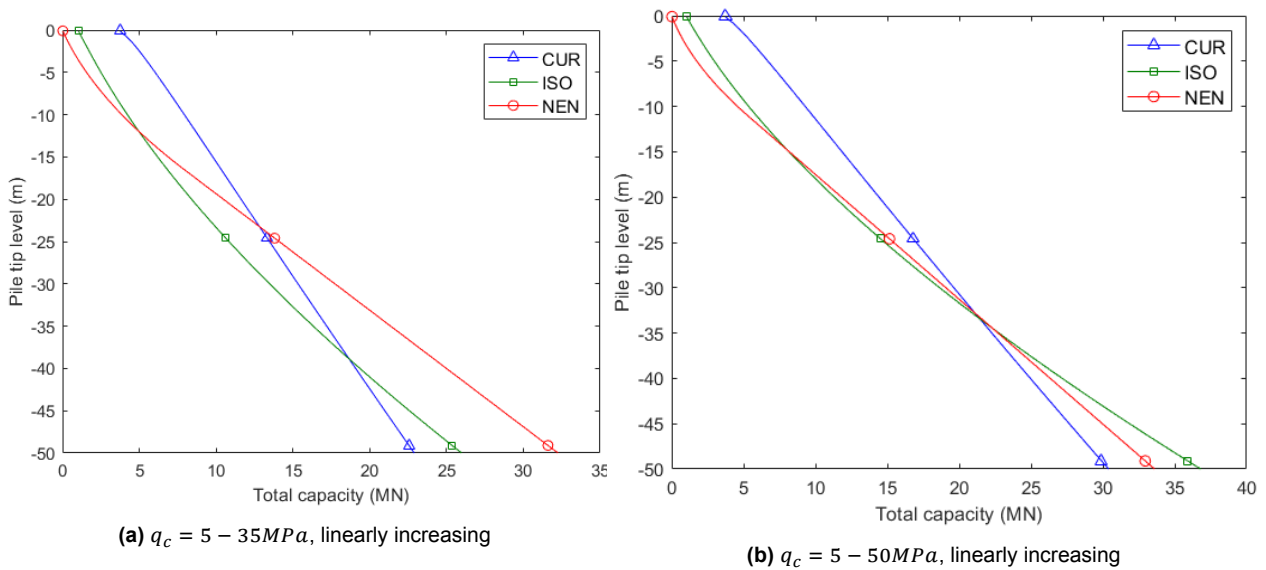


Figure 4.6: Capacities for depth trends for a pile with $D = 1.03 \text{ m}$ and $t = 0.016 \text{ m}$

A depth trend gives a closer approximation of what might be found in the field. In Figures 4.6a and 4.6b, similar conclusions can be observed as before, where the Q_{cur} is highest for shallow depths and/or low q_c . As the ISO has a stronger depth trend than the CUR, Q_{iso} surpasses Q_{cur} at a certain point. This can be explained by the asymptotic vs. depth trend behaviour of the CUR and ISO seen before.

In Figure 4.6a, the strong linear prediction of the NEN makes it surpass the CUR and ISO as penetration depth increases. In both Figures, $Q_{fr,i,nen} < Q_{eb,nen}$ by a wide margin, and thus a non-plugging pile is assumed. It may look like Figure 4.6b contains a point on which the three methods coincide, but this is not the case.

4.2.2. Influence diameter and wall thickness

The capacities were also evaluated for different cross-sectional pile dimensions: the diameter and wall thickness. The diameter was increased from $D = 0.356 \text{ m}$ to $D = 2.5 \text{ m}$ with commonly used diameters in between.

Figure 4.7 shows the capacities of the NEN for different diameters for a constant q_c of 15 MPa .

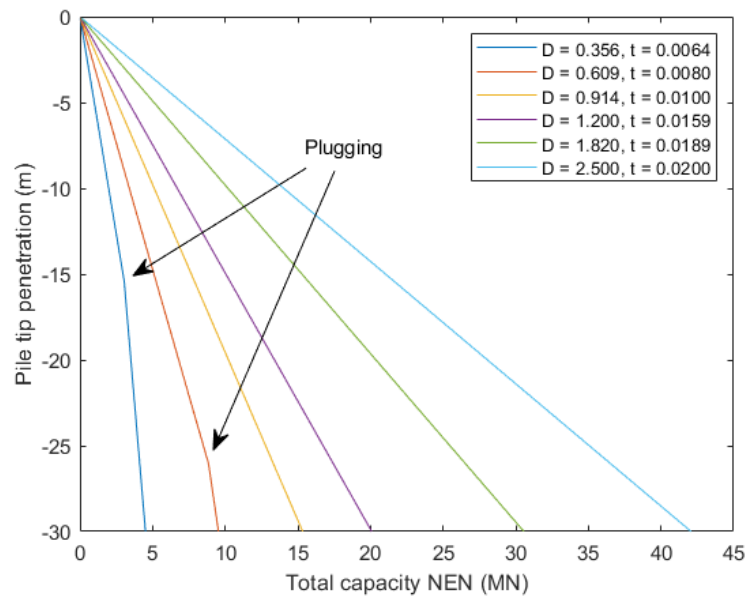


Figure 4.7: Effect of diameter on NEN for increasing diameter in synthetic q_c of 15 MPa

Often, the NEN assumes a non-plugging pile during loading, except below the hinges of the lines of $D = 0.356\text{ m}$ and $D = 0.609\text{ m}$ from which the base capacity is smaller than the inner friction according to equation 2.18.

The magnitude and lines/slopes of Figure 4.7 will not change for higher q_c 's due to the limiting values of the NEN, whereas the CUR and ISO would. For higher q_c , the NEN often predicts the lowest capacity, whereas for low q_c it may sometimes predict the highest due to linear capacity behaviour.

When the CUR and ISO were evaluated for increasing D , the CUR appeared to be much more sensitive to this. An increase in D also gave a big increase in capacity according to the CUR. This effect is here called the 'diameter effect'. There are two explaining mechanisms for why the CUR is so sensitive for an increase in D and the ISO much less is represented. The first is given in Figure 4.8:

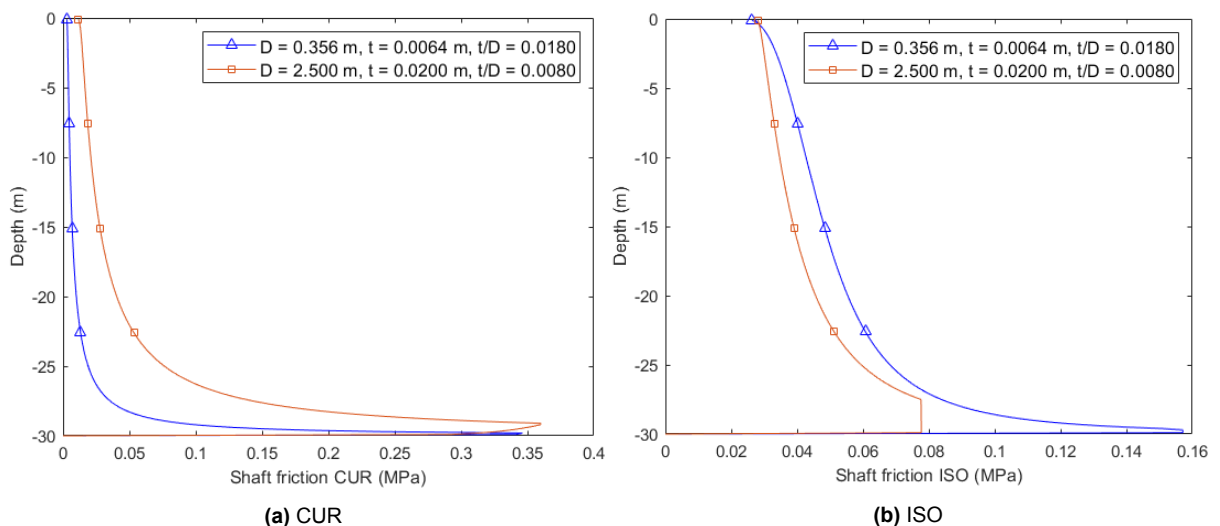


Figure 4.8: Diameter effect on shear stress for $q_c = 15\text{ MPa}$

On Fig. 4.8a it can be seen that an increase in diameter leads to an increase over the shear stress profile. Consequently, the integral from shaft friction to shaft capacity also increases. This is unreason-

able, as piles with diameter $> 1\text{ m}$ are unlikely to plug and cause less soil displacement as they are installed in coring mode. The unit shear stress (i.e. shear stress for an element of the circumference) is unlikely to increase with an increase in D for these cases. The ISO (Fig. 4.8b does not show this effect. Variations of D give more or less similar τ_f profiles for the ISO. Variations occur because of the nature of the empirical formulas and numerical implementation.

The second explaining mechanism for why the CUR is much more sensitive for increases in diameter is given in Figure 4.9.

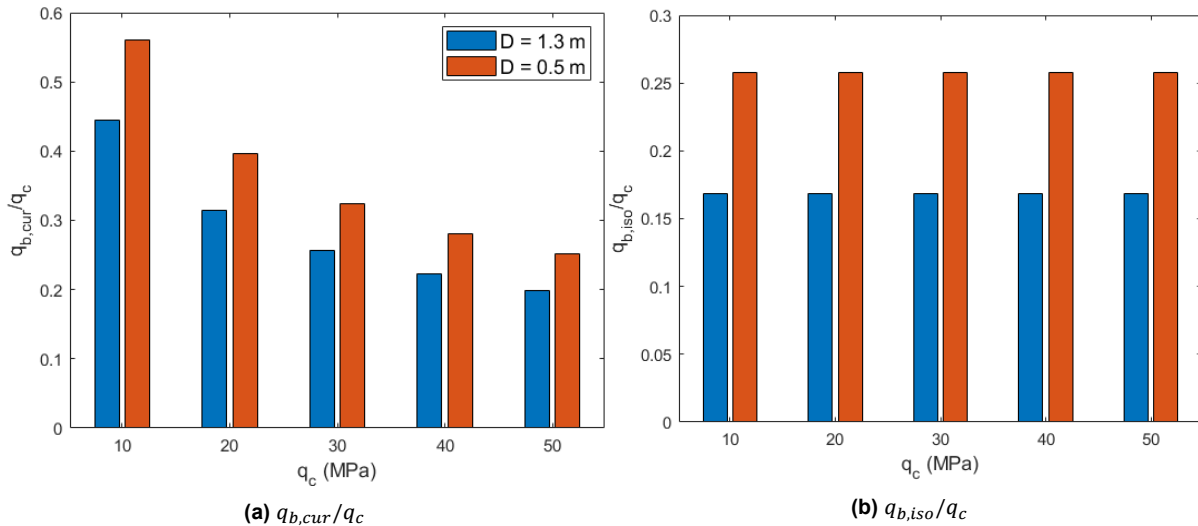


Figure 4.9: Diameter effect on base resistance

Figure 4.9 plots normalised base resistance (q_b/q_c) for the CUR and ISO for two piles on different q_c 's. In real CPT's, q_c would here be $q_{c,avg}$. The difference between the piles for both methods is the degree in which the displace soil around the pile (DR for CUR, A_{re} for ISO), as base resistance is dependent on q_c and pile dimensions. The smaller D pile displaces more soil around it than the higher D pile due to its t/D ratio. The normalised base resistance for the CUR is much higher than for the ISO, especially for lower q_c 's. Another way to interpret this, is that the share of q_c that makes up the base resistance increases as q_c decreases. This leads to the CUR having a stronger diameter effect in low q_c soils or looser sands. When q_c is increased, normalised base resistance of the CUR approaches that of the ISO. The normalised base resistance for the ISO is constant as q_b is directly related to $q_{c,avg}$ with a regression formula on the effective area ratio (a constant).

When plotting the capacities per method over different diameters and thicknesses, the CUR is more sensitive than the ISO. Plotting shaft friction profiles for the CUR and ISO for different D and t , it was found that the $\tau_{f,iso}$ profiles rather equal in size and shape, while the $\tau_{f,cur}$ profiles increase over depth as D increases, Figures 4.8a and 4.8b. This effect makes the CUR more sensitive for increasing D than the ISO. It appears that changing the t/D ratios to $1/60$ or other constants is of minimal influence.

The influence of diameter in Figures 4.8a and 4.8b is also influenced by the q_c . An increase in q_c causes the band of τ_f profiles for the CUR in Figure 4.8a to be more narrowly placed, where those of Figure 4.8b for the ISO incline steeper down. The effect of q_c on capacities of the CUR and ISO for different D and t is better illustrated in Figures 4.10a and 4.10b, in which the capacity of the ISO is subtracted from the CUR for two variations of q_c of 15 MPa and 40 MPa .

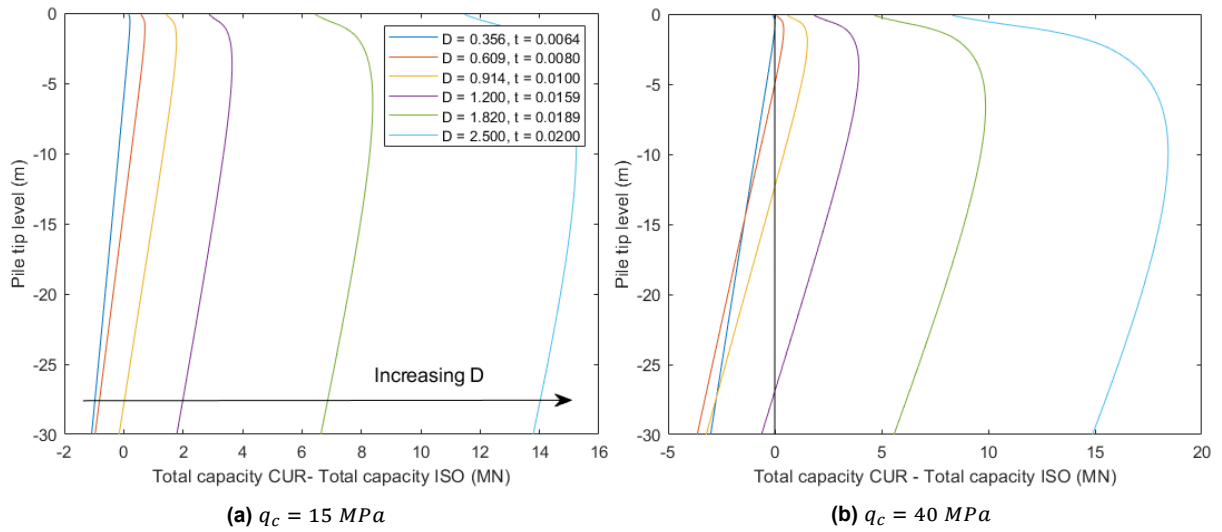


Figure 4.10: Diameter effect on $Q_{cur} - Q_{iso}$ for different q_c

Figure 4.10a shows that for a relatively low q_c and smaller diameters, the CUR and ISO predict roughly similar for small D of 0.356 and 0.609 m, with deviations of about $\pm 1 \text{ MN}$. For larger D 's, the CUR deviates a lot from the ISO, reinforcing the claim that the ISO is less sensitive for changes in D . For higher q_c (Figure 4.10b), the ISO's depth trend becomes more skewed (see also Fig. 4.5), and the capacity of the ISO is higher than the capacity of the CUR for $D < 1 \text{ m}$. Nevertheless, the increasing diameter effect of the CUR takes over for piles with $D > 1 \text{ m}$. Especially for piles with $D > 1.5 \text{ m}$, the predicted capacities can deviate from 5 to even 19 MN for this synthetic case. It is noteworthy that the CUR states its method is valid for a diameter range of 0.25 – 3.00 m.

4.3. Axial capacities with synthetic CPT's, tension

Piles loaded in tension have no base capacity, and so the total capacity equals shaft capacity in tension. For the NEN, this means a reduction to $\alpha_t = 0.004$ instead of $\alpha_s = 0.006$. The CUR has a separate formula for $\tau_{f,t}$ which also looks very much like a magnitude change and the ISO assumes $\tau_{f,t} = 0.75 * \tau_f$. Figure 4.11 shows the synthetic tension capacities for $q_c = 10 \text{ MPa}$ and $q_c = 50 \text{ MPa}$.

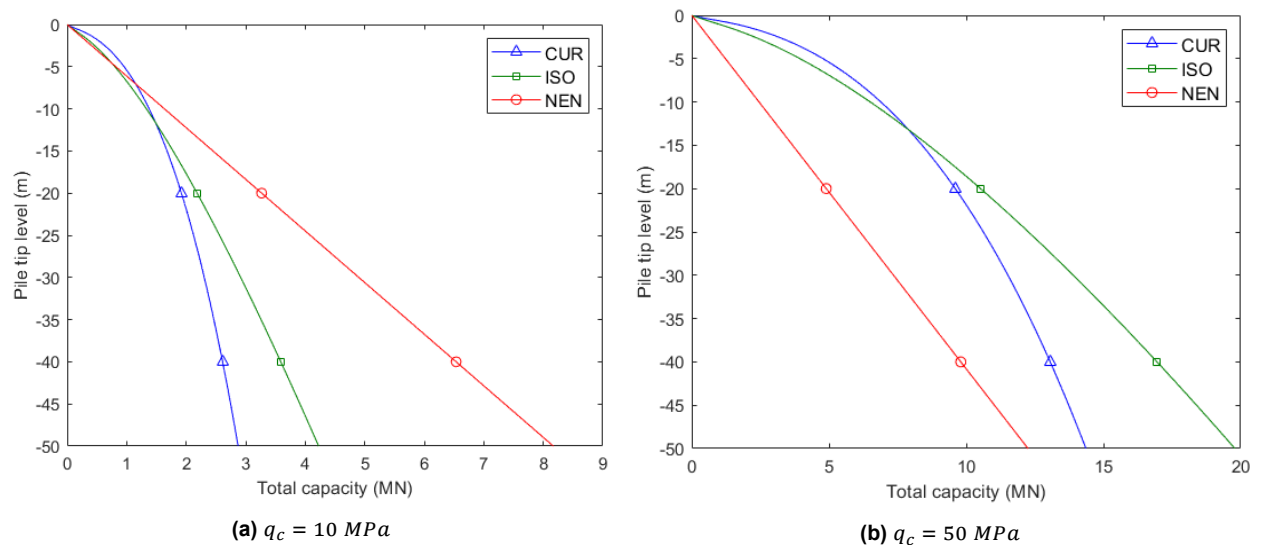


Figure 4.11: Capacities for constant q_c profiles, tension

Again, the NEN is very reductive and minimally influenced by an extreme q_c increase. The CUR and ISO are more sensitive to the q_c difference, and increase roughly fivefold looking at $z = 50 \text{ m}$. Similar depth trends as with compression appear, and it can be said that also in tension the CUR predicts rather asymptotic capacity trend over depth, whereas the ISO shows an increasing depth trend.

4.4. Axial capacities with CPT's

This section shows capacity plots for 3 real CPT's from Maasvlakte, Utrecht and Enschede. For each method per CPT, the capacity is plotted for 2 diameters. In the CPT profiles also the base resistances are plotted to see how they respond to the q_c profile.

4.4.1. Maasvlakte, deep and dense sand layer

Figure 4.12 shows a CPT from the Maasvlakte near Rotterdam of a deep and dense sand layer.

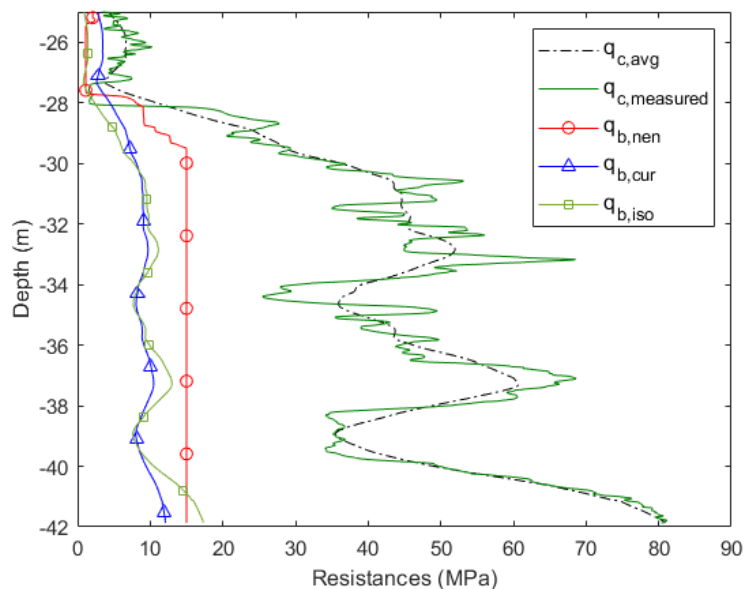


Figure 4.12: Maasvlakte CPT profile with base resistances for a pile with $D = 0.5 \text{ m}$ and $t = 0.008 \text{ m}$

In Figure 4.12, a dense and locally very dense sand layer starts at 28 m depth. The ISO predicts a pile with $PLR = 0.95$ based on its inner diameter. The CUR assumes full plugging after a distance $8D$, being at $z = 32 \text{ m}$ and $z = 38 \text{ m}$ for piles with diameter 0.5 m and 1.3 m respectively.

The ISO's base resistance looks like a scaled version of $q_{c,avg}$, where $q_{b,cur}$ appears more constant and less sensitive for locally very dense zones. For the NEN, q_b is constant at 15 MPa from 30 m on, as q_c values are well over 20 MPa and q_b is limited by 15 MPa .

Figure 4.13 shows the resulting capacities from Figure 4.12 for two piles with $D = 0.5 \text{ m}$ and $D = 1.3 \text{ m}$.

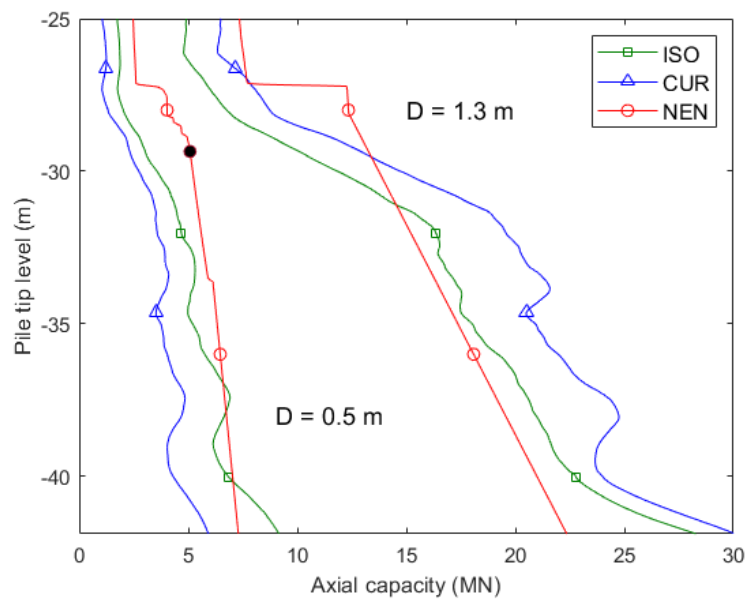


Figure 4.13: Resulting capacities from Fig. 4.12 for two piles. Below left black dot: pile is assumed to plug during loading. Pile does not plug on the right red line of the NEN

Figure 4.13 leads to the following implications:

- *Diameter, CUR and ISO.* The ISO's axial capacity is bigger than the CUR's for the pile with $D = 0.5 \text{ m}$ and that the difference increases over depth due to the stronger depth trend of the ISO in shaft capacity. This is in conformance with the diameter effect of the CUR observed in the synthetic analysis (Fig. 4.10b) and the frictional depth trend of the ISO.
- *Diameter, NEN.* For $D = 0.5 \text{ m}$, it clearly shows the NEN is not necessarily conservative as it is the highest of the three until 37 m depth, but that it is just neglectful of q_c influence. The effect of maximizing q_c for the NEN shows its effect clearly from 28 m depth down where Q_{nen} linearly increases downwards, ignoring dense/loose zones in the sand deposit. The CUR and ISO methods do emphasize the effect of dense/loose zones on the axial capacity better in their capacities.
- *Plugging, NEN.* Below the black dots for the NEN, $Q_{b,nen} > Q_{fr,i,nen}$ and the pile is assumed to be plugging. The linear increase is because $q_{b,nen}$ and $\tau_{f,nen}$ are limited at 15 MPa . As the diameter is increased to 1.3 m , the pile is predicted not to plug.

4.4.2. Utrecht, shallow and loose sand layer

Figure 4.14 shows a CPT from Utrecht. This profile has lower q_c values but is locally quite dense from 14.5 m depth. Below this layer, there is a weaker zone. The base resistance of the CUR is generally higher than the ISO which is also seen in the synthetic analysis.

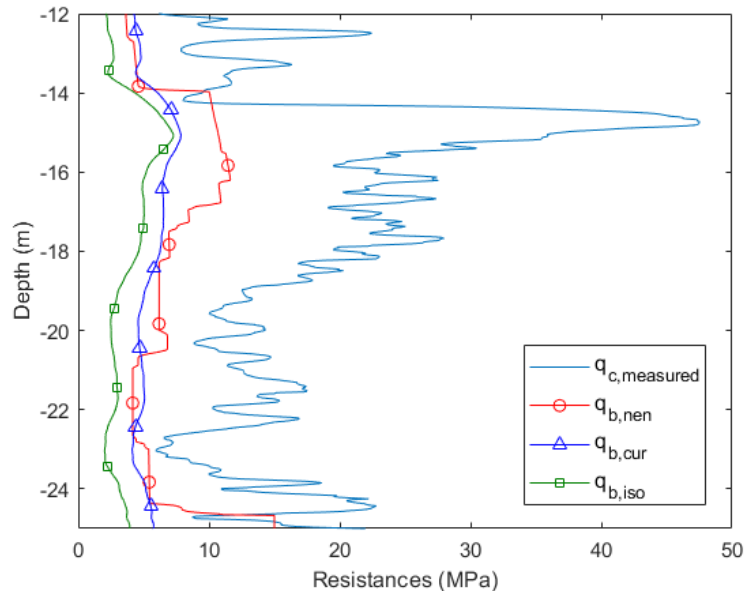


Figure 4.14: Utrecht CPT profile with base resistances for a pile with $D = 0.5$ m and $t = 0.016$ m

With the plugging condition in equation 2.18 for Q_{nen} , the NEN predicts that $Q_b < Q_{fr,i}$ from 18.2 m depth, and from that point down the pile is predicted to plug during loading.

Koppejan q_c averaging in lower q_c

Almost all of the q_c profile is between 10 – 30 MPa and the base resistance for the NEN is less than 15 MPa. The base resistance $q_{b,nen}$ was computed with the method of Koppejan, also in Fig. 4.14. This base resistance looks blocky because $q_{c,I,avg}$, $q_{c,II,avg}$ and $q_{c,III,avg}$ follow minimum path rules and create averages over certain trajectories. The $q_{c,I,avg}$ follows a path of $0.7D - 0.4D$ down from pile tip, and the base resistance increases at a distance above a stronger zone, e.g. $q_{b,nen}$ increases at 14 m depth while a dense sand layer is situated at 15 m. In other words, the base resistance 'feels' the resistance of strong (or weak) layers beneath it, as an assumption of this averaging method is that a pile fails along the weakest zones.

The base resistance of the NEN is dependent on diameter. Figure 4.15 shows the effect of an increase or decrease of D on base resistance. If the diameter is decreased, the trajectories of $q_{c,I,avg}$, $q_{c,II,avg}$ and $q_{c,III,avg}$ also decrease in length and the profile becomes more sensitive for strong zones, as for each level of the pile tip the minimum values over the trajectories have less influence. In other words, it becomes 'less likely' for the influence of a strong zone to be excluded because the influence of the minimum values is taken over shorter intervals. Because of that, $q_{b,nen}$ generally rises as D decreases. For the dense layer at $z = 15$ m, $q_{b,nen}$ with $D = 0.2$ m reaches its maximum of 15 MPa, while for $D = 0.8$ m an increase has the opposite effect. As D increases, the trajectories for $q_{c,I,avg}$, $q_{c,II,avg}$ and $q_{c,III,avg}$ are lengthened and the influence of minimum values is increased.

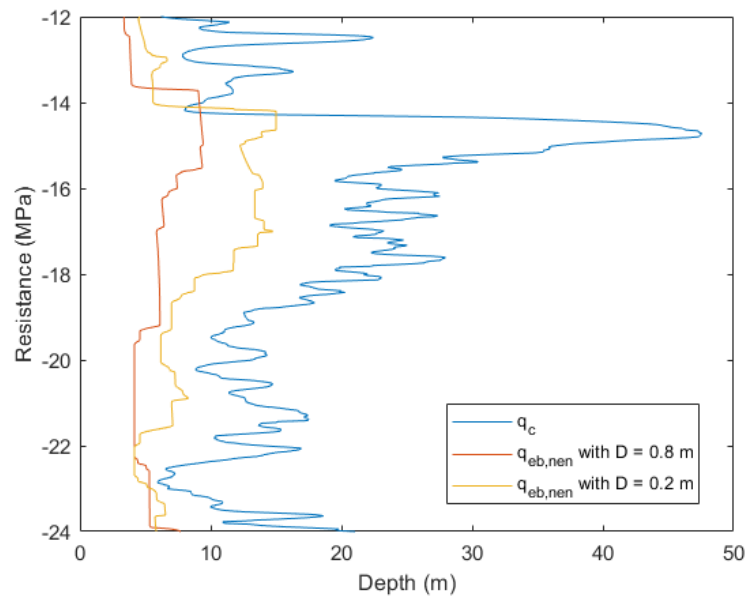


Figure 4.15: Influence of increasing/decreasing D on $q_{b,nen}$

Capacities

Figure 4.16 shows the capacities from Fig. 4.14 for again two piles with $D = 0.5\text{ m}$ and $D = 1.3\text{ m}$.

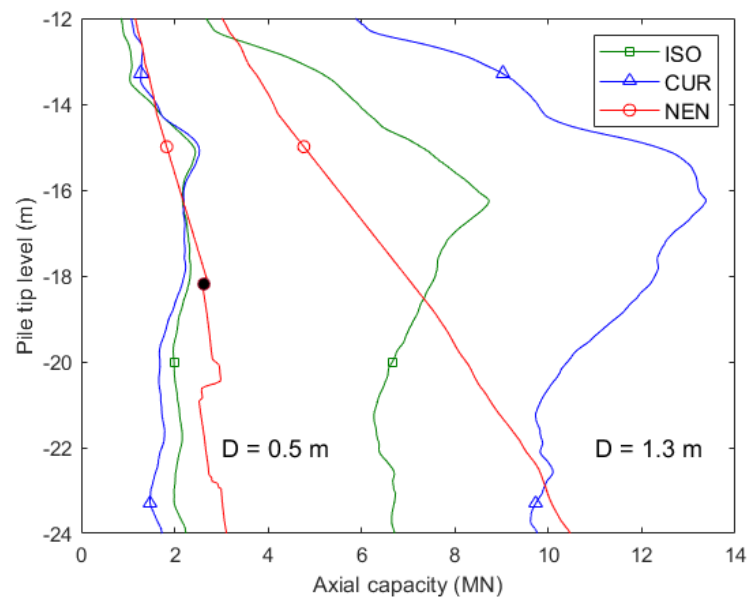


Figure 4.16: Resulting capacities from CPT in Fig. 4.14 for two piles. From black dot, the NEN predicts plugging. Pile is predicted non-plugging in Q_{nen} with $D = 1.3\text{ m}$

Figure 4.16 leads to the following implications:

- *Plugging, NEN.* For the smaller pile, the NEN predicts plugging from the black dot after the dense zones and enough inner friction is mobilised.
- *Capacities.* The choice of method again greatly influences the predicted capacity. The CUR and ISO both notice the strong zone in their capacities and they are roughly equal for the $D = 0.5\text{ m}$ pile. The NEN does not see this is zone in its capacity. Below the dense layer, the NEN predicts

highest capacity and thus is not conservative. The highest capacity of the NEN is at 20 m depth, well below the dense zone.

- *Diameter*. For this looser sand with lower q_c , there is great disagreement on what would be the capacity on the dense layer at 16 m depth. There is over 6 MN capacity difference between the NEN and the CUR at this point.
- *CUR*. It is confirmed there that the CUR predicts much higher capacities for large D in low q_c (the 'diameter effect' concluded in the synthetic analysis, Fig. 4.10a). The breakdown of capacity components in Fig. 4.17 illustrates this better.

Figure 4.17 shows the causes of the diameter effect via breakdown of base and shaft capacities from Figure 4.16.

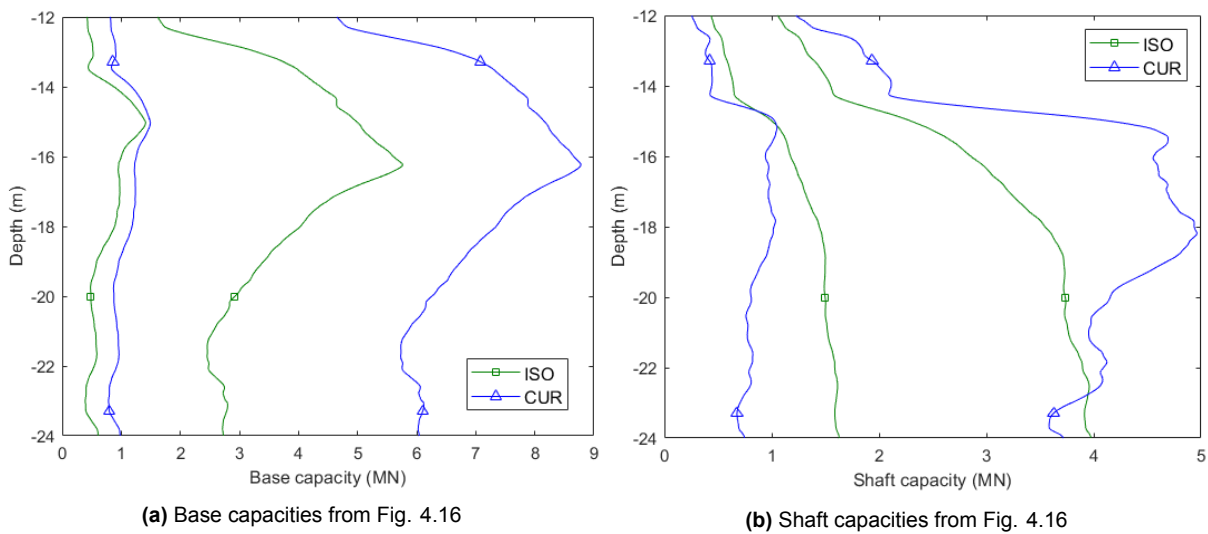


Figure 4.17: Breakdown of capacity components from Utrecht for CUR and ISO for two piles

Figure 4.17 leads to the following implications:

- An increase to very high diameter leads to a big increase in base capacity for the CUR. The explaining mechanism was given in Fig. 4.9a and 4.9b. The base resistance is much higher for the CUR on low q_c sands which is enlarged in base capacity for an increase in diameter.
- There is a big and local increase in shaft capacity when the diameter is increased for the CUR. The explaining mechanism behind this was given in Fig. 4.8a and 4.8b. An increase in D lead to an increase in τ_f with a lot of frictional contribution near the bottom of the pile tip for shaft capacity.

4.4.3. Enschede, two shallow and locally dense sand layers

Figure 4.18 shows a CPT and base resistances from a CPT near Enschede with two locally very dense sand layers, one of which is rather shallow. Also here, the $q_{b,nen}$ is significantly higher than the ISO's and CUR's. The locally dense zones are both equally notified by the CUR and the ISO in base resistance.

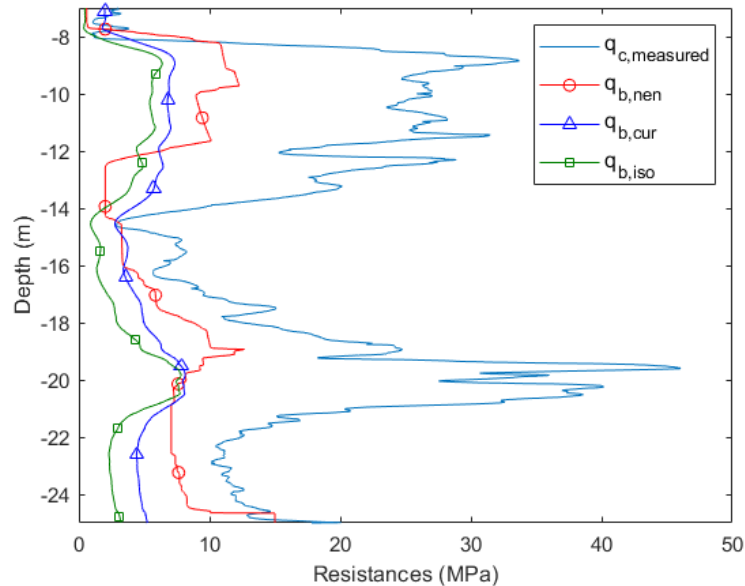


Figure 4.18: Enschede CPT profile with base resistances for a pile with $D = 0.5 \text{ m}$ and $t = 0.008 \text{ m}$

Figure 4.19 shows the resulting capacities from the CPT of Fig. 4.18.

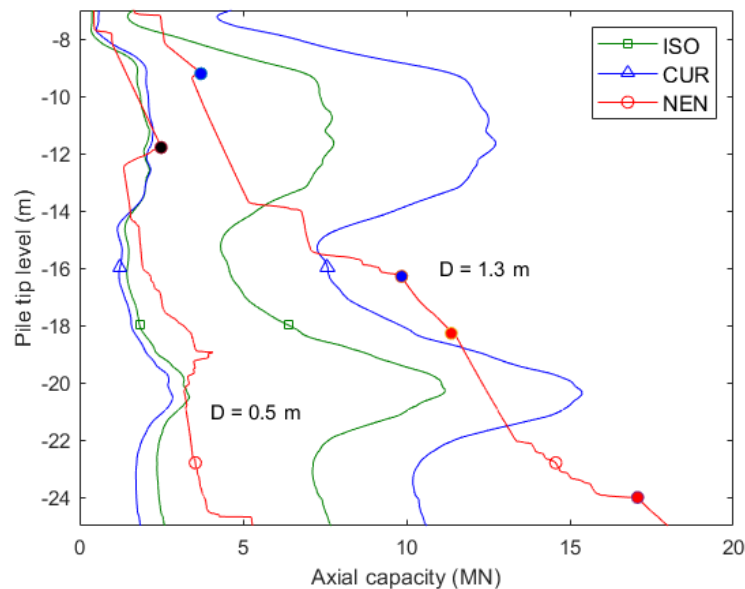


Figure 4.19: Resulting capacities from CPT in Fig. 4.18 for two piles. After black dot and in between blue/red dots, $Q_{b,nen} < Q_{fr,nen,i}$ and pile is assumed to plug

Figure 4.19 leads to the following implications:

- The diameter effect of the CUR is again clearly visible. The CUR predicts the highest capacity for the $D = 1.3 \text{ m}$ pile with a great amount.
- The difference between the ISO and CUR for the pile with $D = 0.5 \text{ m}$ increases over depth due to a stronger depth trend of the ISO from the shaft capacity.

- The NEN fully ignores both strong zones, most notably with the $D = 1.3 \text{ m}$ pile. Because of these, there is a huge difference at around 11 m depth, where $Q_{nen} \approx 4 \text{ MN}$ and $Q_{cur} \approx 12.5 \text{ MN}$, a three-fold difference. This does not mean that the NEN is conservative, as it surpasses both the CUR and ISO at $z = 25 \text{ m}$ with $Q_{nen} \approx 17.8 \text{ MN}$ and $Q_{iso} \approx 7.7 \text{ MN}$, giving a rough 10 MN difference. Also here, the methods seem very much to disagree on capacity for very large diameters.

It is apparent, especially from the Utrecht and Enschede CPT's, that the design methods are unsuited for large D as there is an enormous difference in predicted capacities and pile behaviour. In the Maasvlakte CPT, the CUR and ISO predicted more equal capacities. For weaker sands with lower q_c , there is a larger difference in predicted capacities.

4.5. Database background of CUR and ISO

To better understand the buildup and working of the method, it is relevant to understand the underlying tests on which the methods are based.

The database on which the CUR method was calibrated for open-ended piles in compression consists of 12 tests on 5 sites. An additional 2 tests are done more than 200 days after installation and include effects like pile ageing in their results. Figures C.6a and C.6b show the diameters and t/D ratios.

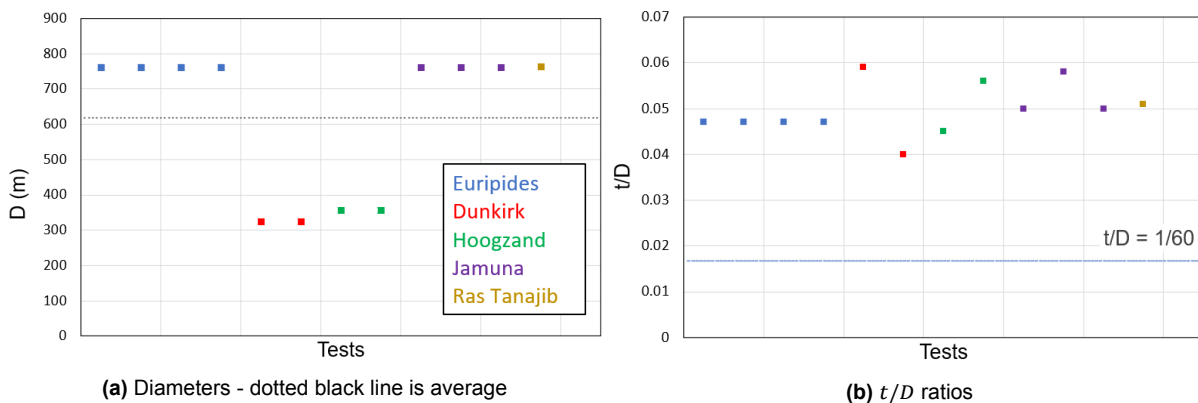


Figure 4.20: Database CUR for open-ended piles loaded in compression - colours indicate test sites

Figure 4.20 leads to the following implications:

- The CUR is effectively based on only 2 values for the diameter, being 0.76 and 0.34 m . This is an underlying reason why the CUR is sensitive for larger diameter piles: there are no tests included that account for capacities for piles with diameters $> 0.8 \text{ m}$.
- The piles in Figure C.6b have an average t/D ratio of around $1/20$ ($= 0.05$), while a common criticism of the CUR is that many open-ended piles in practice have a $t/D < 1/60$, so below the blue line in Figure C.6b, and strictly speaking then the CUR should not apply as valid design method.

Also noteworthy comments of the tests on which the CUR and ISO are based are:

- Of the 5 sites from the CUR only 2 are Dutch, being the EURIPIDES tests and tests in Hoogzand. The EURIPIDES tests are done with relatively large D and deep depths, while those of Hoogzand are with smaller D and shallower depths in over-consolidated sand. A legit response to using a new design method in the Netherlands would be to ask if the method would work or is calibrated on the Dutch soils. Half of the tests from the CUR are of foreign nature, and the ISO is also calibrated on EURIPIDES and Hoogzand.
- One of two tests done in Dunkirk by F. Chow, 1997 was done with a driving shoe (test CS) and compression tests were done 1 day after tension tests. Doing compression and tension tests at the same day is also common (e.g. EURIPIDES and Hoogzand).

- The Jamuna tests for construction of a bridge were done in micaceous sands (Yu and Yang, 2012) which behave different than siliceous sands. Micaceous sands can have high void ratios, and ICP, 2005 argues that design methods for piles in micaceous severely over-predicts frictional capacity and under-predicts base capacity. Performance results from the CUR 2001-8 also confirm this.
- The database on which the ISO was calibrated consists of 17 tests on open-ended steel pipe piles loaded in compression and 12 in tension. The ISO uses almost all tests the CUR is based on for $q_{b0.1}$, except the 3 tests from Jamuna because they were done in micaceous sand. There are separate databases for e.g. $\Delta\sigma'_{rd}$
- For determination of $q_{b0.1}$, the ISO uses 3 tests with diameters of 1.5, 1.5.2.0 m in Tokyo, with lengths of 73.5, 86.0, 30.6 m. This is a considerable calibration for very large diameters that the CUR does not have.

4.6. Summarised conclusions

The most important findings of this chapter are summarised to these conclusions.

- *Plugging*. The NEN and CUR both have 'extreme' plugging predictions, where the NEN is generally non-plugging and the CUR full plugging after a distance $8D$. The ISO is the only method considering partial plugging based on a prediction of the *PLR*. In engineering practice, if a pile plugs or not leads to a lot of uncertainties and discussions.
- *Shaft friction*. The CUR implies a large concentration of shaft friction near the pile tip, causing a lot of friction fatigue. Most of the friction contribution for shaft capacity is located near the pile tip. The ISO assumes friction to be more divided along the pile shaft, but with a bigger concentration at the bottom. The NEN assumes constant shaft friction due to its limiting value and constant α -factors.
- *Base resistance*. Normalised base resistance for the CUR is higher than for the ISO, especially in looser sands (low q_c). Normalised base resistance for ISO is constant, while that for the CUR is very high for low q_c and decreases with increasing q_c . This leads to base capacity being over-predicted in loose sands. This effect is enlarged for increasing diameter.
- *Synthetic capacity*. The methods vary enormously in their predicted capacity. The CUR shows an asymptotic trend in capacity predictions over depth, because it assumes most friction to be near the pile, regardless the pile length. The ISO method shows an increasing capacity prediction as pile penetration depth increases, because shaft friction is more divided on the length of the pile. In general for shallow depths and/or low q_c , the CUR predicts the highest capacity.
- *Diameter - NEN*. Increasing the diameter leads to less base resistance. This is because the Koppejan averaging method follows minimum path rules and an increase in D means an increase in the averaging trajectories. Consequently, the minimum values over trajectories have an influence over a longer trajectory, decreasing the averaged base resistance. At the same time, $Q_{fr,nen,i}$ increases a lot with increasing D . This can lead to counter-intuitive and highly reductive plugging predictions, proposed by the NEN.
- *Diameter - CUR and ISO*. The ISO is considerably less sensitive for increases in D and t than the CUR. There are two mechanisms causing this 'diameter effect'. 1) The CUR predicts an increasing τ_f profile for increasing D , causing a significant diameter sensitivity as the integral. This sensitivity is amplified by locally strong zones due to the large friction fatigue term of the CUR, contributing most of the friction to the bottom of the pile. 2) The normalised based resistance is much higher for the CUR than the ISO for low q_c and this difference decreases as q_c increases. This means the for low q_c , the CUR predicts much more base resistance. This difference becomes less in higher q_c sands.
- *Diameter - all*. There is enormous disagreement between the methods on what happens when the diameter is increased to > 1 m. Differences of 10 MN were calculated for piles with $D = 1.3$ m. This is a critical thing to notice, as the CUR says it applies to D up to 3 m, which would cause enormous disagreement which can be impracticable or even useless.

- *Database background.* The CUR is effectively being based on two sets of diameters (for compression) and uses three tests done in micaceous sands. The ISO is based on all CUR tests except the micaceous sands from Jamuna and incorporates additional large diameter tests, while also relating the degree of plugging to base resistance. ISO included 5 very large diameter tests with $D \geq 0.91 \text{ m}$. There is no base for the $t/D > 1/60$ condition of the CUR, as it is calibrated on $t/D \approx 1/20$ and most piles on-land have $t/D < 1/90$.
- *Limiting values, NEN.* There seems to be no valid reason to either maximize $\tau_{f,nen}$ or $q_{eb,nen}$. It clearly limits capacity predictions and disallows distinction of strong zones. An explaining mechanism behind this limiting cannot be found, and it was shown that it neither is a specifically conservative or save way of predicting capacity.
- *Tension.* Tension shows similar capacity trends, but without base capacity and with a magnitude change for τ_f .

5

Results: Case studies

This chapter aims to link the theory and conclusions from the synthetic analysis with the design methods to instrumented case studies and pile load tests. A number of tests are evaluated for compression and tension. The focus was put on Dutch tests to see how the ISO applies to Dutch soil conditions, a load test in Tokyo and two detailed tests from literature.

The goal of this chapter is to observe performance in a greater perspective as is done in the analysis of the previous chapter in combination with measured plugging data and shaft friction profiles. Some of these tests the methods are already calibrated for.

Two (instrumented) Dutch tests are the EURIPIDES tests and the Hoogzand tests. The CUR and ISO both are calibrated for this test. The EURIPIDES tests are with large diameter and installed at deep depths, while the Hoogzand tests are with smaller diameter and shallow depth in an over-consolidated sand. The axial capacity and its components were modelled over the q_c domain to observe certain trends and explanations. If available, measured shaft frictions were compared with the predicted ones.

For tension, additional tests of Blessington were evaluated in which the effect of pile ageing can be seen. A test from Han et al., 2020 shows the methods' implications in gravel and correction for residual loads and inner shaft friction.

5.1. Euripides I a-c, compression

5.1.1. Dimensions and condition

The EURIPIDES tests were done in Eemshaven to better understand open-ended piles with installed to deep depths and with large D . Site conditions show a thick and soft Holocene layer of around 20 – 25 m and a high q_c Pleistocene layer from 30 m down. The three tests were done with one pile driven down to 30.5, 38.7 and 47 meters depth with compression and tension tests done at each level. The set up time of tests a-c are 7, 2 and 11 days respectively (J. A. Schneider et al., 2008), both for compression as tension.

EURIPIDES site I tests a, b and c were done with a pile of $D = 0.763$ m and lengths $L_{a-c} = 30.5, 38.7, 47$ m respectively into a very dense Pleistocene sand layer starting at about 30 m depth. The relative density tip was a little over 0.8. Both the CUR and the ISO are calibrated for this test.

The tests were a-c were done 7, 2 and 11 days after installation, respectively. The pile was driven in an almost fully coring mode, as can be seen in Fig. 5.1.

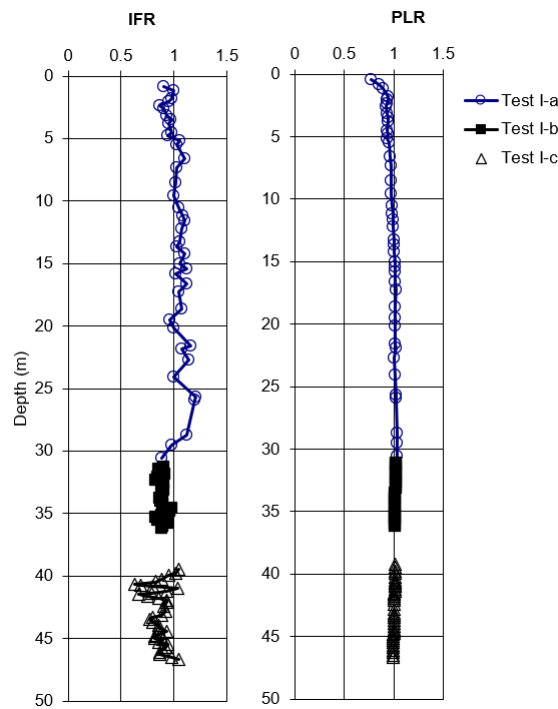


Figure 5.1: *PLR* and *IFR* of EURIPIDES I

The large diameter and soft Holocene layer make the pile to be installed in almost full coring mode. There is a gap in the data on Fig. 5.1 because the apparatus malfunctioned. The values per test for *PLR* and *IFR* over different distances can be seen in 5.1.

Test	PLR avg. 10D	PLR avg. 20D	IFR avg. 10D	IFR avg. 20D
I-a	1.03	1.20	1.03	1.07
I-b	1.02	1.02	0.88	0.95
I-c	1.00	1.01	0.88	0.88

Table 5.1: *PLR* and *IFR* over certain distances for EURIPIDES I tests

5.1.2. Results

Figure 5.2a shows the bottom part of the q_c profile. Figure 5.2 shows the total, shaft and base capacity modelled for the q_c profile. The dotted lines indicate the depths to which the different tests were installed and the black dots their measured capacities given by Yang et al., 2016.

Fig. 5.2 shows what the synthetic and real CPT analyses also show: the CUR gives higher capacity for shallower depths but the depth trend of the ISO at a certain depth takes over. The NEN is neglecting q_c variability and predicts a linear capacity profile.

Fig. 5.2b shows that the total capacity strongly increases for tests a-c that are progressively installed to deeper depths. This is caused by a depth trend in frictional capacity, and not by the base resistance. This depth trend in frictional capacity is noted best by the ISO method. The CUR implies a rapid increase in Q_{fr} while the pile meets the dense sand layer but this quickly reaches an apparent asymptotic value.

The reason for the ISO to note this frictional depth trend is a less extreme friction fatigue component in $\tau_{f,iso}$, which contributes more friction at the pile tip for the shaft capacity. The CUR attributes almost all of its friction for shaft capacity near the pile tip (Fig. 4.1). In other words, the CUR seems to almost neglect the influence of strong zones further removed from the pile tip, and once the pile has penetrated past this zone, the frictional capacity is not increased much by an increase in depth. This is also due to the fact that the dense zone from $z = 30$ m, on average, is more or less constant with $q_c = 60$ MPa. Would it have a stronger depth trend too, the CUR is likely to also follow that trend.

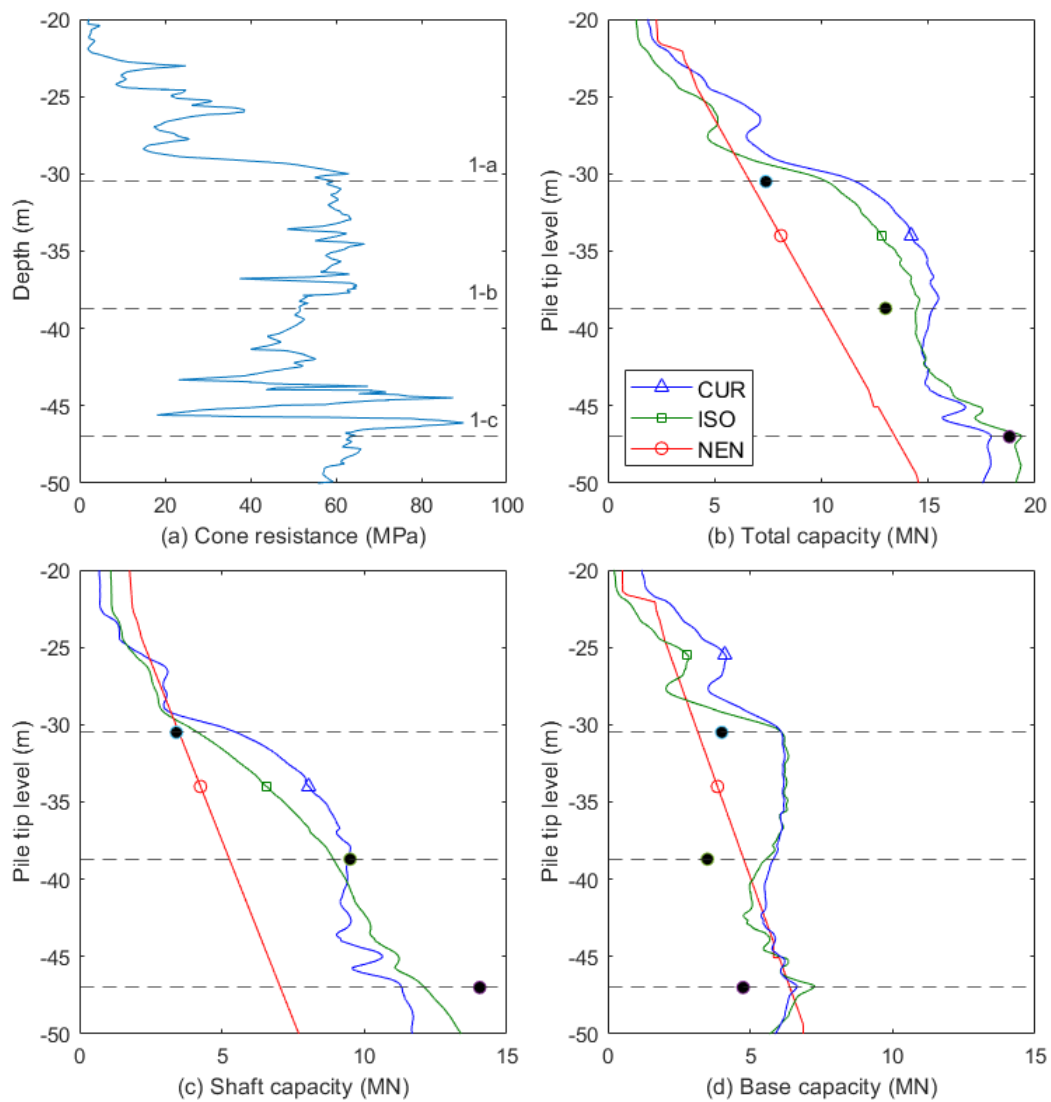


Figure 5.2: Results for EURIPIDES test 1 a-c, black dots are Q_m -values from Yang et al., 2016

In Figure 5.2, the methods over-predict the base capacity, but for tests b and c it constitutes about 25% of the total capacity and of bigger importance here is obtaining an accurate prediction of shaft friction because of the deep depths. For the NEN, base capacity follows equation 2.18.

The base capacity profile is more or less constant for the CUR and ISO, because both methods use a term averaging the q_c profile $\pm 1.5D$ on each point and this is constant by approximation. The measured values also reflect this.

Table 5.2 shows the performance of the tests. The NEN predicted shaft capacity in test 1-a well, but this is more of a coincidence than of an accurate way to calculate shaft capacity with the α factors. Fig. 5.2 shows that for test 1-c a much higher α_s would be required.

	I-a			I-b			I-c		
	CUR	ISO	NEN	CUR	ISO	NEN	CUR	ISO	NEN
$Q_{b,c}/Q_{b,m}$	1.52	1.53	0.79	1.66	1.59	1.36	1.40	1.52	1.35
$Q_{s,c}/Q_{s,m}$	1.62	1.22	1.03	0.99	0.94	0.55	0.80	0.86	0.50
$Q_{t,c}/Q_{t,m}$	1.57	1.38	0.90	1.17	1.11	0.77	0.95	1.03	0.72

Table 5.2: Performance calculations on EURIPIDES I a-c

	I-a	I-b	I-c
$Q_{b,m}(MN)$	4	3.5	4.75
$Q_{s,m}(MN)$	3.4	9.5	14.05
$Q_{t,m}(MN)$	7.4	13	18.8

Table 5.3: Measured capacities for EURIPIDES I a-c from Yang et al., 2016

Figure 5.3 shows the predicted and measured shaft friction profile for the bottom part of test 1-c. The measured profile does show an increase in shaft friction near the bottom of the pile, but not as extreme as the CUR predicts and neither as constant as the NEN predicts.

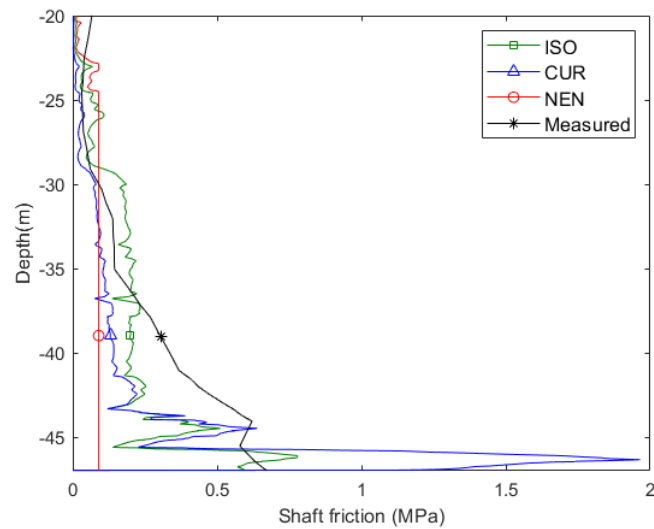


Figure 5.3: Predicted and measured shaft frictions, with measured shaft friction from JIP, 2020

5.2. Euripides II, compression

The second EURIPIDES load test was also done in a deep and dense Pleistocene sand (5.4a). The q_c profile (Fig. 5.4a) is by approximation less constant as in the first tests but still relatively similar.

Measured values for $Q_{b,m}$ and $Q_{s,m}$ are taken from ICP, 2005 and are given as black dots in Fig. 5.4. EURIPIDES test II was done 6 days after installation.

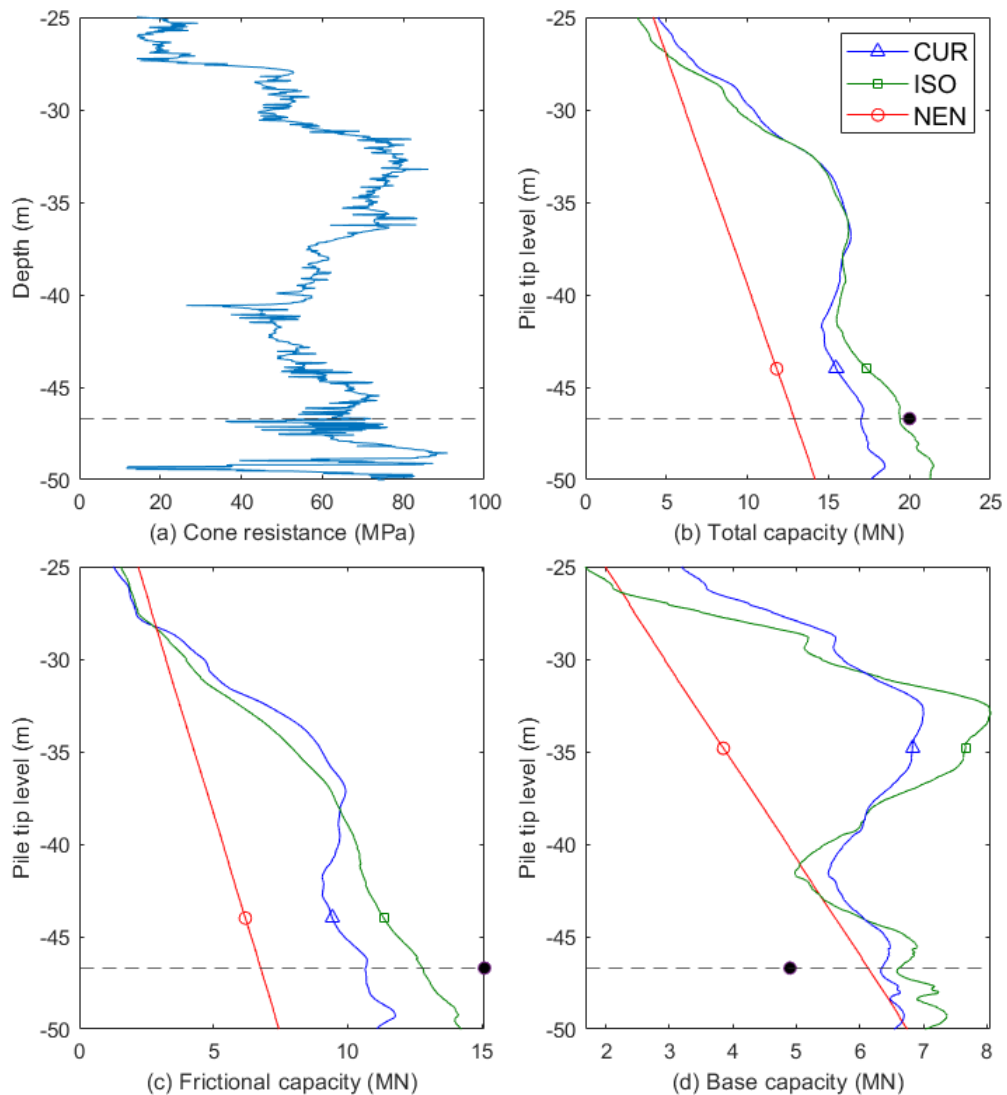


Figure 5.4: CPT profile and capacities for EURIPIDES II

Figure 5.4 confirms what was concluded with the EURIPIDES 1 tests. Also here, the depth trend of $Q_{fr,iso}$ seems to predict $Q_{fr,m}$ best, notably due to its depth trend. Even though the ISO over-predicts base capacity, accurate prediction of Q_{fr} is more important due to the pile's long length.

It is a general trend that the ISO's base resistance is more sensitive to the influence of strong and weak zones (e.g. also in Fig. 5.7). The synthetic analysis also showed this (Fig 4.9b), and that the CUR is less sensitive in changes of q_c for base resistance.

In industry, capacity is often calculated from the depth on which the sand layer starts which in Fig. 5.4 is at about 27 m depth. Depending on the method, this may lead to a reduction of about 5 to 7 MN (Fig. 5.4b).

5.3. Han, F. et al. (2020) - Gravelly sand, compression

A detailed and highly instrumented test was done by Han, F. et al. (2020) on the axial capacity of a long pile with $L = 30.48 \text{ m}$ and large diameter with $D = 0.664 \text{ m}$. A double-walled pile gave insight in capacity components, identified with electrical-resistance and vibrating-wire gauges. Inner and outer shaft resistances, as well as plug and annulus resistances were identified.

Site conditions in Fig. 5.5 indicate a high and varying q_c profile with large gravel content, locally up to 40 – 50%. The piles was highly instrumented and provided great insight in parameters such as β , the coefficient of lateral earth pressure K and a detailed breakdown of stress components and correction for residual loads. For the performance calculations, a lower bound in the CPT profile was suggested by the authors as the resistance response is not only caused by the cone and gravel particles, but also the gravel particles pushing on each other and interlocking, giving local peaks. This effect is also accounted for in the NEN, where a reduction in q_c is needed based on mean particle diameter.

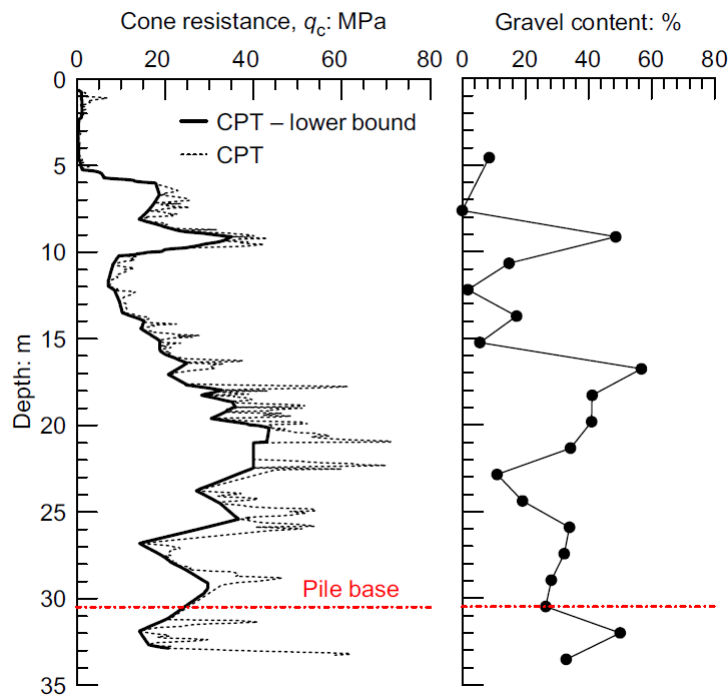


Figure 5.5: q_c profile and gravel content from Han et al., 2020

The measured PLR was 0.777 of this test, while the PLR predicted by the ISO is 0.838, a rather acceptable deviation of 7.8%. The NEN assumes an unplugged pile in this case during loading as $Q_{fr,i,NEN} < Q_{b,NEN}$, but it is apparent the pile is not unplugged and has significant base resistance contribution of 52.7% of the Q_t , while $Q_{fr,i,measured}$ is 6 times smaller than $Q_{b,measured}$ (without residual load correction). The NEN is significantly off in prediction of pile behaviour and stress distribution in this case.

The performance calculation for each method are given in table 5.4 and the measured capacities in table 5.5.

	excl. residual load correction			incl. residual load correction		
	CUR	ISO	NEN	CUR	ISO	NEN
$Q_{s,c}/Q_{s,m}$	1.70	2.03	1.66	1.93	2.30	1.88
$Q_{b,c}/Q_{b,m}$	1.44	0.99	1.70	1.27	0.88	1.50
$Q_{t,c}/Q_{t,m}$	1.58	1.55	1.68	1.58	1.55	1.68

Table 5.4: Q_c/Q_m results on Han et al., 2020

	excl. resid. load correction	incl. resid. load correction
$Q_{b,m}(MN)$	2.22	2.518
$Q_{s,m}(MN)$	2.562	2.264
$Q_{t,m}(MN)$	4.782	4.782

Table 5.5: Measured capacities from test by Han et al., 2020

The residual load correction (see also chapter 2.4.1) does not influence $Q_{t,m}$, but influences the distribution of $Q_{b,m}$ and $Q_{s,m}$. This correction reduces $Q_{b,m}$ and increases $Q_{s,m}$, and the two components almost seem to swap in magnitude. The individual capacity components per method are now even more off and all three methods show poor results in obtaining the shaft capacity. Han et al., 2020 also note the overestimation of frictional load due to high gravel content by design methods.

The ISO is accurately predicting the base resistance. The CUR and NEN are over-predicting this, too, by a rather wide margin.

Figure 5.6 shows the measured unit shaft friction and the predicted shaft friction profiles for the CUR, ISO and NEN.

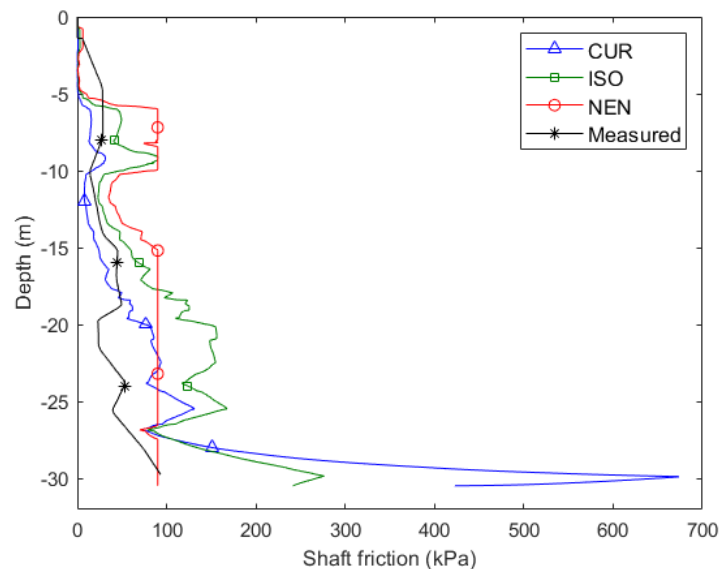


Figure 5.6: Predicted and measured shaft frictions

It is apparent that the concentration of the large friction component predicted by the CUR at the bottom of the pile is absent in the measured profile. The NEN predicts a predominantly constant shaft friction profile. The CUR and the ISO seem to give a reasonable approximation of τ_f until $z = 15$ m. After 15 m depth, the gravel content also rises significantly to about 30 – 40%. A potential reason for this overestimation may be a smaller amount of particle contacts and thus less friction due to the large particle size. Another reason may be a short time in between installation and static load test (8 days).

5.4. Hoogzand I and III, compression

5.4.1. Dimensions and conditions

The Hoogzand tests were done in 1979 and consist of two compression and tension tests (*I* and *III*) with piles of small D and shallow L in a dense, over-consolidated sand. A test *II* was also done but this was a closed-ended pile.

The q_c profile (Fig. 5.7a, obtained from Yang et al., 2016) shows a shallow, dense sand layer appearing from $z = 3 - 10$ m. This is unusual for Dutch soil condition as often a soft Holocene layer is on top of a denser Pleistocene (sand) layer. What should be noted is that the profile of $q_{c,avg}$ is very similar to q_c , suggesting that the apparent q_c is already smoothed or was of poorer precision than current measurements. This may have influenced the results.

Pile dimensions were $D = 0.356$ m, $L_I = 7$ m and $L_{III} = 5.3$ m, and $t_I = 0.016$ m and $t_{III} = 0.020$ m. Due to the different wall thicknesses giving different capacity predictions, the results could not be plotted clearly in one graph.

Test 1-c was done 37 days after installation, test 3-c 19 days after installation (J. A. Schneider et al., 2008).

5.4.2. Results

Figure 5.7 shows the predicted results for total capacity, frictional capacity and base capacity of Hoogzand 1-c.

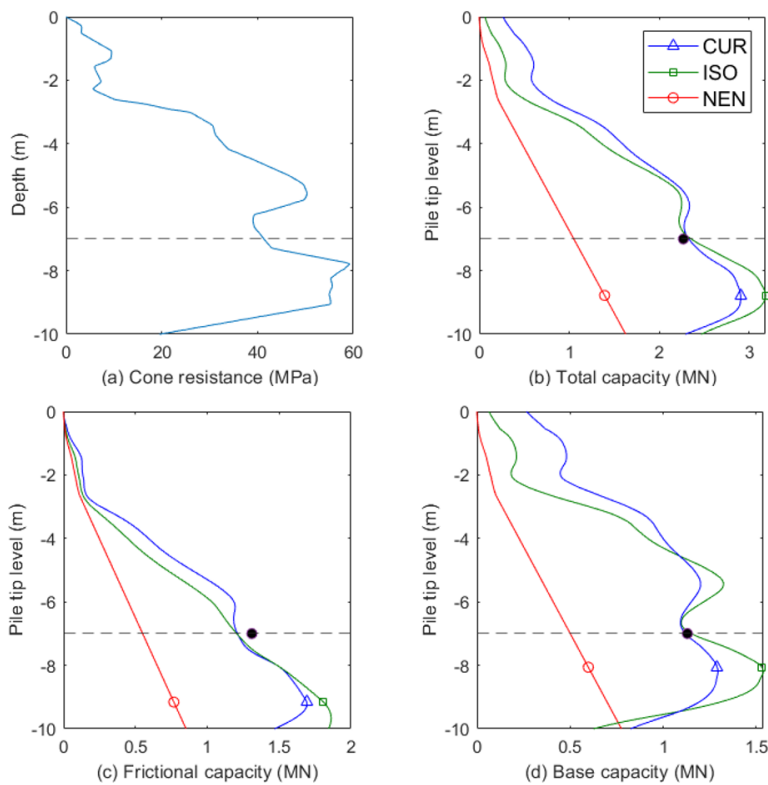


Figure 5.7: Hoogzand 1-c

Both the ISO and the CUR are predicting the capacity very well. There is hardly any disagreement between the two methods for both base and frictional capacity at the installed level. The NEN, again, is very off in capacity prediction and predicts less than 40% of the measured capacity.

Fig. 5.7c shows a big difference in shaft capacity after the dense zone. The CUR implies most of the frictional capacity to be caused by friction near the pile, while the CUR assumes a more gradual increase nearing the pile. The ISO still accounts for the effect of the strong zones up the pile, while the CUR neglects their importance, causing a large difference in capacity predictions.

The measured PLR was 0.66 (J. A. Schneider et al., 2008) and contribution of measured base capacity on the total capacity is 46.3%, while that of the shaft capacity is 53.7%. The results of performance calculations are given in table 5.6.

	1-c			3-c				1-c	3-c
	CUR	ISO	NEN	CUR	ISO	NEN			
$Q_{b,c}/Q_{b,m}$	0.99	1.02	0.44	1.26	1.38	0.34	$Q_{b,m}(MN)$	2.44	1.95
$Q_{s,c}/Q_{s,m}$	0.92	0.92	0.42	1.12	0.88	0.40	$Q_{s,m}(MN)$	1.31	0.95
$Q_{t,c}/Q_{t,m}$	0.95	0.97	0.43	1.19	1.13	0.37	$Q_{t,m}(MN)$	1.13	1

Table 5.6: Performance of Hoogzand tests and measured capacities

Table 5.6 shows that the CUR and the ISO both predict capacities well, with the ISO obtaining a nearly perfect prediction on the total capacity.

The NEN predicts the pile unplugged during loading as $Q_{fr,i,NEN} < Q_{b,NEN}$. Also in capacity predictions, the NEN lacks significantly. The α -factors do not seem to predict pile behaviour well, especially not in this over-consolidated sand deposit.

Figure 5.8 shows the results for test 3-c, which was installed slightly higher than 1-c in a denser zone.

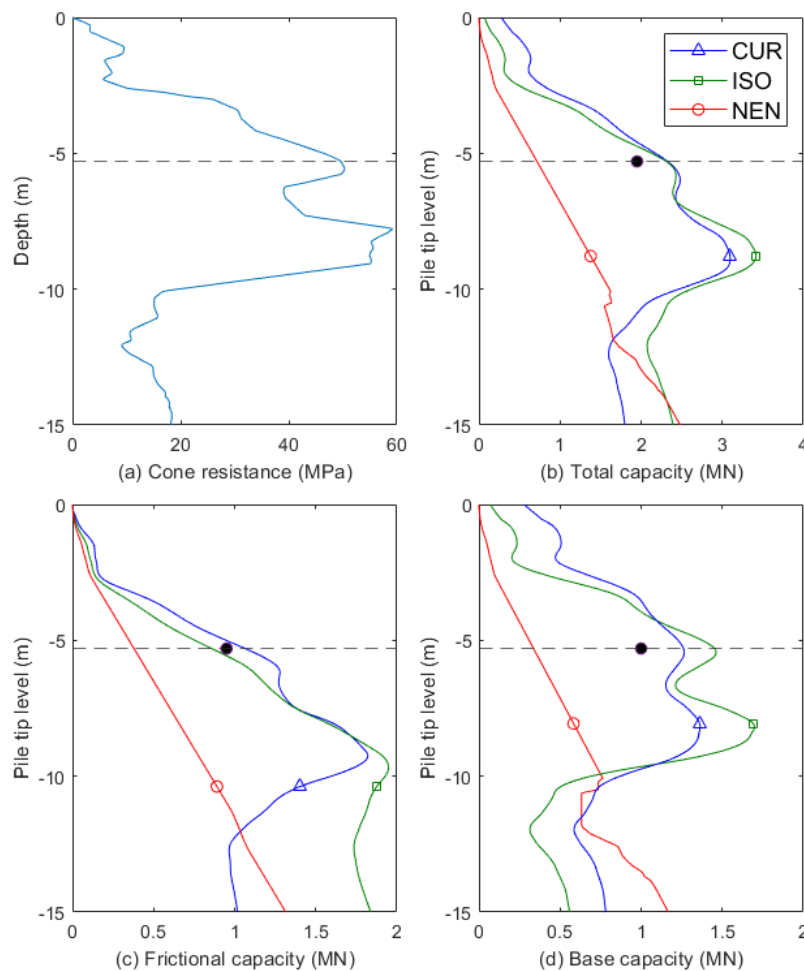


Figure 5.8: Hoogzand 3-c

The CUR and the ISO both over-predict the total capacity. The CUR over-predicts both shaft and base capacity, while the ISO strong over-predicts the base capacity which is slightly balanced by an under-prediction of frictional capacity.

Figure 5.9 shows the predicted and measured shaft friction on Hoogzand 1-c test.

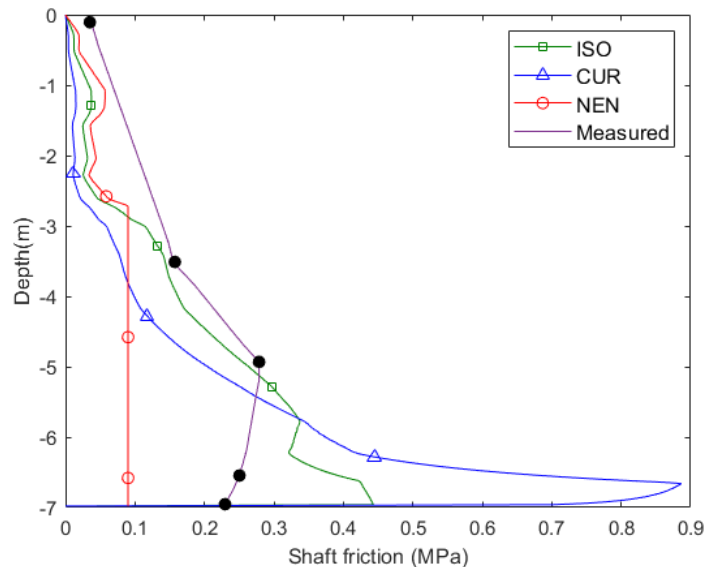


Figure 5.9: Hoogzand 1-c shaft friction profiles, measured values from JIP, 2020

It can be seen that the large friction fatigue term implied by the CUR is not apparent in the measured profile. The constant shaft friction implied by the NEN also is nowhere near the measured shaft friction. There is not an apparent reason or an explaining mechanism to limit τ_f of the NEN. The ISO is closest to the measured profile and prediction of $Q_{s,c}$ and it follows the trend that there is a higher concentration of shaft friction near the pile tip, but not an enormous amount as implied by the CUR.

5.5. Tokyo, compression

A pile test in Tokyo was done with very large diameter of $D = 2.00 \text{ m}$ and thickness $t = 0.034 \text{ m}$ ($t/D = 0.017$). It is one of the few instrumented tests with a diameter $> 1.5 \text{ m}$. The CPT profile is simplified but this is of lesser importance for base capacity as it uses an averaged cone resistance, while for shaft capacity this matters more because the area under friction profiles determines shaft capacity.

In chapter 4, the effect of increasing diameter was discussed on the CUR and the ISO. The Tokyo load test confirms the conclusion that the CUR over-predicts base capacity for high diameters. Figure 5.10 shows the simplified cone resistance and resulting base capacity.

The CUR over-predicts the measured base capacity at 30.5 m depth 2.5 times the measured capacity, with a difference of 13.2 MN . Over the whole profile, the CUR predicts a significantly higher base capacity than the ISO. The ISO over-predicts the base capacity with a factor 1.44. The measured capacity is likely lower than predicted due to the weaker zone below the pile tip. Both the CUR and the ISO average the q_c for a distance $\pm 1.5D$ above/below the pile tip, but perhaps the zone below the pile tip matters more than the zone above the pile tip because it has to resist the compressive load more.

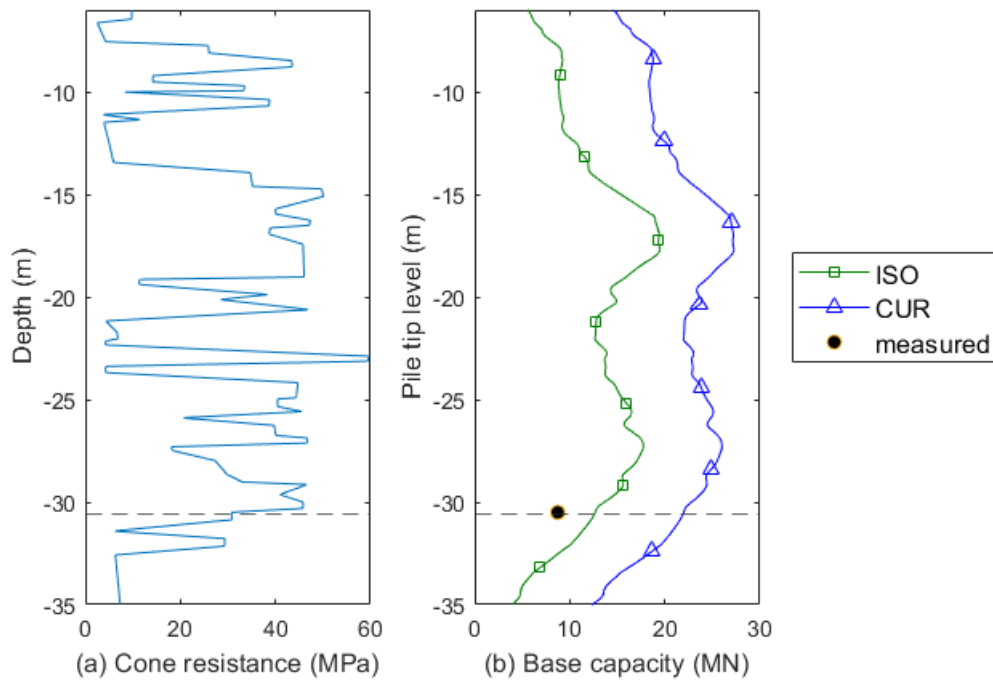


Figure 5.10: Tokyo load test cone resistance and resulting base capacity

5.6. Tension

The EURIPIDES and Hoogzand tests were also done for tension. Often this is done on the same day as a compression test. Apart from these, detailed tests done in Blessington (Ireland) by K. G. Gavin et al., 2013 show the effect of pile ageing in respect to the design methods.

For piles loaded in tension, there is no base capacity contributing to the axial capacity and $Q_t = Q_{fr}$ with Q_t defined as maximum force instead of $Q_{0.1D}$ for compression.

5.6.1. EURIPIDES and Hoogzand

Figures 5.11a, 5.11b, 5.12a and 5.8 show the results for the previous case studies on EURIPIDES and Hoogzand. The black dots are measured capacities $Q_{t,m}$ and dotted lines represent the depth to which a pile is installed. Performance calculations of $Q_{t,c}/Q_{t,m}$ is shown in Table 5.7.

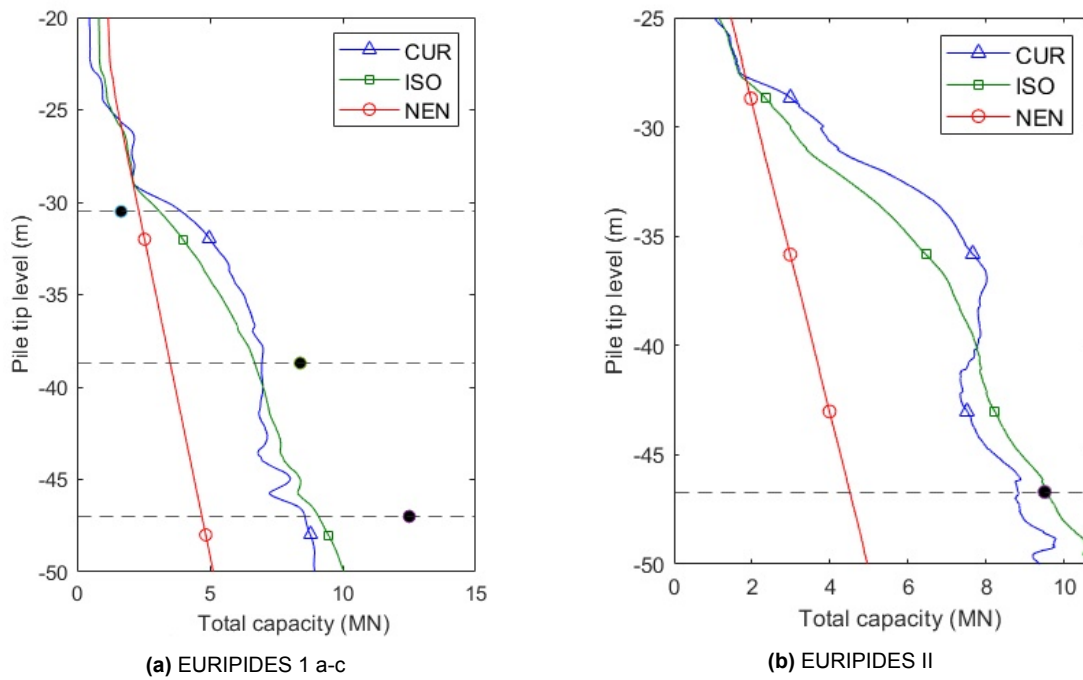


Figure 5.11: EURIPIDES capacity prediction for tension, black dots are $Q_{t,m}$

EURIPIDES test 1-a is over-predicted by all methods, notably by the CUR with a performance well over 2. The opposite is shown in tests 1-c, where the methods severely under-predict tension capacities. For the EURIPIDES tests 1-c it can be seen that there is a strong increase in capacity for piles that are installed deeper. This depth trend is caught best by the ISO method.

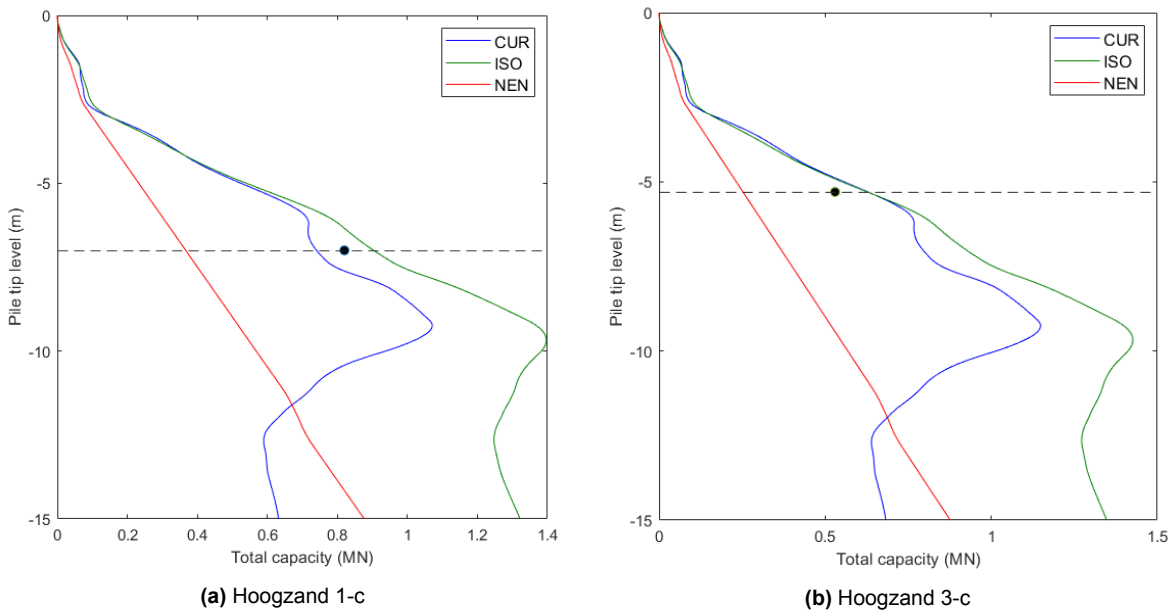


Figure 5.12: Hoogzand capacity prediction for tension, black dots are $Q_{t,m}$

$Q_{t,c}/Q_{t,m}$	CUR	ISO	NEN
EURIPIDES I-a	2.37	1.87	1.40
EURIPIDES I-b	0.83	0.80	0.42
EURIPIDES I-c	0.69	0.73	0.38
EURIPIDES II	0.93	1.01	0.47
Hoogzand 1-c	0.90	1.10	0.45
Hoogzand 3-c	1.19	1.18	0.48
Average	1.15	1.12	0.60
Stand. dev.	0.56	0.37	0.36

Table 5.7: $Q_{t,c}/Q_{t,m}$ results on tension tests

Table 5.7 shows performance calculations and averages for the discussed Dutch tension tests. It can be seen that the ISO does best, but that the CUR is not much worse. The ISO does however a smaller tendency to deviate from its average, while the CUR has a standard deviation of over 0.5 which is significant. The NEN under-predicts all tests except EURIPIDES I-a.

5.6.2. Blessington

The effect of pile ageing for piles in tension was tested by K. G. Gavin et al., 2013 for 4 piles with $L = 7\text{ m}$, $D = 0.34\text{ m}$, $t = 0.014\text{ m}$. The q_c profiles for each of the individual tests were equal enough to allow for averaging into 1 average q_c profile. Each of the 4 piles was tested later for capacity, given in Tab. 5.8.

Figure 5.13 shows the q_c profile and predicted capacities of the methods over depth.

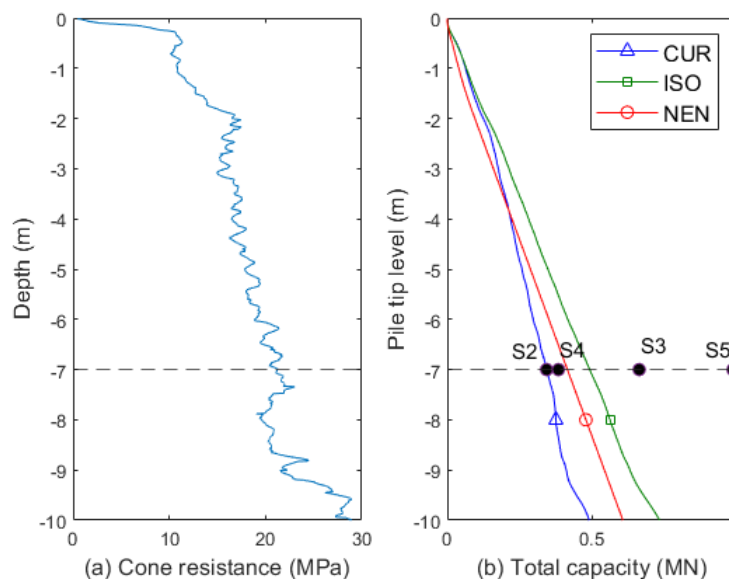


Figure 5.13: q_c profile and capacity predictions for Blessington tests S2-S5 (tension)

Table 5.8 shows the measured capacities and performance calculations for the methods.

Test	Time (days)	$Q_{t,m}$ (kN)	$Q_{t,c}/Q_{t,m}$ CUR	$Q_{t,c}/Q_{t,m}$ ISO	$Q_{t,c}/Q_{t,m}$ NEN
S2	2	344	1.00	1.43	1.19
S3	12	665	0.52	0.74	0.62
S4	30	385	0.89	1.28	1.07
S5	219	990	0.35	0.50	0.42
		Average	0.69	0.99	0.82
		Standard dev.	0.27	0.38	0.32

Table 5.8: Data and performance calculations Blessington tests

Figure 5.13a shows a relatively linear q_c profile from 10 MPa on ground level to 30 MPa at 10 m depth. Consequently the predicted capacity profiles per method are also linear by approximation. From $z = 4$ m down, the CUR predicts lowest capacity, NEN in the middle and ISO highest capacity profile.

Piles S2, S3 and S5 show increasing capacity as time of testing increases, except for pile S4. Pile S4 was driven in a more unplugged state and significantly showed less axial capacity than pile S3 (tested earlier).

The results of the performance calculations show that, on average, the ISO performs best and CUR performs worst. However, the ISO also has a bigger tendency to deviate for this case. Pile S5 was severely under-predicted by all methods. The CUR under-predicts S5 by 75%, the NEN with 58% and the ISO does best but still with an under-prediction of 50%. Apart from pile S1, the CUR under-predicted each pile in capacity.

5.7. Accuracy on performance and plugging prediction

Multiple factors influence the accuracy of performance calculations. Also, the PLR used in the ISO requires an indication of the degree of plugging before installation. It is evaluated what effect this change of predicted and measured PLR has on the capacity.

5.7.1. Performance calculations

There is certain ambiguity in the Q_c/Q_m tables in this chapter, as certain definitions and approaches differ throughout the data and literature of this chapter. There are different ways to obtain $Q_{t,m}$, often it is defined as the load to create a displacement of 10% of the diameter (denoted as $Q_{0.1D}$), but it can also be extrapolated from a load test that did not reach failure. Different discretisations and averaging of q_c profiles (such as smoothing, choosing lower bound values or picking a q_c every 1 m) also may strongly influence results of Q_c , as well as certain other assumptions (such as correlating/measuring σ'_v or assuming $\sigma'_v = \gamma' \cdot z$ with $\gamma' = 10 \text{ kN/m}^3$) and rounding off. Sometimes, the upper part of a q_c profile is neglected in capacity calculations if it consists of weak zones assumed not to contribute to the capacity.

An example is the value $Q_{t,m}$ of EURIPIDES 1-c compression, where ICP, 2005 note $Q_{t,m} = 20.4 \text{ MN}$, while J. A. Schneider et al., 2008 state $Q_{t,m} = 19.5 \text{ MN}$ and Yang et al., 2016 state $Q_{t,m} = 18.8 \text{ MN}$. All three sources define $Q_{t,m}$ when a displacement of 0.1D has occurred. Another example is EURIPIDES 1-a tension, where J. A. Schneider et al., 2008 state $Q_{t,m} = 3 \text{ MN}$ and Yang et al., 2016 state $Q_{t,m} = 1.66 \text{ MN}$, while both adhering the same definition of $Q_{t,m}$ (for tension, $Q_{t,m} = Q_{fr,m} = Q_{max,m}$).

Work from Yang et al., 2016 has data on all case studies shown here, while also including load-displacement curves and performance calculations, this was judged most coherent and applicable to this research.

5.7.2. PLR_{ISO}

The ISO makes use of a statistical PLR incorporated in shaft and frictional capacity (Fig. 2.15 and eq. 2.24). This implies the calculating the capacity with a plug without knowing the PLR . The effect of this statistical PLR was observed to see how the approximation of this calculated PLR_c matters.

Table 5.9 shows the measured PLR and the calculated PLR from the ISO method for the Dutch case studies. In nearly all cases, except Hoogzand I, the calculated PLR under-predicts the measured PLR (meaning more plugging, as a lower PLR indicates stronger development of the plug), occasionally as much as 12% between the two PLR 's, but in these cases often within a 10% limit.

		PLR_m	PLR_c	PLR_c/PLR_m
EURIPIDES	I-a	0.99	0.87	0.88
	I-b	0.97	0.87	0.89
	I-c	0.96	0.87	0.90
	II	0.95	0.87	0.91
Hoogzand	I	0.66	0.72	1.09
	III	0.77	0.71	0.93

Table 5.9: PLR measured (from J. A. Schneider et al., 2008) compared to calculated PLR from the ISO

To see if under-prediction matters, the PLR in Hoogzand III was replaced with the measured PLR to back-calculate the capacity. The result is shown in Figure 5.14.

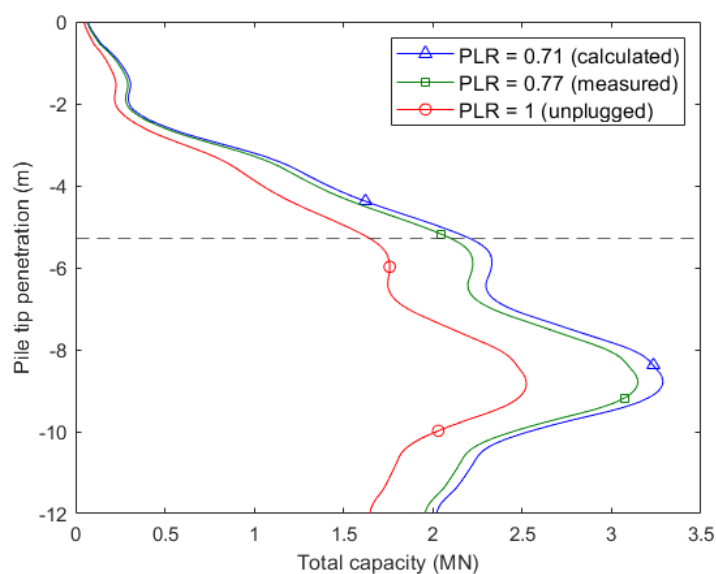


Figure 5.14: Variations of PLR on Q_{iso} for Hoogzand III

The capacity related to PLR_c ($= 0.71$) divided by capacity related to PLR_m ($= 0.77$) gives 0.952, indicating a 4.8% difference, while $PLR_c/PLR_m = 0.93$, or a 7% difference. It can be seen in the whole trajectory of Fig 5.14 the predicted capacities decreases when PLR decreases over the whole trajectory.

5.8. Future load tests

There is still considerable improvement on the design of pipe piles, and it is likely that tests in the future will be done to optimise capacity and plugging predictions. Chapter 4.6 showed that the biggest uncertainty for open-ended piles in Dutch soil deposits comes from looser sands and/or very large diameter. There are quite some good tests available in dense/high q_c sands, but hardly any in very variable or weaker deposits, as may be common in the Netherlands.

The ISO's base capacity expression is accurate and robust enough for varying soil conditions and parameters to given a reasonable prediction. The CUR's base capacity shows significant over-prediction in weaker soil and/or larger diameter. However, obtaining an accurate shaft capacity is a key factor in good performance as it often of the larger share of total axial capacity, especially for deeper piles.

Also the degree of plugging is essential to measure. The IFR is the best way indicator of (the degree of) plugging, but it is realised this might be difficult to measure in the field and implement in a design code. Incorporating plugging during installation may start with the PLR , an easier parameter to measure.

5.9. Summarised conclusions case studies

- *Trends and sensitivity.* Most of the trends and sensitivity analyses from chapter 4 are reflected in the case studies. Most notable are the ISO's depth trend in capacity due to the depth trend in shaft capacity, the CUR's asymptotic behaviour in capacity and the CUR being highest of the three in shallow sands.
- *Performance, compression and tension.* Of the three methods, the ISO performed best for Dutch soil conditions, while NEN performed the worst. The NEN often severely under-predicts pile capacity in dense sands, but this does not necessarily mean it is conservative. The α -factors, the limiting values and the plugging condition are a poor way of predicting axial capacity. The CUR is generally more off than the ISO. Multiple factors influence performance calculations and for the same test different performance results can be obtained.
- *Shaft friction and capacity.* The extreme friction fatigue effect of the CUR does not appear in any of the measured shaft friction profiles. Shaft friction does tend to increase near the pile tip. Neither does the limiting of shaft friction by the NEN appear in any of the measured profiles. When q_c is relatively constant, the ISO predicts a depth trend in shaft capacity where the CUR predicts an asymptotic profile. Measured values indicate that the ISO is correct on this trend. This is important as shaft capacity has a greater contribution on the capacity the deeper a pile is installed. The ISO is, in general, most accurate in predicting shaft capacity.
- *Tension.* In tension, the ISO performs best. This is true for the Dutch tests and the Blessington tests. The methods differ even more during tension because it only includes shaft capacity and denser zones farther from the pile tip have different contributions per method.
- *Soil conditions.* All the design methods seem to over-predict a pile's axial capacity in gravel. The CUR and ISO both predict the capacity in the over-consolidated sand from Hoogzand well. From the data available, the ISO seems to work best in Dutch soil conditions.
- *Installation effects.* Correcting for residual loads does not influence total measured capacity, but reduces shaft capacity and increase base capacity. The design methods are poorly suited to account for pile ageing, but this is also includes many uncertainties.
- *Future load tests.* The biggest uncertainties appear in typical Dutch soil conditions (variable and relatively weak deposits) and for very large diameter. Performance calculations and comparisons with measured shaft friction profiles show that, in order to optimize design, the biggest gain can be made in obtaining an accurate approximation of the shaft resistance. If pile dimensions (D and L) are increased, inaccurate shaft friction profiles become more notable in capacity predictions.
- *Base resistance and capacity.* The ISO predicts higher q_b in strong zones than the CUR which is not always correct (e.g. Hoogzand 1-c). The large capacity increase by an increase in diameter (the diameter effect) for the CUR partly caused by a big increase in base capacity, confirmed by the Tokyo test. Base capacity becomes a smaller part of the total capacity as the pile is installed deeper.
- *Plugging in design.* The ISO uses a statistical *PLR* to predict capacity before installation. Often, measured *PLR*'s after installation are off within a 10% bound. The capacity with this 'corrected' *PLR* for Hoogzand 1-c changed with about 5%, which is not extremely influential. This in combination with the conclusions above makes the ISO method currently the best way to incorporate the effect of plugging in the design of open-ended steel pipe piles.

6

Recommendations and conclusion

This thesis focused on the following research question. *How can the design of open-ended pipe piles in the Netherlands be optimised?*

The research questions was broken down into 4 sub-questions.

1. How is the capacity of pipe piles obtained and how do design methods calculate axial capacity

Depending on the degree of plugging, open-ended piles obtain their capacity from components on the interior and exterior of the pile. The degree of plugging suggests a degree of soil displacement, and plugging greatly influence the capacity of an open-ended pile, as a fully plugged pile behaves similar to a full displacement pile. Measuring plugging can be done with the Incremental Filling Ratio or Plug Length Ratio. The Incremental Filling Ratio better indicates the degree of plugging but is harder to measure. Many factors influence plug formation. Notable is the diameter which inherently is also strongly related to an open-ended pile's capacity. However, plugging is often poorly accounted for in a design method. Often, the effect of the plug is not individually accounted for in a design method but included in empirical factors in a method's formulations. Plugging can occur during loading or installation and influences piles in compression as well as tension.

Design methods empirically approach the capacity of a pile with formulations for shaft and base capacity. The NEN is a reductive method and considers a fully plugged or unplugged condition for loading. It directly relates q_c to shaft friction with α factors and limiting values, implying no friction fatigue. The origin of this constant α_s is unknown, as is other data that support the NEN's formulations.

The CUR considers a large friction fatigue component, resulting in almost all shaft friction to be concentration near the pile tip. It considers only a fully plugged condition in its base resistance.

The ISO is a new international method that combines other methods that have risen internationally. It incorporates a predicted plug length in both shaft and base capacity.

Base resistances for CUR and ISO are only dependent on $q_{c,avg}$ and pile dimensions D and t . Base resistance of the NEN is determined by the Koppejan averaging method, which assumes failure to occur on the weakest zones below and above the pile tip.

2. What are the characteristics for capacity, shaft resistance and base resistance of the discussed design methods?

The three methods vary significantly in predicted capacities. In general, the CUR predicts highest capacities for shallow depths and/or low q_c , while the ISO often predicts highest capacity at deeper depths. This is because the CUR generally predicts a higher base capacity, while the ISO has a depth trend in shaft capacity. The NEN is often lowest, though this does not mean it is necessarily conservative.

Shaft friction profiles indicate that the CUR assumes most shaft friction to be close to the pile tip, while the NEN assumes a rather constant spread along the pile length and the ISO assumes a larger concentration near the pile tip but not as extreme as the CUR. This concentration of shaft friction near

the pile tip causes a large friction fatigue effect for the CUR. This implies that most of the shaft capacity comes from the zone near the pile tip, and that weaker/stronger zones further from the pile tip hardly contribute to shaft capacity. Shaft friction for the NEN and ISO are more evenly distributed along the pile length.

For the CUR q_b/q_c increases with decreasing q_c , which causes a significant over-prediction for base resistance in looser sands. For the ISO, q_b/q_c is constant, a relationship confirmed by research (JIP, 2020).

The shaft friction profile for the CUR causes the shaft capacity over depth to be asymptotic or slightly sloping. This is because the CUR assumes most shaft friction concentrated near the pile tip and the length of the pile itself is less significant, whereas the NEN and ISO assume it to be distributed along the length of the pile and so the frictional capacity increases with depth. The ISO has a stronger depth trend. The NEN's shaft friction profile is by approximation linear often due to limiting values. There is no reason to put limiting values on τ_f and q_b , because there is no explaining mechanisms why nor does the NEN give any. The NEN often severely under-predicts capacity because of the linear capacity trend caused by the limiting values. This does not make the NEN conservative.

Tension shows the same capacity trends as compression, but without base capacity and a magnitude change for shaft friction.

3. What are the implications of these methods for varying parameters and soil conditions?

As the diameter is increased, the CUR's capacity significantly enlarges compared to that of the NEN and ISO. There are two reasons for this diameter effect of the CUR:

1. An increase in diameter causes an increase in shaft friction profiles even though there is less soil displacement around the pile. This causes the area under the shaft friction profile to be further enlarged. This causes an additional increase from shaft friction to shaft capacity. Locally dense zones give a peak in the frictional capacity profile.
2. The CUR's relationship of q_b/q_c becomes more prominent in base capacity when diameter is enlarged. It was already concluded that q_b/q_c significantly increased for the CUR while that of the ISO remains constant. This causes over-prediction of base capacity in looser sands (or low q_c). This effect is enlarged for larger diameters, because a diameter increase gives an increase to the power 2.

Changing the t/D ratio of the CUR so it suits the $t/D > 1/60$ condition increases this effect. If $t/D > 1/60$, the thickness has to be increased compared to standard pile dimensions and, in general, a thicker pile has higher capacity. An underlying reason is that the CUR is only based on 2 different values for diameter (0.34 m and 0.76 m). An increase in diameter for the NEN gives lower base resistance as the averaging trajectories increase in length and thus minimum values become more influential over length. For diameters > 1 m, the NEN and CUR disagree so much that it can be argued if these methods should even be accepted in Dutch standards for these diameters. The CUR states it applies to piles for diameters up to 3 meters, which would lead to too big uncertainties and structural risks due to over-prediction.

In dense sands, the ISO and CUR are in agreement for piles with $D \approx 0.7$ m. Varying the diameter, the CUR becomes easily lowest or highest of the three methods due its sensitivity. The NEN severely under-predicts the capacity in dense sands. In looser or locally dense sands, the diameter effect of the CUR is increased. The NEN can predict capacities higher than the CUR and ISO due to its linear behaviour in shaft capacity. Consequently, the NEN neglects/overlooks locally dense zones in capacity predictions.

4. How effective are these methods and their characteristics based on real load tests?

The trends from synthetic q_c can be seen in real CPT's. With the case studies it is confirmed that the CUR generally under-predicts capacities for long piles. The ISO generally performs best. The ISO appears to work effectively in two Dutch load tests. An important aspect as to why ISO in general performs better than the CUR is a stronger depth trend in shaft capacity.

The shaft friction profile of the CUR with the extreme friction fatigue component near the pile tip was not seen, not even in the over-consolidated sand of Hoogzand. In general, the ISO seems to be most right at predicting shaft friction with a larger concentration near the pile tip which decreases up the shaft.

All discussed design methods are unsuited to predict shaft capacity in sand with high gravel content. The base capacity however, especially the ISO's, is predicted adequately. A correction for residual stress does not change total measured capacity but increases base capacity and reduces shaft capacity, leading to an even bigger over-prediction of shaft capacity.

The ISO makes use of a predictive *PLR*. For available Dutch data, this *PLR* deviates with a little over 10%. A corrected capacity for Hoogzand III with the measured *PLR* gives about 5% reduction in capacity. This is a reasonable deviation, and this is an improvement in incorporating plugging in the design of open-ended piles.

How can the design of open-ended pipe piles in the Netherlands be optimised?

Ideally one efficient and well-performing method would be the norm instead of different norms/options as is currently the case (NEN and CUR). The NEN and CUR both differ enormously in approach and assumptions. Consequently, the NEN and the CUR were shown to vary with 8.5 *MN* in capacity and with a threefold difference for the same pile in the same soil. With the demonstrable limitations that were discussed in detail, it raises the question if any of the two are suited for designing open-ended piles.

The ISO is in many ways an improvement on current design methods. It is based on a larger and more varying database, collects formulations from former methods that were proven effective and different formulations are evaluated and optimised. The author argues the ISO should be adopted as current standard for open-ended pile design in the Netherlands. An evaluating committee on a potential improvement of current design norms is set up, but there is no need to set up a new or improved method.

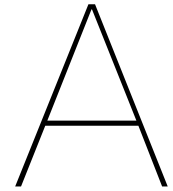
The method from the CUR is currently scheduled to be adopted in the NEN, but according to this research should come with the following changes or remarks

- The condition that piles should have $t/D > 1/60$ be removed. There is no argumentation or relevance why this condition is a prerequisite of the CUR.
- The condition that the CUR applies to piles with diameter up to 3 *m* should either be reduced to 1 *m* and/or come with the notion that it over-predicts capacities for piles with diameter larger than 1 *m*.

Plugging is very essential for predicting the axial capacity of a pile. Optimising the design of open-ended piles starts with incorporating plugging in shaft and base resistance. The best knowledge there is so far is collected in the ISO.

However, the ISO is still far from perfect. There still is considerable uncertainty of shaft friction profiles and installation effects (evaluated were residual loads in gravel and pile ageing) show the methods still fail to catch these accurately. Also, the complexities from Dutch soils requires additional load tests to get a better understanding on the workings of open-ended piles. There is a reasonable amount of load tests available in dense sands, but only the EURIPIDES tests are representative for Dutch soil conditions. More tests with a considerable Holocene top layer would be recommended, ideally with larger diameters. Especially for piles with deeper lengths, predicting shaft capacity right proves to be the leading factor in good performance. The biggest gain is to be made by accurate measurements of shaft friction, as good prediction of shaft capacity is often the deciding factor in the performance of a method.

Besides open-ended piles, the ISO also applies to closed-ended piles. It may be worth researching how this method behaves on closed-ended piles in the Netherlands.



Summarised equations per design method

$$Q = Q_b + Q_{fr} \quad (\text{A.1})$$

$$Q_{fr} = \pi D_0 \int_0^L \tau_f(z) dz \quad (\text{A.2})$$

$$Q_b = A_b \cdot q_b = (0.25\pi D_o^2) q_b \quad (\text{A.3})$$

$$\sigma'_v(z) = \int_0^z \gamma'(z) + p(0) dz \quad (\text{A.4})$$

NEN 9997-1

The equations below can be found in chapter 7.6.2.3 ("*Uiterste draagkracht op druk gebaseerd op resultaten van grondonderzoek*") from NEN 9991-7, 2017.

$$Q_{nen} = Q_{fr} + \min(Q_b; Q_{fr,i} + Q_{ann}) \quad (\text{A.5})$$

Shaft

$$\tau_f = \alpha_s \cdot q_{c,mod} < 12 \quad (\text{A.6})$$

$$Q_{fr} = \pi D \int_0^L \tau_f(z) dz \quad (\text{A.7})$$

Base

$$Q_b = A_b \cdot q_{b,max} \quad (\text{A.8})$$

$$q_b = \frac{1}{2} \cdot \alpha_p \cdot \beta \cdot s \left(\frac{q_{c,I,avg} + q_{c,II,avg}}{2} + q_{c,III,avg} \right) \quad (\text{A.9})$$

Some notes on the equations provided by NEN 9997-1

- In equation A.9, β is a pile class factor (not the friction ratio)
- Parameters $q_{c,I,avg}$, $q_{c,II,avg}$ and $q_{c,III,avg}$ follow minimum rules based on trajectories up or below the pile tip for a lengths 4 to 8 times the diameter, see NEN 9997-1.

CUR 2001-8

The equations below have been retrieved from the CUR commission C18 report, titled *CUR Rapport 2001-8 Bearing capacity of steel pipe piles*, as a design method for piles in sand.

Shaft

$$\tau_f = q_c 0.08 (\sigma'_v/p_a)^{0.05} (h/R^*)^{-0.90} \quad \text{with } h/R^* \geq 4 \quad (\text{A.10})$$

$$\tau_f = q_c 0.08 (\sigma'_v/p_a)^{0.05} (h/R^*)^{-0.90} (h/(4R^*)) \quad \text{with } h/R^* < 4 \quad (\text{A.11})$$

$$h = L - z \quad (\text{A.12})$$

$$R^* = 0.5 D_0 (DR)^{0.5} = (R_0^2 - R_i^2)^{0.5} \quad (\text{A.13})$$

Base

$$Q_b = (\pi D_0^2/4) q_b < \left(\pi D_i \int_0^L t_{f,i}(z) dz + Q_{b,wall} \right) \quad (\text{A.14})$$

$$q_b = p_a 8.5 (q_{c,avg}/p_a)^{0.5} (DR)^{0.25} \quad (\text{A.15})$$

$$q_{c,avg} = \frac{1}{3D_0} \int_{L-1.5D_0}^{L+1.5D_0} q_c(z) dz \quad (\text{A.16})$$

$$DR = 1 - (D_i/D_0)^2 \quad (\text{A.17})$$

Some notes on the equations provided by the CUR 2001-8

- Equation A.11 contains a reduction factor that is given in the CUR as $(h/4R^*)$, but this should arithmetically be $(h/(4R^*))$, as $(h/4R^*)$ effectively means $((h/4)R^*)$ or $(0.25 \cdot hR^*)$. Plotting with $(h/4R^*)$ gives a highly unrealistic τ_f and makes it not a reduction factor (< 1) anymore.
- Equation A.16 is the mathematical representation of determining the average q_c of a distance $1.5D$ above and below the pile tip level. It is equal to q_p of the ISO/API method.
- The condition in equation A.14 is called the plugging condition. The CUR 2001-8 notes that the condition of equation A.14 is met after driving a depth of $8D$, thereby saying that the pile is fully plugged after a driven depth of $8D$.
- Note how equation A.17 for DR is equal to equation A.21 for A_{re} when FFR or PLR in equation A.21 is equal to 1.

ISO

The equations below are retrieved from the Joint-Industry Project report, titled *Unified, unaffiliated CPT-based method for axial pile capacity calculation*

Shaft

$$\tau_f = (f_t/f_c)(\sigma'_{rc} + \Delta\sigma'_{rd}) \tan 29^\circ \quad (\text{A.18})$$

$$\sigma'_{rc} = \frac{q_c}{44} A_{re}^{0.3} [\max(1, h/D)]^{-0.4} \quad (\text{A.19})$$

$$\Delta\sigma'_{rc} = \frac{q_c}{10} \left(\frac{q_c}{\sigma'_v} \right)^{-0.33} \frac{d_{CPT}}{D} \quad (\text{A.20})$$

$$A_{re} = 1 - FFR \cdot (D_i/D_0)^2 \approx 1 - PLR(D_i/D_0)^2 \quad (\text{A.21})$$

$$PLR = L_{plug}/L \approx \tanh \left[0.3 \left(\frac{D_i}{d_{CPT}} \right)^{0.5} \right] \quad (\text{A.22})$$

$$f_t/f_c = 1 \text{ (compression) or } 0.75 \text{ (tension)}, \quad d_{CPT} = 0.0356 \text{ m} \quad (\text{A.23})$$

Base

$$Q_b = q_{b0.1} (\pi D_0^2/4) \quad (\text{A.24})$$

$$q_{b0.1} = (0.12 + 0.38 A_{re}) q_p \quad (\text{A.25})$$

$$q_p = \frac{1}{3D_0} \int_{L-1.5D_0}^{L+1.5D_0} q_c(z) dz \quad (\text{A.26})$$

B

Database overview of pile load tests

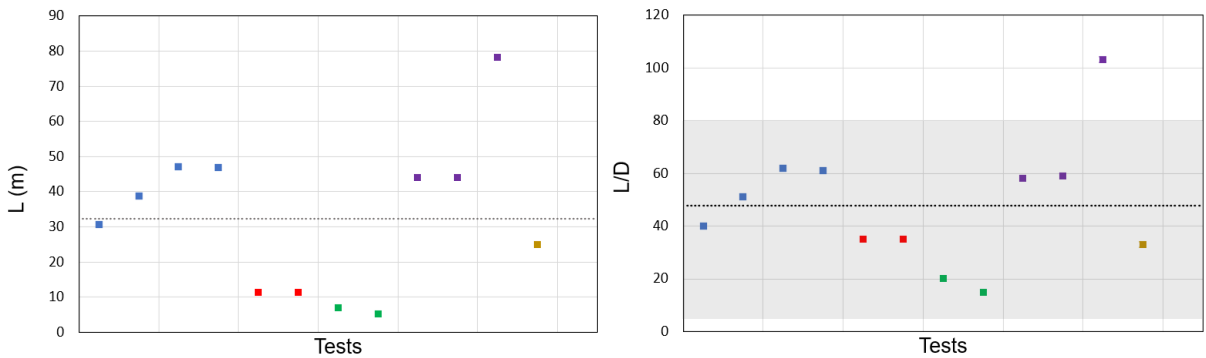
B.1. CUR

CUR data compression open end						
Site	Test	L/D	t/D	D (mm)	t (mm)	L (m)
Euripedes	I-30-c	40	0.047	760	36	30.7
	I-38-c	51	0.047	760	36	38.7
	I-47-c	62	0.047	760	36	47
	II-47-c	61	0.047	760	36	46.8
Dunkirk	CS	35	0.059	324	19	11.3
	CL	35	0.04	324	13	11.3
Hoogzand	I-c	20	0.045	356	16	7
	III-c	15	0.056	356	20	5.3
Jamuna	PS1	58	0.05	760	38	44
	PS3	59	0.058	760	44	44
	PS 1-D	103	0.05	760	39	78.3
Ras Tanajib II	25a	33	0.051	763	39	25.08
Average		47.67	0.050	620.25	31.00	32.46

Table B.1: Database on which the CUR is based for compression, from CUR, 2001

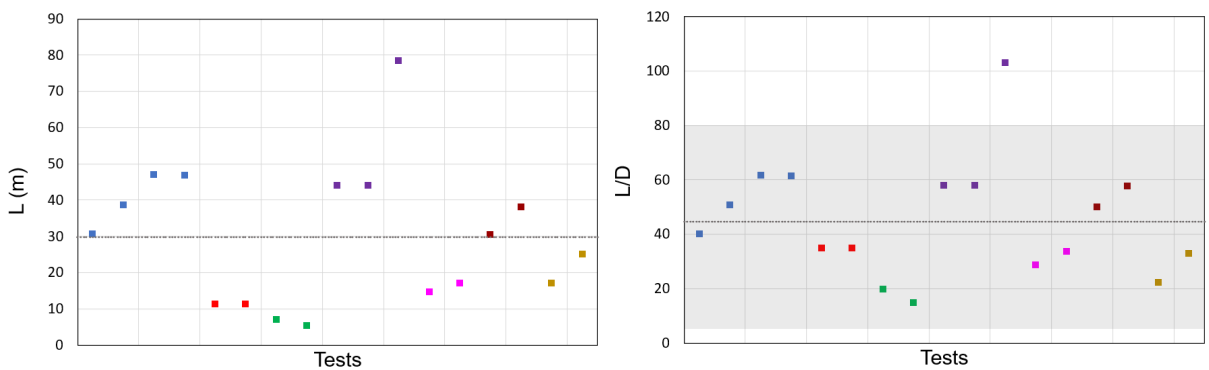
Site	Test	L (m)	D (m)	t (m)	days	t/D	L/D
EURIPIDES	I-30-t	30.7	0.762	0.036	7	0.047	40.3
	I-38-t	38.7	0.762	0.036	2	0.047	50.8
	I-47-t	47	0.762	0.036	12	0.047	61.7
	II-47-t	46.8	0.762	0.036	7	0.047	61.4
Dunkirk	CS	11.3	0.324	0.019	186	0.059	34.9
	CL	11.3	0.324	0.013	173	0.040	34.9
Hoogzand	I-t	7	0.356	0.016	37	0.045	19.7
	III-t	5.3	0.356	0.02	19	0.056	14.9
Jamuna	PS1	44	0.76	0.038	9	0.050	57.9
	PS3	44	0.76	0.044	11	0.058	57.9
	PS1-D	78.3	0.76	0.038	4	0.050	103.0
Padre Island	A	14.6	0.508	0.013	2	0.026	28.7
	A	17.1	0.508	0.013	1	0.026	33.7
Leman Bank	AD	30.5	0.61	0.016	80	0.026	50.0
	BD	38.1	0.66	0.032	80	0.048	57.7
Ras Tanajib	17a	17	0.763	0.039	10	0.051	22.3
	25a	25	0.763	0.039	102	0.051	32.8
Average		29.8	0.618	0.028	44	0.046	44.9

Table B.2: Database on which the CUR is based for tension, from CUR, 2001



(a) Diameters - dotted black line is average **(b)** L/D ratios - shaded area is 5 – 80D to which the CUR applies

Figure B.1: Database CUR for open-ended piles loaded in compression - colours indicate sites



(a) Diameters - dotted black line is average **(b)** L/D ratios, shaded area is 5 – 80D to which the CUR applies

Figure B.2: Database CUR for open-ended piles loaded in tension - colours indicate sites

B.2. ISO

Site	Test	D	L	IFR	A_{re}	σ_{v0}	$q_{b0.1}$	$q_{c,tip}$	$q_{1.5D}$	q_{dutch}	q_{LP}
Dunkirk	Csa	0.32	11.3	0.45	0.65	141	7	26.7	24	21	20.7
	Cla	0.32	11.3	0.48	0.59	141	6.1	26.7	24	21.8	20.7
EURIPIDES	I30c	0.76	30.5	0.99	0.19	320	12.3	61.5	60.08	55	60.2
	I38c	0.76	38.7	0.9	0.26	403	9.9	50.8	50.8	47.3	50.8
	I47c	0.76	47	0.89	0.27	488	15.3	65.9	66.4	53.1	63
	II47c	0.76	46.7	0.82	0.33	477	16	63.3	63.1	53.4	63
	Ia	0.76	8.5	0.99	0.19	70.9	9.6	62.2	60.9	55	58.6
	IbC2	0.76	16.7	0.9	0.26	404.2	9.6	51.4	51.2	45.7	51.3
	IcC3	0.76	25	0.89	0.27	488.7	15.5	63.6	66.9	50.8	61.9
Hoogzand	I	0.36	7	0.66	0.45	100	10.9	37.7	42.3	38.7	32.9
	III	0.36	5.3	0.77	0.39	82	11.2	45.5	45.5	39.1	35.4
Pigeon	OEP	0.36	7	0.8	0.46	94	5.9	19.5	19.7	18.4	20.5
Rastanajib	25a	0.76	25	1.13	0.09	306	12.3	77.1	86.8	75	85.9
Shanghai	ST1	0.91	79	0.8	0.27	637	5.9	23.3	23.3	23.3	23.2
	ST2	0.91	79.1	0.85	0.22	637	5.1	23.3	23.3	23.3	23.2
Lafayette	-	0.66	31	0.7	0.5	340	7.4	25	26.5	22.1	25
Tokyo P Bay	TP4	1.5	73.5	1	0.07	661.5	8.9	80.7	84.4	57.2	72
	TP5	1.5	86	1	0.07	774	6.4	42.1	47.9	36	41
Tokyo	TP	2	30.6	1.08	0.01	275	2	30.4	23.9	9.7	21.7

Table B.3: ISO database for determination of base resistance

B.3. Collected pile load tests from Yang et al., 2016

Below is a table based on work from Yang et al., 2016, that might be used as a collection of tests on circular open-ended steel pipe piles for further reference or research.

Location	Test	D (m)	t (m)	L (m)	Age (days)	average IFR
Mobile Bay	AL1	0.324	0.0254	15.2	-	0.71
Mobile Bay	AL2	0.324	0.0254	42.7	-	0.71
ABEF Foundation	7	0.5	0.09	9	-	0.73
ABEF Foundation	8	0.5	0.09	7.5	-	0.73
Hoogzand	1-C	0.356	0.016	7	37	0.66
Hoogzand	3-C	0.356	0.02	5.3	19	0.77
Hound Point	P(0)-C	1.22	0.0242	26	21	0.95
Dunkirk	C1-C	0.457	0.0135	10	68	0.78
Euripides	Ia	0.763	0.0356	30.5	7	0.99
Euripides	Ib	0.763	0.0356	38.7	2	0.97
Euripides	Ic	0.763	0.0356	47	11	0.96
Euripides	II	0.763	0.0356	46.7	6	0.95
Tokyo Bay	TP	2	0.0306	30.6	52	1
Drammen	16-P1-11	0.813	0.0125	11	2	0.88
Drammen	25-P2-15	0.813	0.0125	15	2	0.88
Drammen	25-P2-25	0.813	0.125	25	2	0.88
Shanghai	ST-1	0.914	0.02	79	23	0.8
Shanghai	ST-2	0.914	0.02	79.1	35	0.85
Pigeon Creek	2	0.356	0.032	7	4	0.83

Table B.4: Collected database of open-ended tests in compression from Yang et al., 2016

Location	Test	D (m)	t (m)	L (m)	Age (days)	average IFR
Dunkirk	CL-T	0.324	0.0127	11.3	175	0.72
Dublin	S2	0.34	0.014	7	2	0.73
Dublin	S3	0.34	0.014	7	13	0.73
Dublin	S5	0.34	0.014	7	220	0.73
Horstwalde	P2B	0.711	0.0125	17.61	43	0.86
Horstwalde	P2D	0.711	0.025	17.69	34	0.85
Horstwalde	P5B	0.711	0.0125	17.71	36	0.86
Horstwalde	P5D	0.711	0.0125	17.76	29	0.86
Horstwalde	P4B	0.711	0.0125	17.67	37	0.86
Horstwalde	P4D	0.711	0.0125	17.66	32	0.86
Horstwalde	P3D	0.711	0.0125	17.63	116	0.86
Horstwalde	P3D	0.711	0.0125	17.74	30	0.86
Larvik	L1	0.508	0.0063	21.5	43	0.8
Larvik	L2	0.508	0.0063	21.5	135	0.8
Larvik	L3	0.508	0.0063	21.5	218	0.8
Larvik	L4	0.508	0.0063	21.5	365	0.8
Larvik	L5	0.508	0.0063	21.5	730	0.8
Larvik	L6	0.508	0.0063	21.5	730	0.8
Larvik	L7	0.508	0.0063	21.5	30	0.8
Hoogzand	1-T	0.356	0.016	7	37	0.66
Hoogzand	3-T	0.356	0.02	5.3	19	0.77
Hound Point	P(0)-T1	1.22	0.0242	34	11	0.95
Hound Point	P(0)-T2	1.22	0.0242	41	4	0.95
Lemen	BD	0.66	0.019	38.1	-	0.84
Dunkirk	CS-T	0.324	0.0191	11.3	187	0.72
Dunkirk	R1-T	0.457	0.0135	19.3	9	0.78
Dunkirk	C1-T	0.457	0.0135	10	69	0.78
Euripides	Ia-T	0.763	0.0356	30.5	7	0.99
Euripides	Ib-T	0.763	0.0356	38.7	2	0.97
Euripides	Ic-T	0.763	0.0356	47	11	0.96
Euripides	II-T	0.763	0.0356	46.7	7	0.95

Table B.5: Collected database of open-ended tests in tension from Yang et al., 2016

C

Additional plots

Not all plots were equally relevant to put in the main document, but this appendix collects some remaining plots. Perhaps they might prove helpful for better understanding and insight in the future.

Figure C.1 shows the $q_{c,avg}$, the average q_c at distances $1.5D$ above and below PTL . It effectively smooths out the q_c profile to obtain a representative value for q_b . Often in load tests, the q_c profile is already processed with this smoothing.

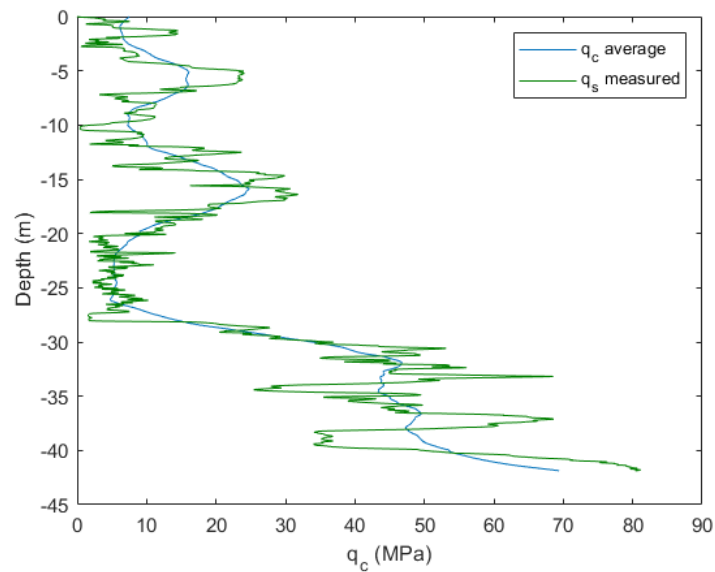


Figure C.1: CPT from Maasvlakte (q_c measured with $q_{c,avg}$)

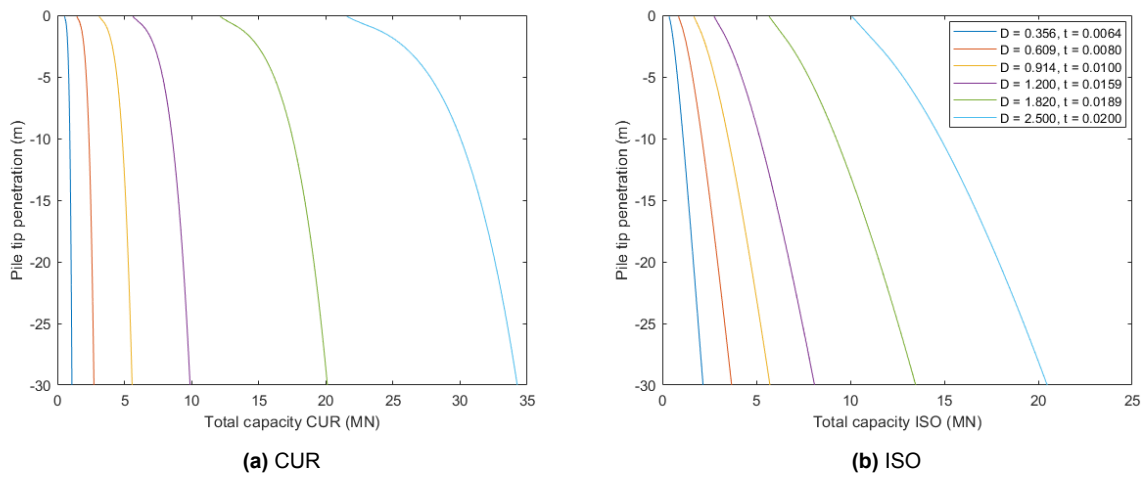


Figure C.3: Effect of increasing diameter on CUR and ISO for $q_c = 15 \text{ MPa}$

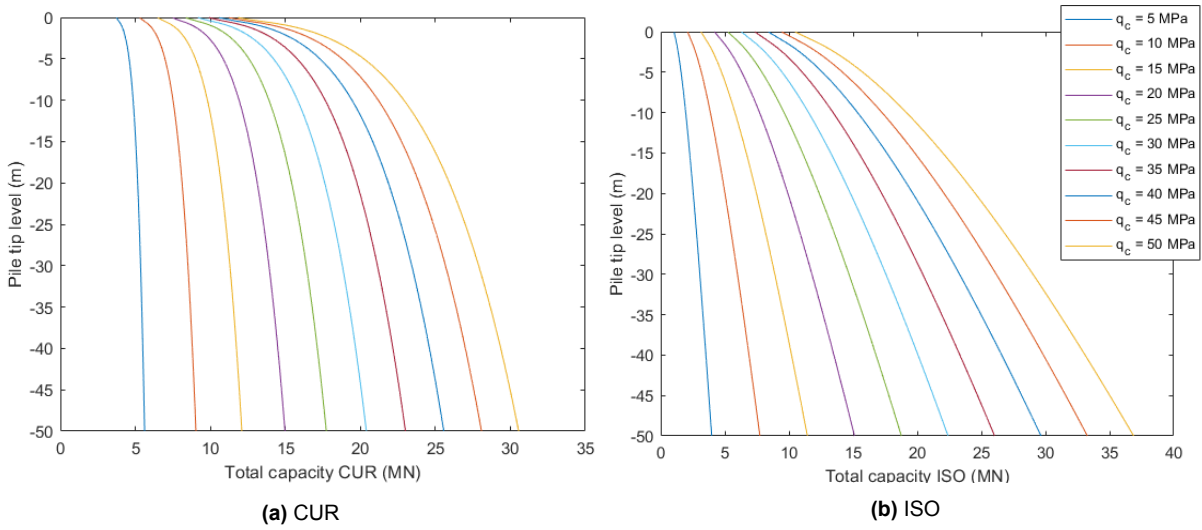


Figure C.2: Effect of varying synthetic q_c on capacities CUR and ISO

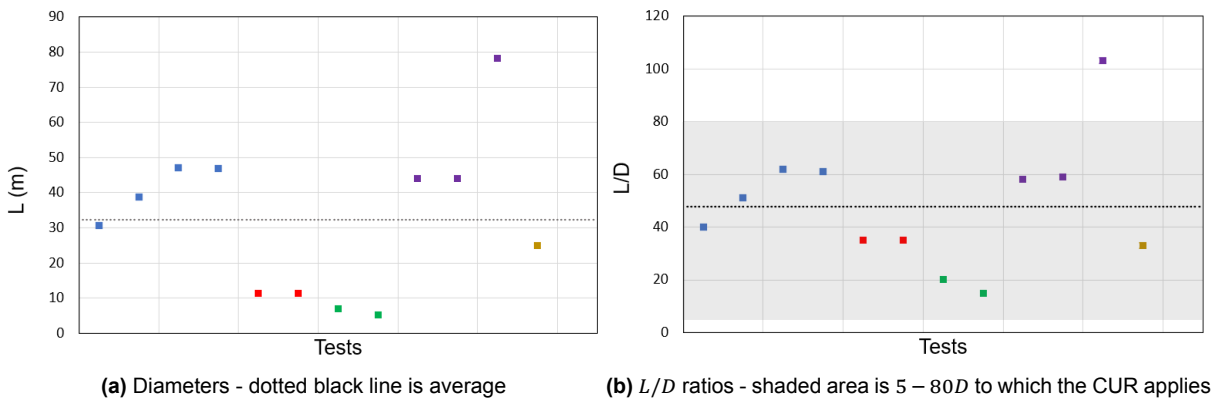


Figure C.5: Database CUR for open-ended piles loaded in compression - colours indicate sites

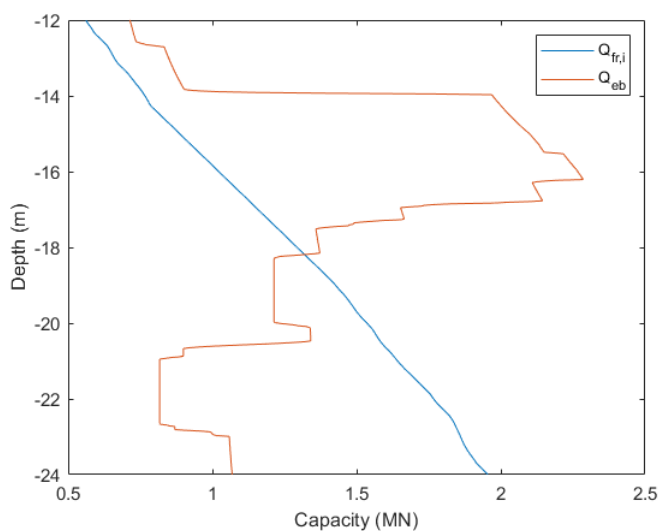
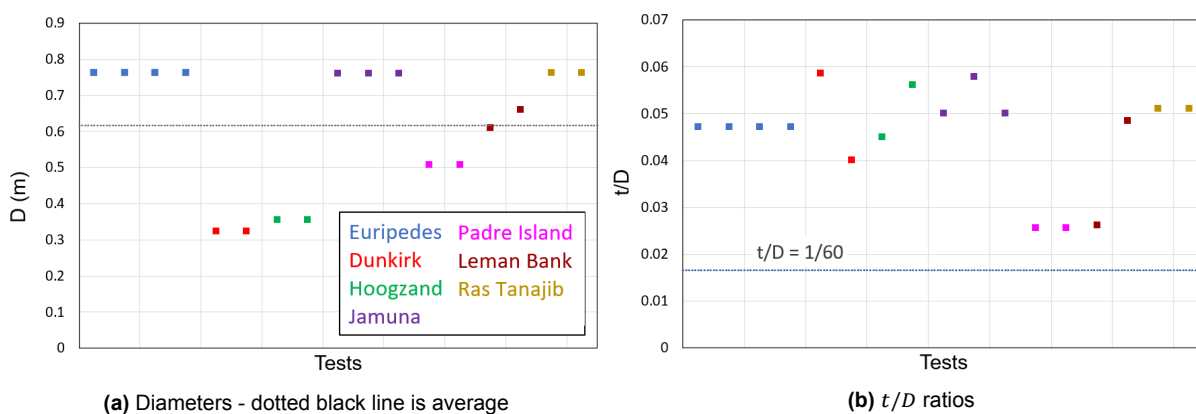


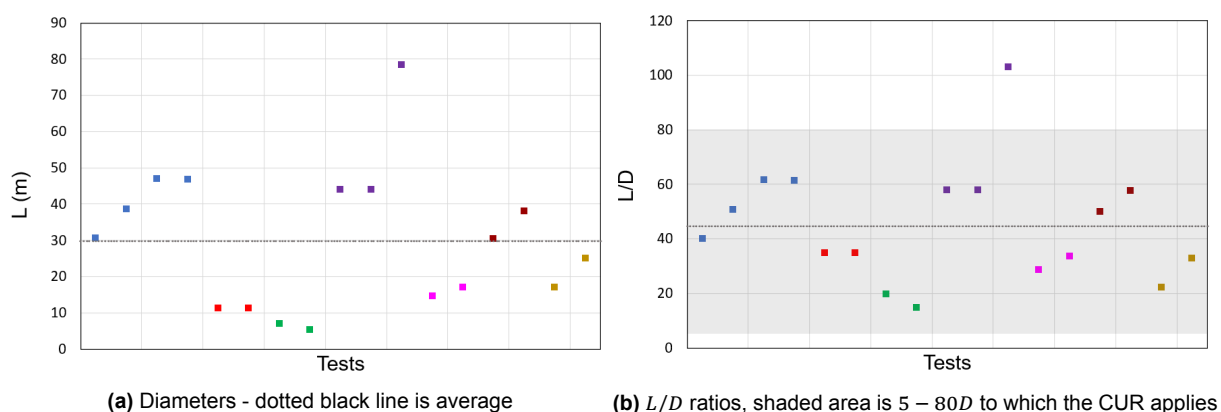
Figure C.4: $Q_{fr,i}$ and Q_b for NEN in CPT Utrecht for a pile with $D = 0.5$ m. When $Q_{fr,i} < Q_b$, the pile plugs (according to the NEN)



(a) Diameters - dotted black line is average

(b) t/D ratios

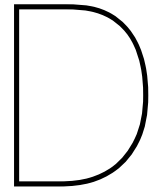
Figure C.6: Database CUR for open-ended piles loaded in tension - colours indicate sites



(a) Diameters - dotted black line is average

(b) L/D ratios, shaded area is $5 - 80D$ to which the CUR applies

Figure C.7: Database CUR for open-ended piles loaded in tension - colours indicate sites



The 1D plugging equation

The 1D plugging equation is often referred to in certain papers evaluating aspects of plugging. It is of lesser relevance for the main content of this research, but included as Appendix for completion.

Randolph et al., 1991 proposed an analytical model based on a 1D approximation of a soil plug. Figure D.2 shows the approximation of the plug as a series of disks of height dz on which a change in vertical stress $d\sigma_v$ acts.

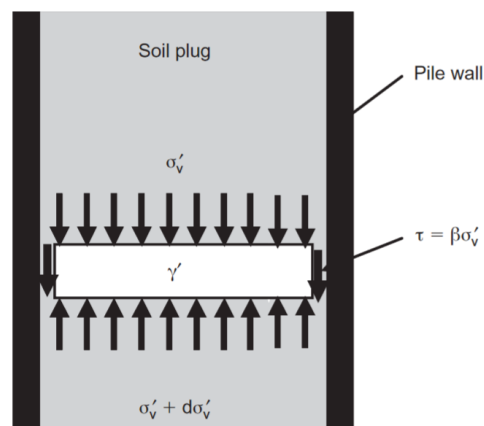


Figure D.1: Equilibrium of soil element, from Randolph, 2003

The equation for vertical equilibrium is now

$$\frac{d\sigma_v}{dz} = \gamma_w + \gamma' + \frac{4}{D_i} \tau_{f,i} \quad (\text{D.1})$$

The internal friction $\tau_{f,i}$ can be related to the vertical stress σ_v with a friction ratio β in

$$\tau_{f,i} = \beta \sigma'_v = K_0 \sigma'_v \tan \delta \quad (\text{D.2})$$

The equilibrium equation for effective stress then becomes

$$d\sigma'_v/dz = \gamma' + 2\beta\sigma'_v/R_i \quad (\text{D.3})$$

Using Mohr's circle and assuming active failure near the edge of the plug, it was found by Randolph et al., 1991 that β can be expressed as

$$\beta = \frac{\tau_{f,i}}{\sigma'_v} = \frac{\sin\phi}{1 + \sin\phi} \cdot \frac{\sin(\Delta - \delta)}{\cos(\Delta - \delta)} \quad (\text{D.4})$$

with

$$\Delta = \frac{\sin\delta}{\sin\phi} \quad (\text{D.5})$$

The assumption was made that the upper part of the plug hardly contributes to plug capacity, and introduced a boundary condition that a surcharge pressure acts for $z = 0 \text{ m}$ and that $z = 0 \text{ m}$ now is defined at the horizon where the wedged plug starts. Integrating eq. D.3 results for plug resistance with

$$q_{plug} = (\gamma' L_{unwedged} + (R_i \gamma' / (2\beta))) e^{(2\beta/R_i)L_{wedged}} - R_i \gamma' / (2\beta) \quad (\text{D.6})$$

Equation D.6 is theoretically interesting, but in practical use hard to apply as the determination of the unwedged/wedged plug is hard or impossible to determination, as are accurate expressions for β .

Lehane and Gavin, 2001 found the inner shear stress to be directly proportional to the vertical effective stress, validating equation D.4. Jeong et al., 2015 proposed a relationship for the inner skin friction and the IFR. This relationship can be seen in

$$\frac{t_{f,i}}{K_0 \sigma'_v \tan \delta} = 33.4 (IFR \cdot D)^{-0.48} \quad (\text{D.7})$$

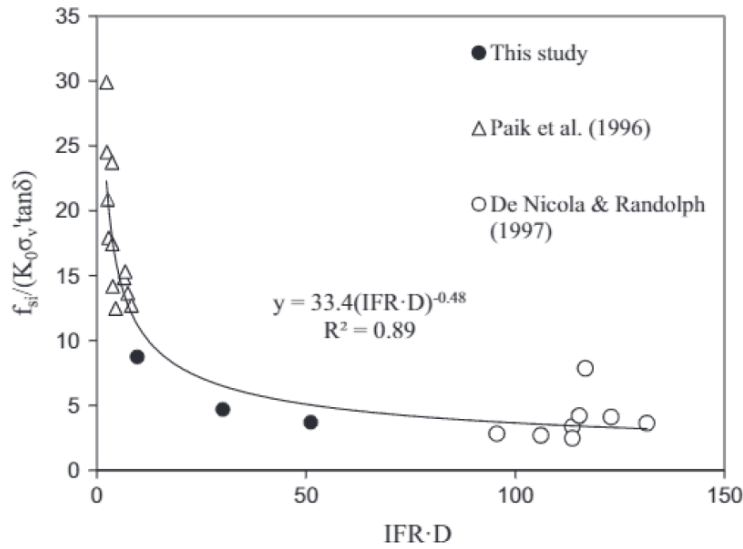


Figure D.2: Equation from Jeong et al., 2015

Bibliography

- Chow, F. (1997). Investigations into the behaviour of displacement piles for offshore foundations. *PhD thesis, Imperial College, London*.
- Chow, F. C., & Jardine, R. J. (1996). New design methods for offshore piles. *MTD96/103*.
- CUR. (2001). *Cur rapport 2001-8 bearing capacity of steel pipe piles* (tech. rep.).
- Gavin, D., Igoe. (2011). Piles for offshore wind turbines: A state-of-the-art review. *Proceedings of the ICE - Geotechnical Engineering*, 164(4), 245–256. <https://doi.org/10.1680/geng.2011.164.4.245>
- Gavin, K., & Igoe, D. (2021). A field investigation into the mechanisms of pile ageing in sand. *Géotechnique*, 71(2), 120–131. <https://doi.org/10.1680/jgeot.18.p.235>
- Gavin, K. G., Igoe, D. J. P., & Kirwan, L. (2013). The effect of ageing on the axial capacity of piles in sand. *Proceedings of the Institution of Civil Engineers - Geotechnical Engineering*, 166(2), 122–130. <https://doi.org/10.1680/geng.12.00064>
- Gudavalli, S. (2014). Effect of soil plugging on axial capacity of open-ended pipe piles in sands.
- Han, F., Ganju, E., Prezzi, M., Salgado, R., & Zaheer, M. (2020). Axial resistance of open-ended pipe pile driven in gravelly sand. *Géotechnique*, 70(2), 138–152. <https://doi.org/10.1680/jgeot.18.p.117>
- ICP. (2005). <https://doi.org/10.1680/idmfdpisac.32729>
- Iskander. (2010). *Behavior of pipe piles in sand*. Springer.
- Jamiolkowski, M., Presti, D. C. F. L., & Manassero, M. (2003). Evaluation of relative density and shear strength of sands from cpt and dmt. *Soil Behavior and Soft Ground Construction*. [https://doi.org/10.1061/40659\(2003\)7](https://doi.org/10.1061/40659(2003)7)
- Jardine, R. J., & Chow, F. C. (1996). *New design methods for offshore piles*. Marine Technology Directorate.
- Jeong, S., Ko, J., Won, J., & Lee, K. (2015). Bearing capacity analysis of open-ended piles considering the degree of soil plugging. *Soils and Foundations*, 55(5), 1001–1014. <https://doi.org/10.1016/j.sandf.2015.06.007>
- JIP. (2020). *Unified, unaffiliated cpt-based method for axial pile capacity calculation* (tech. rep.). Joint-Industry Project.
- Kim, K., Salgado, R., & Lee, J. (2002). Load tests on pipe piles for development of cpt-based design method. <https://doi.org/10.5703/1288284313263>
- Ko, J., & Jeong, S. (2015). Plugging effect of open-ended piles in sandy soil. *Canadian Geotechnical Journal*, 52(5), 535–547. <https://doi.org/10.1139/cgj-2014-0041>
- Labenski, J., Moormann, C., Aschrafi, J., & Bienen, B. (2016). Simulation of the plug inside open steel pipe piles with regards to different installation methods. *Proceedings of 13th Baltic Sea Geotechnical Conference*. <https://doi.org/10.3846/13bsgc.2016.034>
- Lehane, B. M., & Gavin, K. G. (2001). Base resistance of jacked pipe piles in sand. *Journal of Geotechnical and Geoenvironmental Engineering*, 127(6), 473–480. [https://doi.org/10.1061/\(asce\)1090-0241\(2001\)127:6\(473\)](https://doi.org/10.1061/(asce)1090-0241(2001)127:6(473))
- Lehane, B. M., Jardine, R. J., Bond, A. J., & Frank, R. (1993). Mechanisms of shaft friction in sand from instrumented pile tests. *Journal of Geotechnical Engineering*, 119(1), 19–35. [https://doi.org/10.1061/\(asce\)0733-9410\(1993\)119:1\(19\)](https://doi.org/10.1061/(asce)0733-9410(1993)119:1(19))

- Li, L., Wu, W., Naggar, M. H. E., Mei, G., & Liang, R. (2019). Dem analysis of the sand plug behavior during the installation process of open-ended pile. *Computers and Geotechnics*, *109*, 23–33. <https://doi.org/10.1016/j.compgeo.2019.01.014>
- NEN 9991-7. (2017). *Nen 9997-1+c2, geotechnisch onderwerp van constructies - deel 1: Algemene regels* (tech. rep.). Nederlandse Norm.
- Paik, K., Salgado, R., Lee, J., & Kim, B. (2003). Behavior of open- and closed-ended piles driven into sands. *Journal of Geotechnical and Geoenvironmental Engineering*, *129*(4), 296–306. [https://doi.org/10.1061/\(asce\)1090-0241\(2003\)129:4\(296\)](https://doi.org/10.1061/(asce)1090-0241(2003)129:4(296))
- Paik, & Salgado. (2003). Determination of bearing capacity of open-ended piles in sand. *Journal of Geotechnical and Geoenvironmental Engineering*, *129*(1), 46–57. [https://doi.org/10.1061/\(asce\)1090-0241\(2003\)129:1\(46\)](https://doi.org/10.1061/(asce)1090-0241(2003)129:1(46))
- Randolph, M. F. (2003). Science and empiricism in pile foundation design. *Géotechnique*, *53*(10), 847–875. <https://doi.org/10.1680/geot.2003.53.10.847>
- Randolph, M. F., Leong, E. C., & Houlsby, G. T. (1991). One-dimensional analysis of soil plugs in pipe piles. *Géotechnique*, *41*(4), 587–598. <https://doi.org/10.1680/geot.1991.41.4.587>
- Schneider, J., Lehane, B., & Xu, X. (2005). The uwa-05 method for prediction of axial capacity of driven piles in sand. *Frontiers in Offshore Geotechnics*. <https://doi.org/10.1201/noe0415390637.ch76>
- Schneider, J. A., Xu, X., & Lehane, B. M. (2008). Database assessment of cpt-based design methods for axial capacity of driven piles in siliceous sands. *Journal of Geotechnical and Geoenvironmental Engineering*, *134*(9), 1227–1244. [https://doi.org/10.1061/\(asce\)1090-0241\(2008\)134:9\(1227\)](https://doi.org/10.1061/(asce)1090-0241(2008)134:9(1227))
- van Dalen, J. (2013). Effect installatiemethode van open stalen buispalen op de conusweerstand. *Geotechniek*. https://issuu.com/uitgeverijeducom/docs/geo_2013_nr1-jan
- White, D. J., & Lehane, B. M. (2004). Friction fatigue on displacement piles in sand. *Géotechnique*, *54*(10), 645–658. <https://doi.org/10.1680/geot.2004.54.10.645>
- Yang, Z., Jardine, R., Guo, W., & Chow, F. (2016). *A comprehensive database of tests on axially loaded piles driven in sands*. Academic Press.
- Yu, F., & Yang, J. (2012). Base capacity of open-ended steel pipe piles in sand. *Journal of Geotechnical and Geoenvironmental Engineering*, *138*(9), 1116–1128. [https://doi.org/10.1061/\(asce\)gt.1943-5606.0000667](https://doi.org/10.1061/(asce)gt.1943-5606.0000667)